Stony Brook University

Functionalized Nanofibrous Materials for Water Purification

A Dissertation Presented

by

Rui Yang

to

The Graduate School

in Partial Fulfillment of the

Requirements

for the Degree of

Doctor of Philosophy

in

Chemistry

Stony Brook University

May 2014

Stony Brook University

The Graduate School

Rui Yang

We, the dissertation committee for the above candidate for the

Doctor of Philosophy degree, hereby recommend

acceptance of this dissertation.

Benjamin Chu – Dissertation Advisor
Distinguished Professor, Department of Chemistry

Benjamin S. Hsiao – Dissertation Advisor
Professor, Department of Chemistry

Robert B. Grubbs – Dissertation Advisor & Third Member
Associate Professor, Department of Chemistry

Jonathan G. Rudick - Chairperson of Defense
Assistant Professor, Department of Chemistry

Devinder Mahajan – Outside Member
Professor, Department of Materials Science & Engineering

This dissertation is accepted by the Graduate School

Charles Taber
Dean of the Graduate School

Abstract of the Dissertation

Functionalized Nanofibrous Materials for Water Purification

by

Rui Yang

Doctor of Philosophy

in

Chemistry

Stony Brook University

2014

The world faces urgent problems related to global water pollution. New fast, efficient, green, and cost-effective purification technologies can play a crucial role in solving contamination issues and offering fresh water supplies. In this research, two of the most abundant natural polysaccharides, cellulose and chitin, are extracted from wood pulp and shrimp shells, respectively, by using a series of chemical/physical treatments to produce nanofibers of 5 nm to 20 nm in width and a few microns in length, and investigated as functional components in water purification membranes. These naturally occurring nanofibers were thiol-modified to improve their ability to adsorb heavy metal ions, such as chromium, lead and arsenic from polluted water. In addition, these thiol-modified nanofibers were incorporated into high-flux fibrous microfiltration membranes fabricated by electrospinning to make nanofibrous composite membranes with high adsorption capacity of heavy metal ions (such as chromium, lead and arsenic), due to the large surface area-to-volume ratio and effective chemical functionality. The

modified nanofibrous composite membranes also demonstrated good stability and could be used and regenerated multiple times with high recovery efficiency after metal ion removal. Furthermore, novel ultrafiltration membranes were created by radical polymerization within the cellulose nanofibrous top barrier layer of the composite membrane. One example membrane could reject contaminated particles with sizes larger than 15 nm from water and also demonstrated excellent chemical resistance.

Dedication Page

To My Beloved Parents

Table of Contents

List of Figures

List of Tables

List of Abbreviations

MF	Microfiltration
UF	Ultrafiltration
NF	Nanofiltration
RO	Reverse Osmosis
PAN	Polyacrylnitrile
PET	Polyethylene Terephthalate
DMF	Dimethylformamide
CNF	Cellulose Nanofiber
EDC	1-Ethyl-3-(3-dimethylaminopropyl)carbodiimide
NHS	N-Hydroxysuccinimide
TEMPO	(2,2,6,6-tetramethylpiperidin-1-yl)oxidanyl
DVB	Divinylbenzene
AIBN	Azobisisobutyronitrile
SEM	Scanning Electron Microscope
tm-CNF	Thiol-modified Cellulose Nanofiber

Acknowledgments

I would like to take this opportunity to express my sincere gratitude to my advisors Prof. Benjamin Chu, Prof. Benjamin S. Hsiao and Prof. Robert B. Grubbs for their time in instructing my research, sharing comments and suggestions on my writing, presentations and professional career development. I would also like to thank Prof. Jonathan G. Ruddick, who has been serving as chair in my research committee in the past few years, giving comments and advice. Thanks to Prof. Devinder Mahajan for serving as my defense outside member. Thanks Professor Katherine Aubrecht for project instructions and AAS facility help.

In addition, thanks to facility mangers in Chemistry, Materials Science and Life Sciences Departments: Dr. James Marecek for FT-IR, Dr. Jim Quinn for SEM & EDS analysis and Dr. Susan Vanhorn for TEM. Moreover, I want to thank Dr. Troy Wolfskill, Dr. Susan Oatis, Dr. Eric Patterson, Dr David Hanson, Dr. Fernando Raineri, Dr. Roy Lacey, Dr. Joseph Lauher and Dr. Mohammad Akhtar for all the help and instruction with my 8 semesters' practical and professional teaching and training both in general chemistry lectures and labs.

Thanks to all my lab mates and chemistry department graduate students for the research advice and discussions, I would not be able to complete the study without your help. Thanks, Dr. Hongyang Ma, Dr. Dufei Fang, Dr. Christine Burger, Dr. Yu Cai, Dr. Ran Wang, Dr. Yang Liu, Dr. Mason Yeh, Dr. Xiao Wang, Dr. Justin Che, Zhe Wang and Ying Su, Hao Zhou, Sihui Guan, Zhirui Mo, Hui Gao, Edward Lu, Tianyuan Wu, Bingyin Jiang, Zhe Sun, Deborah Barkley, Meng Yang, Jue Liu, Shouhang Bo, Gaowei Wu, Dongyue Xin.

Thanks to my parents, family and friends for all the love and support!

Chapter 1 Introduction

1.1 Global water crisis

1.1.1 Fresh water scarcity

Currently, it is one of the biggest challenges to provide safe and clean drinking water to the world's 7.2 billion and growing population. However, the uneven regional distribution of the global water supply, industrial pollution, and inadequate sanitation has led to water resource scarcity [1]. Moreover, over 70% of fresh water withdrawals are for agriculture purposes, leading to conflicting issues of decreasing water supplies for agricultural production and an increase in human water demands [2]. According to the 2012 World Water Development Report [3], there were more than 700 million people in 43 countries suffering from water scarcity. By the year 2025, this number could rise to 1.8 billion. As shown in Figure 1.1, sub-Saharan Africa areas are the most water-stressed regions and between 75 million and 250 million people are living in some arid and semi-arid places. What is worse is the difficulty in the prediction of regional hydrology, resulting from uncertainty of climate changes, leading to insufficient water supply plans and potential damage in both drylands and wetlands[4]. According to the EM-DAT 2009 annual report, there were about 10 million people in the U.S. exposed to drought (with zero annual deaths), and about 25 million exposed to drought in China (with over 100 annual deaths) (Figure 1.2) [4].

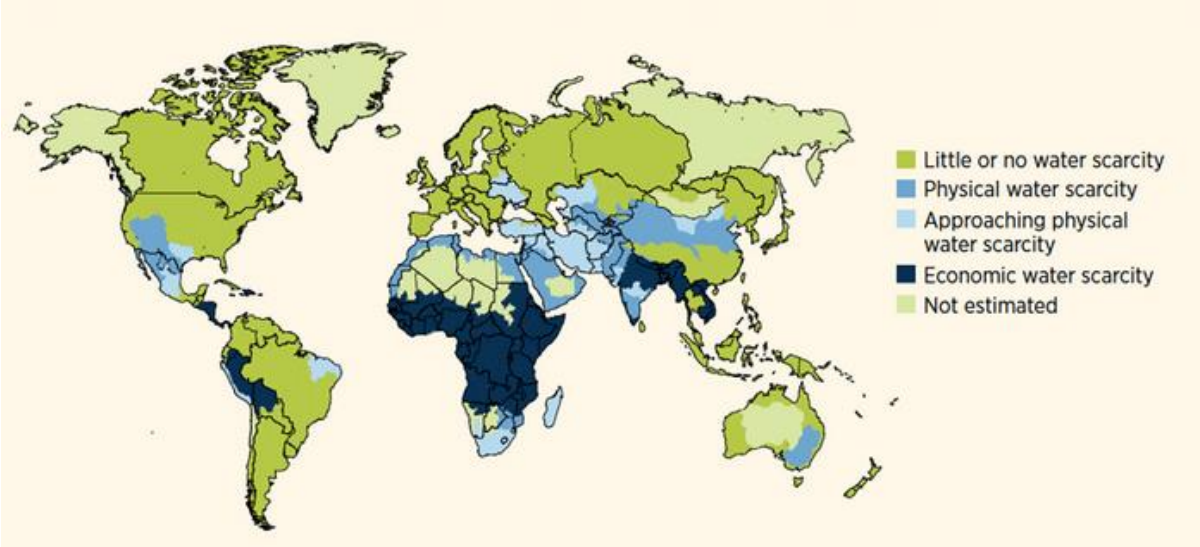

Figure 1.1 Global water scarcity (2012)[3]

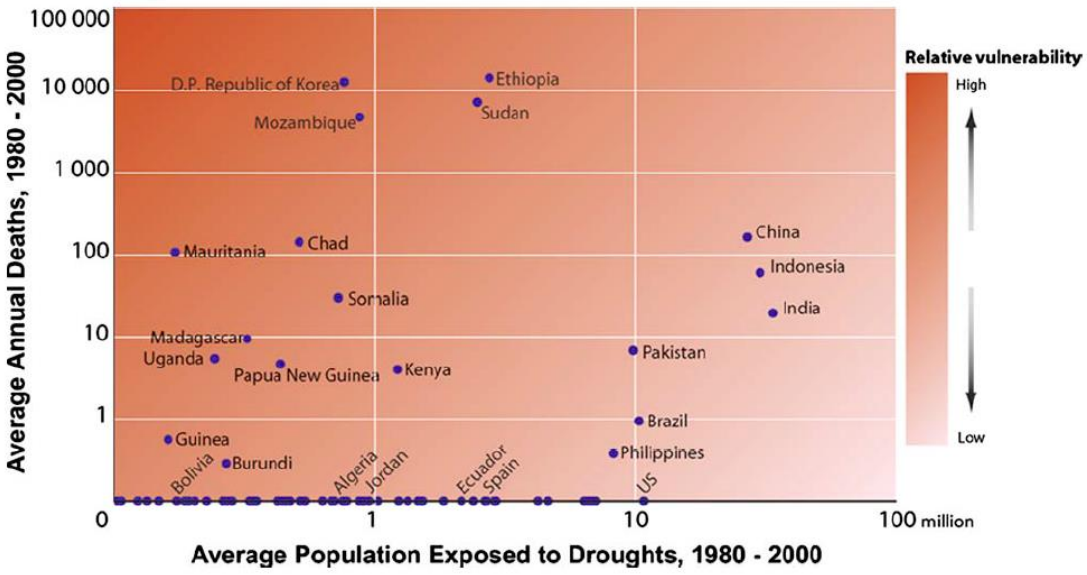

Figure 1.2 Relative global droughts induced human vulnerability (www.emdat.net) [4]

1.1.2 Water contamination and related human health Problems

Water pollution could be caused by various reasons, such as manufacturing, production, and mining. For example, mining operations consume large amounts of water and produce large waste deposits that can be oxidized in the air and precipitate causing polluted rainfall into rivers and lakes leading to contamination of water resources. The extraction of one kilogram of rare metals could result in up to 1000 tons of wastewater production [5]. These waste streams are massively contaminated with heavy metal ions (such as chromium, lead, arsenic and copper) and with mining chemicals. Such contaminated water has both short-term and long-term effects on aquatic life and human health [6]. Figure 1.3 demonstrates a representative relationship between various types of pollution and corresponding health effects. As illustrated, the contaminants include bacteria, viruses, heavy metal ions, pesticide chemicals, and other toxic chemical compounds and particles from air pollution that could cause headaches, fatigue, respiratory illness, cardiovascular illness, gastroenteritis, and increase the risk of cancer, nausea, and skin irritation, respectively [7]. In fact, water pollution is one of the major threats to human health, because contaminants in air and soil may dissolve in rainfall and eventually go to pollute rivers, lakes, and watersheds. Therefore, water purification plays a crucial role in providing a healthy life standard.

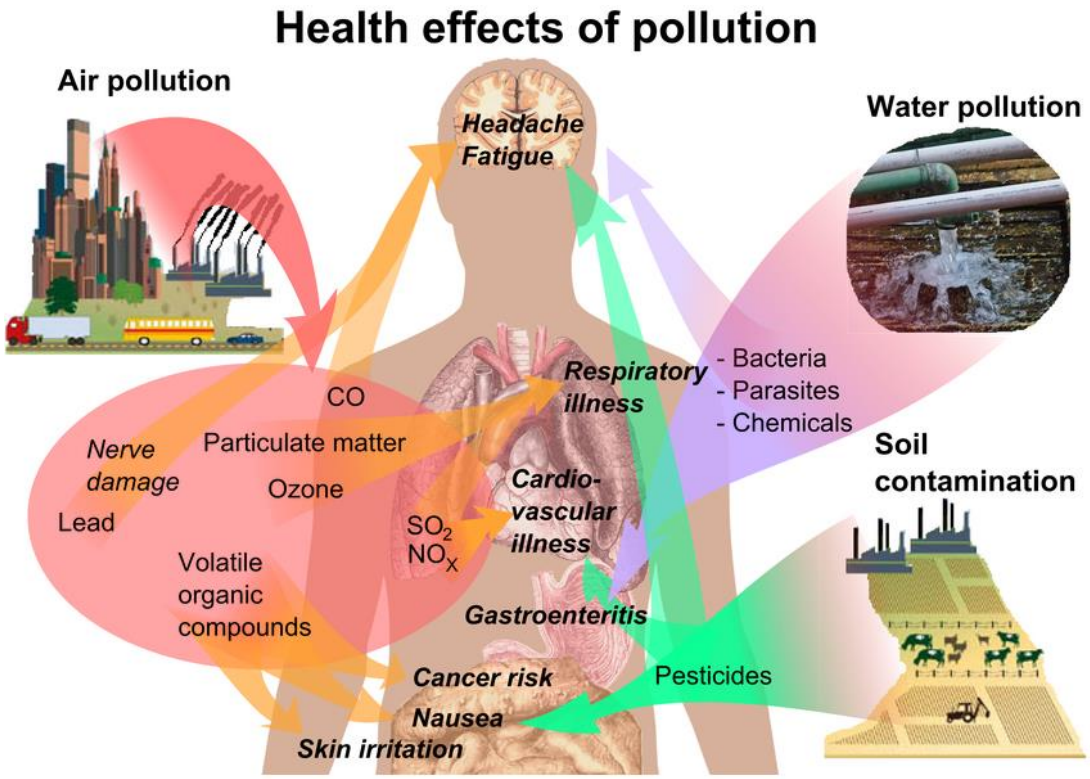

Figure 1.3 Health effects by various types of pollution [7]

To be more specific, both long term and short term intake of heavy metal ions in polluted water could cause the following human health problems as listed in Table 1.1. Heavy metal ion pollution can be generated by both agriculture and heavy industry, such as welding, painting, pesticide use, coal burning, mining, paper making, battery fabrication and unappropriated disposal. In water resources in many regions of the world, the heavy metal ion contamination levels are a 50 to 100 times higher than the World Health Organization (WHO) safety standard. The contaminations and their corresponding purification technologies will be discussed in the following chapters.

Table 1.1 Types of heavy metal and corresponding health effects [8, 9]

Heavy Metal Ions	Pollution Resources	Human Toxicity	WHO Safety Level
Chromium	Welding	Allergic dermatitis	500 ppb
Lead	Paint, pesticide, automobile emission, coal burning	Liver, kidney damage, mental retardation in children	100 ppb
Arsenic	Pesticides, fungicides, metal smelters	Cancer in liver, kidneys, lungs, bladder, skin lesion and dermatitis	20 ppb
Mercury	Pesticides, batteries, paper industry, mining	Damage to nervous system, protoplasm poisoning	10 ppb

1.2 Water purification nanotechnologies

Faced with urgent problems related to global water pollution, purification technologies involving fast, efficient, green, and cost-effective means can play a crucial role in solving contamination issues and offering fresh water supplies. There are diverse types of water purification technologies, such as bio-sorption[10], inorganic adsorbents[11], chemical precipitation[12], and ion exchange[13]; the methods are based on different chemical and physical affinities. Also, membrane filtration [14] is a well-known method widely used both in industry and home supplies. Membrane filtration types do not have strict definitions, but generally can be categorized as microfiltration (MF) (pore size larger than hundreds of nanometers) [15], ultrafiltration (UF) (pore size ranging from 10 nm ~ 100 nm) [16], nanofiltration (NF) (pore size ranging from 1 nm to 10 nm) [17] and reverse osmosis (RO) (pore size less than 1 nm) [18], which are based on the size-exclusion relation between particle filtrate sizes and membrane pore sizes.

1.2.1 Nanomaterial-based adsorption technology

Adsorption describes a mechanism of molecules or particles of a substance, known as adsorbate, adsorbing on some solid surface, known as adsorbent [9]. There is a diversity of factors that can influence the adsorption performance, such as adsorbent size, surface contact area, contact time, solution temperature and pH [19]. Among the natural and synthetic adsorbents, nanomaterials stand out due to their small particle (or fiber diameter) size and their porous or nanofibrous structure which can provide large surface-to-volume ratio and tremendous amounts of adsorption sites.

In recent years, carbon-based nanomaterials have become a hot topic in various fields of basic study and application-based work. A number of studies on both single-walled carbon nanotubes (SWCNTs) and multi-walled carbon nanotubes (MWCNTs) were applied to remove natural organic matter (NOM), consisting of a variety of organic compounds that were generated by plant deposition and animal residues [20], and to remove heavy metal ions [21, 22] from various water resources. Researchers have found out that the mechanism of NOM adsorption by CNTs was based on both the hydrophobic effect between the two substrates and the π–π electron donor–acceptor effect. In addition, some researchers took advantage of the large surface-to-volume properties of carbon nanotubes and combined it with the coagulation of aluminum sulfate[23] or ferric chloride to remove NOM efficiently from water [20].

Natural polysaccharides such as cellulose- and chitin-based nanomaterials are another research area that has drawn much attention. After extraction from the natural bio-residues, followed by a series of chemical and mechanical treatments, and owing to the inherent

hierarchical structure, they can be applied for waste water disposal including heavy metal ion removal. For instance, negatively charged ions can be adsorbed on the positively charged deacetylated chitin due to protonation of the amine in acidic conditions; or positively charged ions can be attracted by negatively charged sulfate-functionalized cellulose nanocrystals providing an Ag^+ maximum adsorption capacity of 34.4 mg/g , as shown in Figure 1.4 [24].

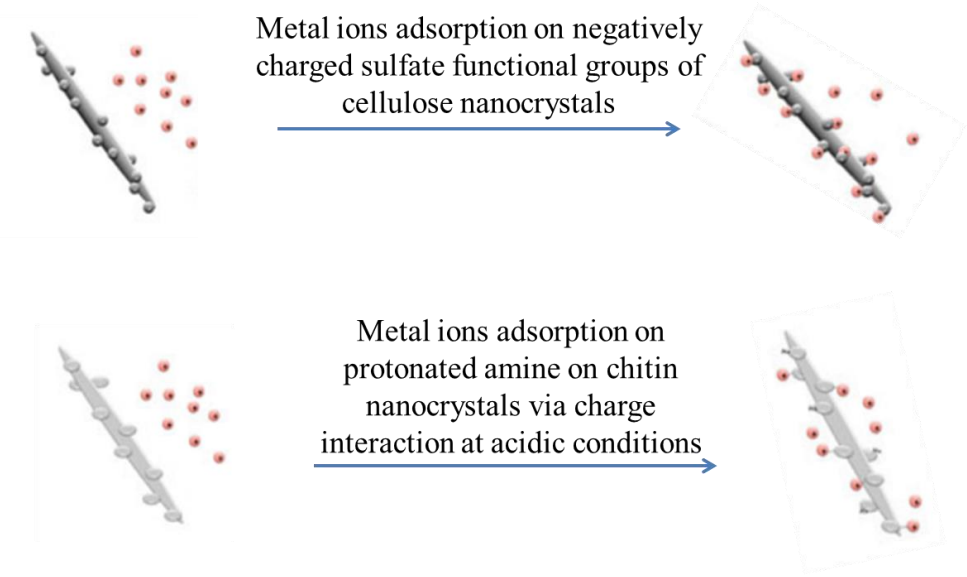

Figure 1.4 Schematic representation of Ag^+ adoption mechanism to modified cellulose and chitin nanocrystals by opposite charge interactions (figure reprinted with permission from reference [24])

Furthermore, there are studies on adsorption performance by synthesis of nanocellulose hybrids such as a class of hybrids containing reactive polyhedral oligomeric silsesquioxane (POSS) [25]. As described in this study, bleached cellulose fabrics from cotton fibers were cross-

linked by the reactive-POSS structure, as shown below in Figure 1.5. The large amount of hydroxyl groups and amino groups from POSS could provide tremendous amount of active sites for chelating complex formation with copper and nickel ions with, respectively, 24.5 mg/L and 8.1 mg/g [25]. Since the cellulose-hybrid adsorbents were neutral at all pH conditions, the adsorption mechanism was based on the chelating effect among metal ions and amino, hydroxyl groups. In addition, POSS could have higher adsorption of Cu^{2+} than Ni^{2+} because of the high stability of the copper amino complex, for which copper complexes formed the predominant species [26].

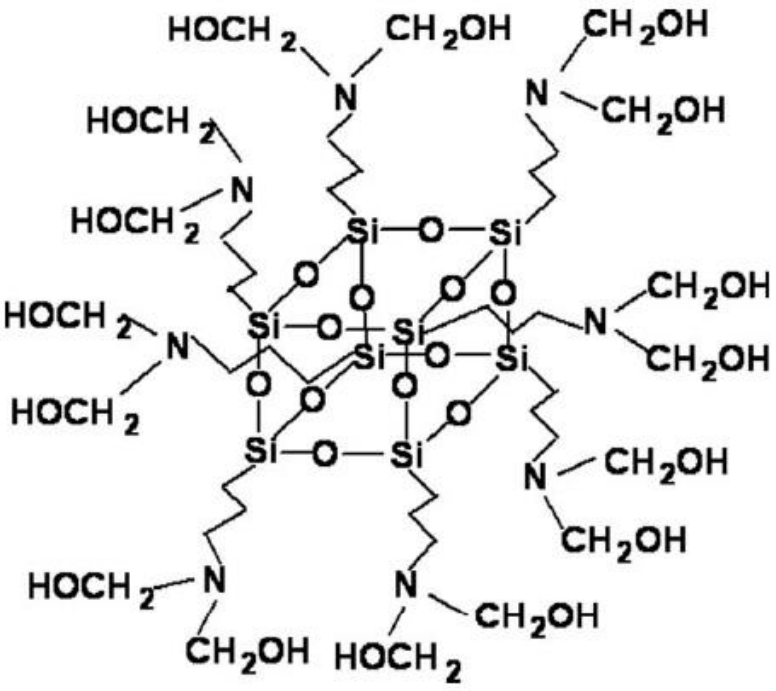

Figure 1.5 Chemical structure of reactive POSS (figure reprinted with permission from reference [25])

1.2.2 Nanofibrous media filtration technology

Membrane filtration has been widely used in water purification to separate solids and liquids or particles with different sizes by size exclusion [14]. Nanofibrous media based membrane filtration can provide high fluid flux efficiency, which is strongly corresponding to fiber sizes, uniformity, mechanical properties, and life time. As shown in Figure 1.6, smaller fiber diameters composed membrane with same pore size can generate higher fluxes.[27]

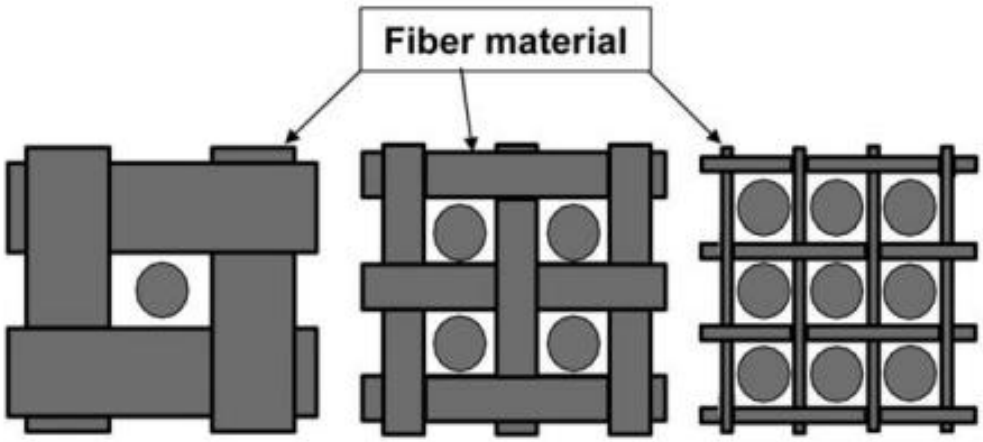

Figure 1.6 Nanofibrous media fiber size and pore size relationship [27]

As briefly mentioned previously, the nanofibrous filtration membrane can be categorized into the following four types based on pore sizes: microfiltration (MF), ultrafiltration (UF), nanofiltration (NF) and reverse osmosis (RO). All are shown in Figure 1.7.

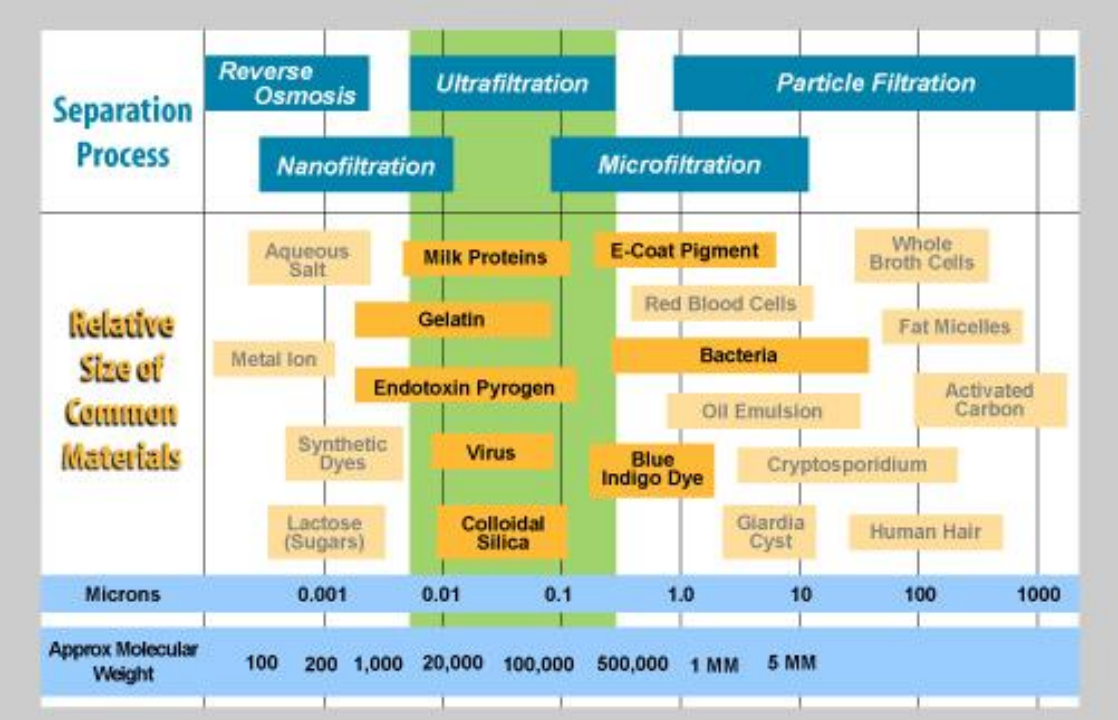

Figure 1.7 Various filtration types based on size exclusion [28]

The microfiltration (MF) membrane is commonly a polymeric filter that contains millions of microscopic pores ranging from 0.1 μm to 10 μm, sizes targeting the removal of bacteria, oil emulsion, and pathogens usually with operating pressure 5 to 25 psi [29]. MF membrane filters made of different materials have been created, developed and commercialized, such as ceramic membranes [30, 31], e-spun nanofiber membranes [32, 33], and phase inversion polymeric membranes [34], as shown in Figure 1.8.

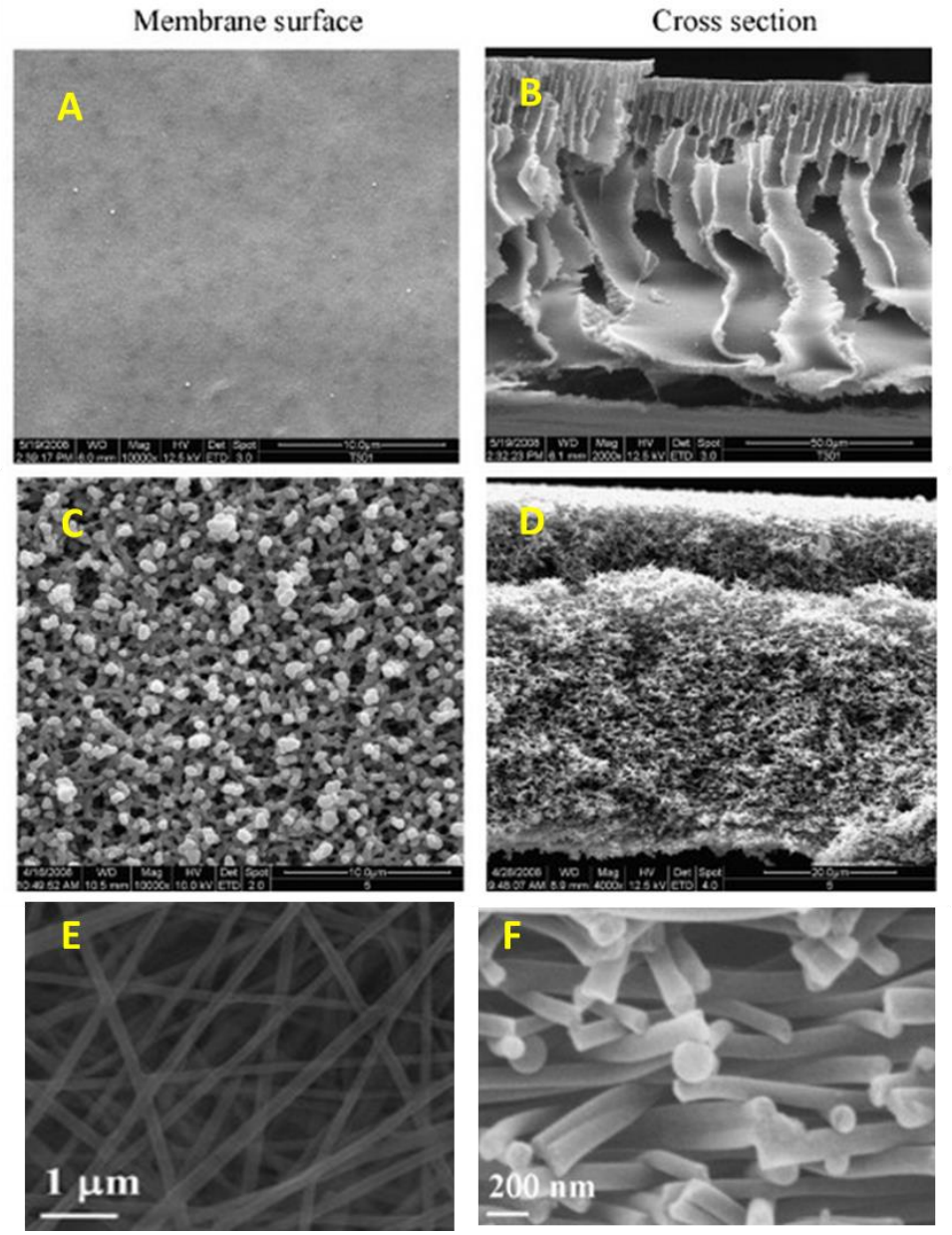

Figure 1.8 SEM images of top view (A, C, E) and cross-section (B, D, F) of MF membranes fabricated from different materials. (A, B) MF membrane made by using the phase inversion method of poly (ethylene glycol) [34]; (C, D) MF membrane made of ceramic materials [31]; (E, F) MF membrane made from E-spun nanofibers of polyvinylacohol (PVA) [33].(Figures reprinted with permission from the corresponding references)

Ultrafiltration (UF) membranes, made of polymers, such as polysulfone, cellulose acetate, and regenerated cellulose, have been widely used in a variety of industries, including food, beverage [35], and medical applications due to its small pore sizes, ranging from 10 nm to 100 nm, to remove particles, such as proteins, gelatin and viruses [36]. The mechanism of UF membrane filtration can be categorized as physical rejection, with particles bigger than the pore size being rejected [37]; with chemical interactions, particles could still be rejected even though the contaminate particle sizes are smaller than the membrane pore size. Thus, by taking advantage of membrane properties, such as functional groups [38], the UF membrane can be incorporated with certain media reactors of microbial organisms, such as biofilms to degrade biodegradable contaminates [39]. The fabrication of UF membranes can be as simple as coating a top fibrous barrier layer with finer fibers of comparable porosity, such as cellulose or chitin nanofibers to reach the pore size requirement [40].

Nanofiltration (NF) membranes refer to membranes with pore sizes ranging from 1 nm to 10 nm, aiming to remove particles such as sugar (lactose), certain salts, and metal ions in aqueous solution [41]. In particular, membranes can be fabricated by cellulose acetate, polyamide, or polyimide, which can either have symmetric or asymmetric structures [42]. The separation mechanism of NF membranes can be a complex combination of steric hindrance effects, Donnan effects, and dielectric effects. Correspondingly, the membrane top barrier layer, which is commonly composed of a 3D network structure of polymer chains, plays the crucial and dominant role in separation efficiency [43].

Reverse osmosis (RO) membranes refer to membranes with pore sizes ranging from 0.1 nm to 1 nm, that mostly reject metal ions or anything larger than ions. This technology has been developed ever since 1970s for seawater desalination [44]. It is a high pressure-dependent and

pressure-driven process; the membrane could be asymmetric with highly condensed layers (usually polyamide generated by interfacial polymerization), and the mechanism could be by size exclusion rejection, charge exclusion rejection, and physical-chemical interactions among the solute, solvent, and membrane [45]. Additionally, one of the biggest challenges in dealing with membrane filtration is the fouling problem. That is why, industrially, cross flow filtration is widely applied rather than direct (dead-end) filtration [39, 46].

1.2.3 Electrospinning in nanofibrous media preparation and applications

Electrospinning technology has been widely used for providing membranes with relatively more uniform pore sizes both in academic research and in industry. There are a variety of materials that can be used in electrospinning, such as ceramic materials [47], natural polysaccharides (chitin, chitosan) [48] and polymeric hybrid composite materials [49, 50].

Though a variety of electrospinning instruments exist, fundamentally, the basic mechanism of electrospinning is similar, as shown in Figure 1.9. A fluid, usually composed of a solute (e-spun material) and a solvent or solvent mixture, is slowly but continuously flowing from a spinneret to a collector under an applied electric field [51]. Specifically, the surface tension of the fluid at the spinneret tip is overcome,, causing the polymer solution to form a conical cone, known as the Taylor cone [52], as shown in Figure 1.9 (a). A jet stream is then formed, as shown in Figure 1.9 (b). Eventually, the polymer solution jet coming out of the tip forming a steady ejection, as shown in Figure 1.9 (c) [53]. After a certain period of time, the e-spun fibers collected would demonstrate a similar matrix morphology as schematically shown in the Figure 9 (d) and in the SEM image as shown in Figure 1.9 (e)

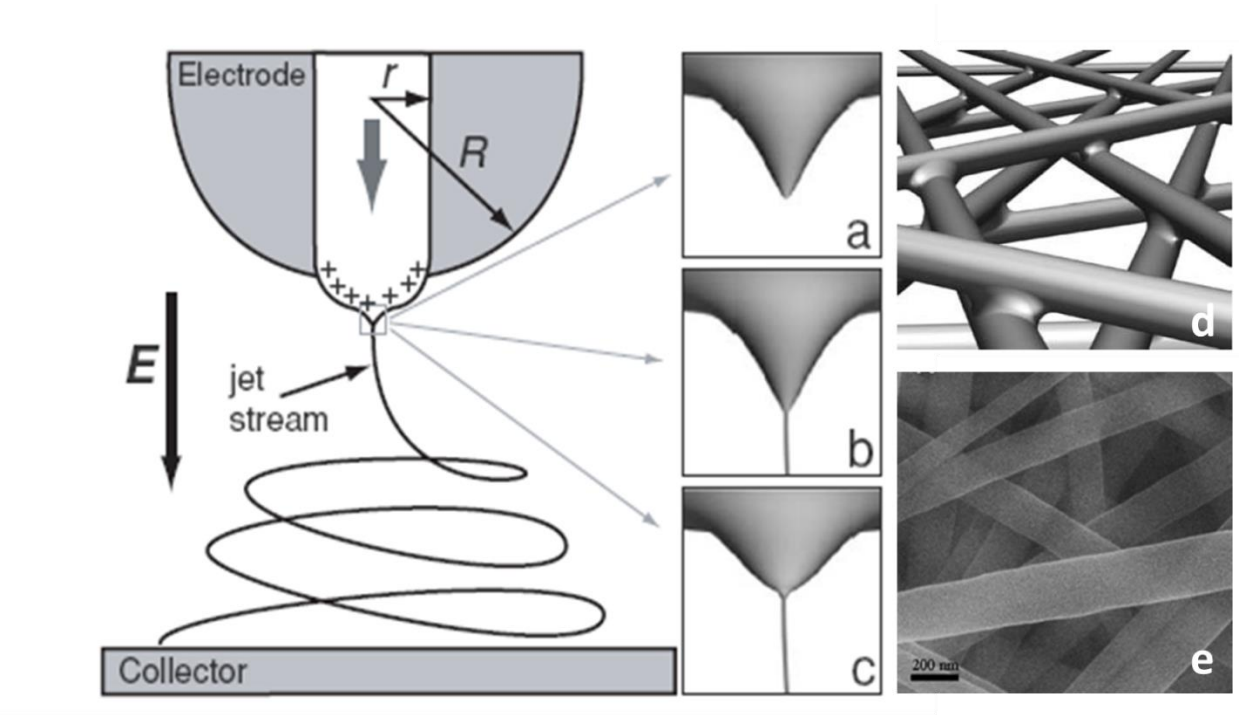

Figure 1.9 Schematic representations of electrospinning in which represent the radius of the capillary that contains e-spun materials, R refers to the curvature radius of the electrode used. (a) Taylor cone formed in applied electric field, (b) fluid e-spun solution ejects out of Taylor cone, (c) Taylor cone relaxation induced by surface tension, (d) 3D cartoon of nonwoven electrospun matrix with "soldered junctions" [53] and (e) SEM image of e-spun polyacrylonitrile (PAN) nanofibers [38] (figure reprinted with permission).

A multiple spinnerets instrument for continuous electrospinning production is shown in Figure 1.10 (A). The instrument was designed, constructed, and tested in the Department of Chemistry at Stony Brook University. Figure 1.10 (B) shows a schematic representation of the essential components of a single jet apparatus: an automatic syringe pump continuously injects a measured amount of solution out of the syringe; a certain voltage is applied between the spinneret and the speed-adjustable rotating collector; at the same time, temperature and humidity can be monitored and controlled during the electrospinning process [49, 50].

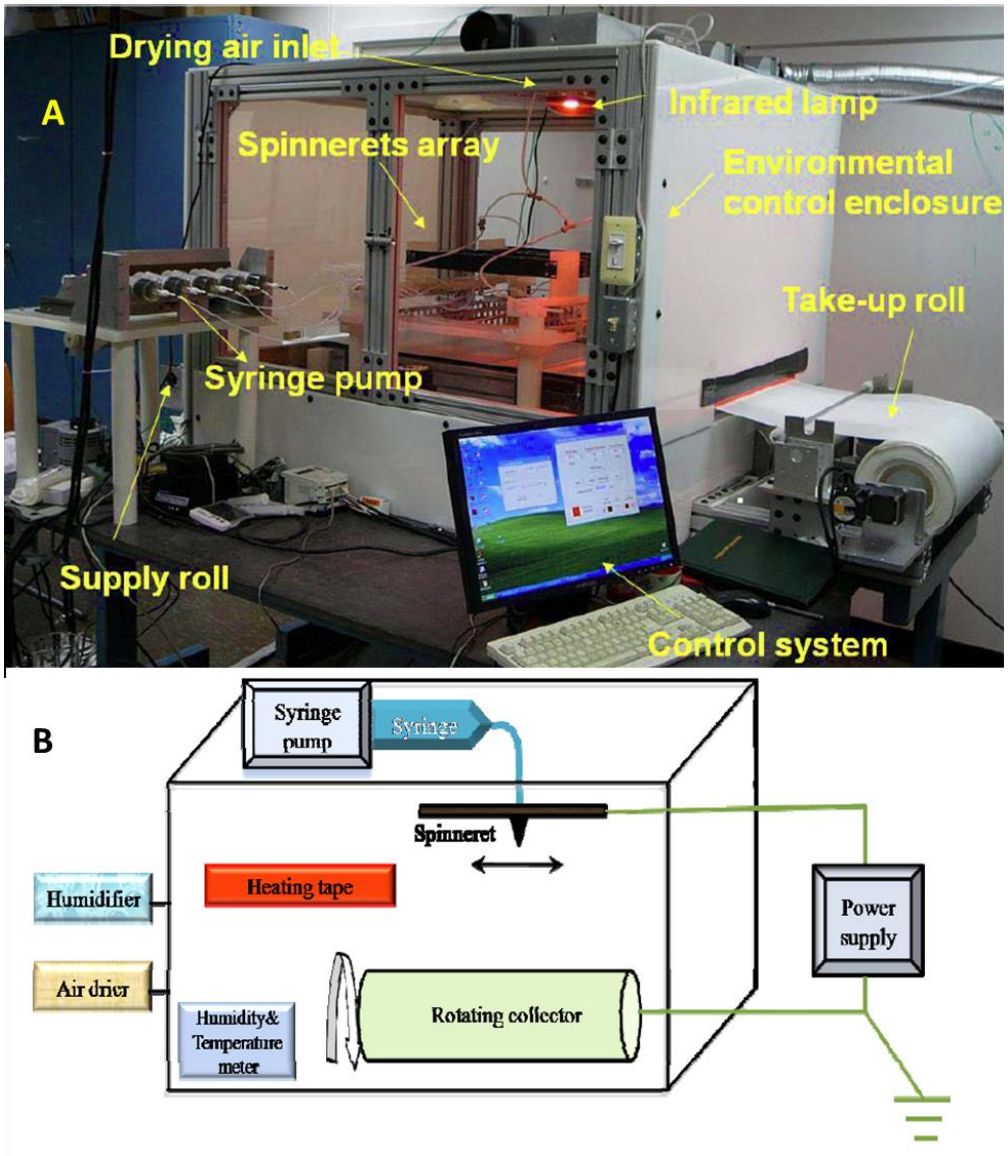

Figure 1.10 Professor Benjamin Chu, Benjamin Hsiao's research lab continuous electrospinning workstation in the Department of Chemistry, Stony Brook University. (A) Photo image of electrospinning working station, (B) Schematic representation of a single-jet electrospinning unit [54]

As mentioned above, e-spun nanofibers can be a good candidate for producing the membrane filtration media and scaffolds. In addition , e-spun nanofibers have also gained

popularity for many different applications, such as cosmetic skin mask, tissue engineering scaffolding, nanosensors, electrical engineering, military protective clothing, et al [53].

1.3 Polysaccharides as potential water purification materials

Polysaccharides are naturally abundant and renewable resources. They can be used for a variety of applications: for instance, starch as food supplies, cotton or jute as clothing materials, paper for communication purposes, sea shells for decorations, and wood for construction [55]. To summarize, there are mainly three different types of polysaccharides: cellulose, chitosan, and starch, as listed in Table 1.2. Among those materials, cellulose and chitin are the most abundant structural polysaccharides and their chemical structures are shown in Figure 1.12.

Table 1.2 Three major polysaccharides products and production

Polysaccharide Materials	Global Production
Man-made Cellulose Fibers	4700 kton in 2011 [56]
Starch Polymers	40 kton in 2006 [57]
Chitin/chitosan	7800 kton in 2010 [58]

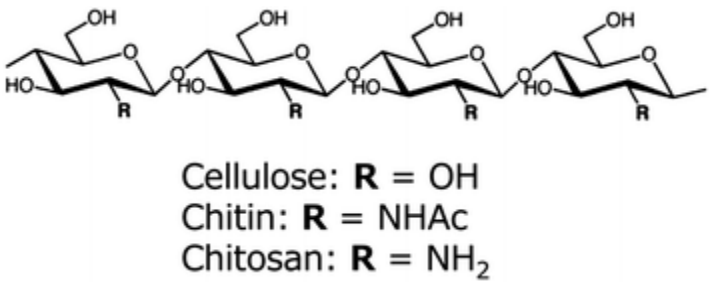

Figure 1.12 Cellulose, chitin and chitosan chemical structure (figure reprinted with permission from reference [59])

Cellulose nanofibers can be extracted from plant cells; the most abundant resource is trees. Figure 1.13 gives out a schematic process of cellulose extraction from the hierarchical structure: the cellulose chains aggregate and form a fiber structure with a dimension of several nanometers in width; then the fibers form bundles in a fiber-matrix structure, which comprises the scaffold and the major component of the cell wall; the cellular structure is composed of cells arrayed in micrometer scales leading to the millimeter scale of the growth ring of trees.

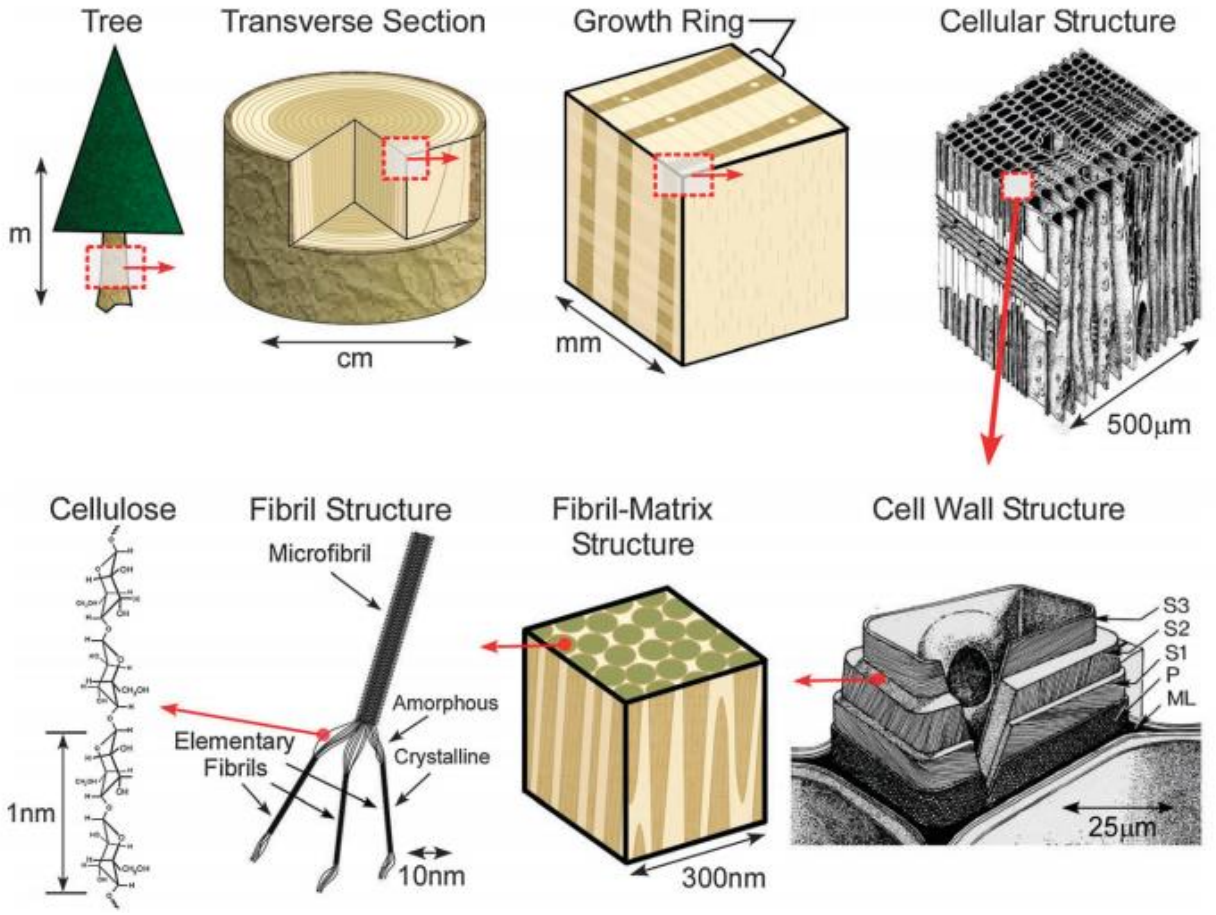

Figure 1.13 Schematic representation of cellulose extraction process from tree (figure reprinted with permission from reference [60])

Different methods have been applied for the extraction of cellulose from its original resource. There are generally two types of cellulose particles in nanoscale: one is cellulose nanocrystals and the other is micro-fibrillated cellulose [61]. The major processes of cellulose nanoparticle production are shown in Figure 1.14. Previous studies have used H_2SO_4 hydrolysis and homogenization to produce cellulose nanowhiskers, cellulose nanocrystals and microfibril cellulose (MFC) from grass fiber, cotton filter paper, and bacterial cellulose [62-64]. In addition to hydrolysis and mechanical treatments, the TEMPO oxidation method [65, 66] is another popular and efficient way to produce ultra-fine cellulose nanofibers with even smaller sizes and higher uniformity, which will be further detailed in the dissertation research.

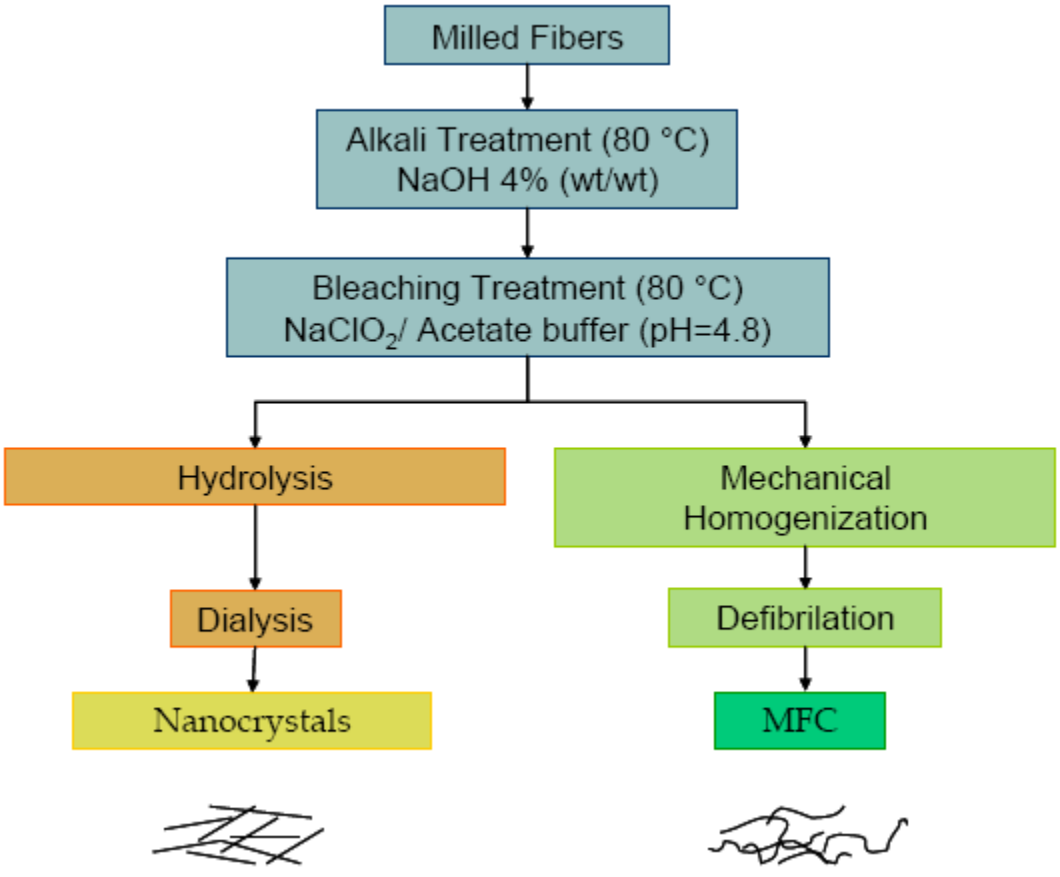

Figure 1.14 Cellulose nanoparticle production process (figure reprinted with permission from reference [60])

Chitin is a linear copolymer consisting of 2-acetamido-2-deoxy-β-d-glucose through a β (1 →4) linkage that can be extracted from crab and shrimp shells or from some natural fungi as a support layer [67]. Based on Figure 1.12, it is easy to see that chitin and chitosan are of similar scaffold structure units, where chitosan is the N-deacetylated derivative of chitin. There is no clear boundary between the definition of chitosan and chitin [68]. As presented in Figure 1.15, based on the chitin extraction from crab shell, the chitin molecules can form crystalline structures which are encapsulated by protein layers at the nanometer scale. The fiber matrices aggregate to form large bundles of chitin nanofibers. In a certain orientation, the rigid bouligand structure can be formed by the nanofiber network, and minerals, such as carbonates, are incorporated in it. Eventually, the shell structure is formed from certain patterns of stacking sequences.

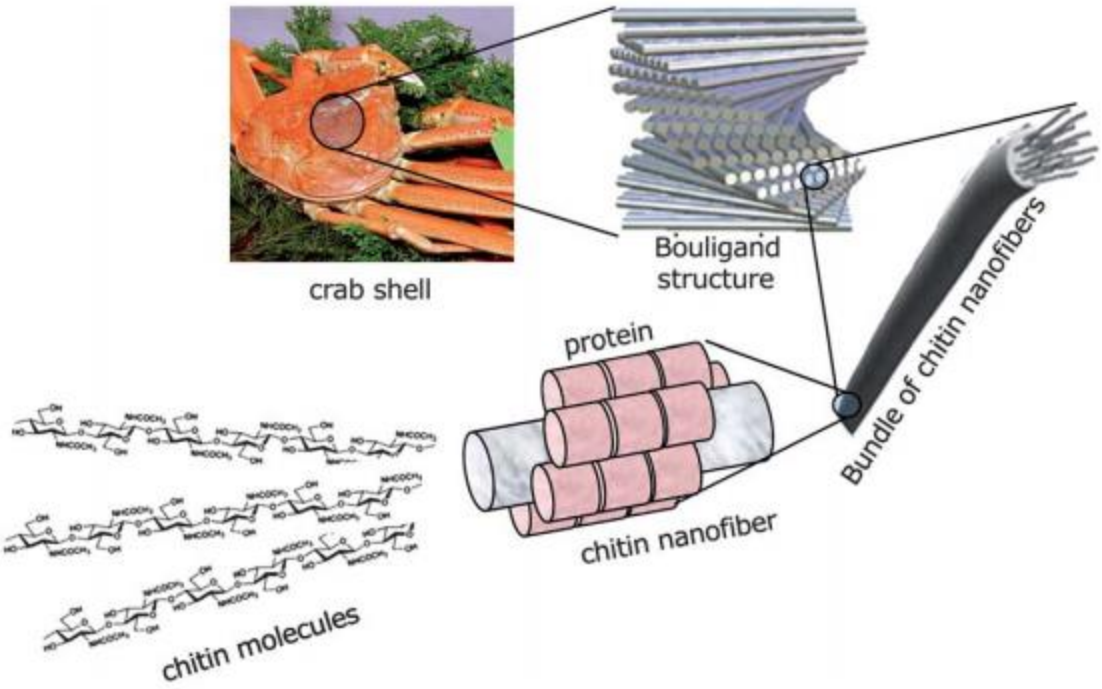

Figure 1.15 Schematic representation of chitin extraction from crab shell (figure reprinted with permission from reference [59])

For past decades, researchers have been using various methods and chemicals to extract chitin nanoparticles from the original resources. The chitin extraction scheme from seashells can be summarized in the following typical way in Figure 1.16. Strong acid HCl and strong base NaOH are the two essential chemicals to treat raw materials to remove minerals (such as carbonate) and protein from the bouligand network structure; mechanical treatment, such as grinding or sonication, are also important to bring down the fiber from the network bundles and to isolate the fibers.

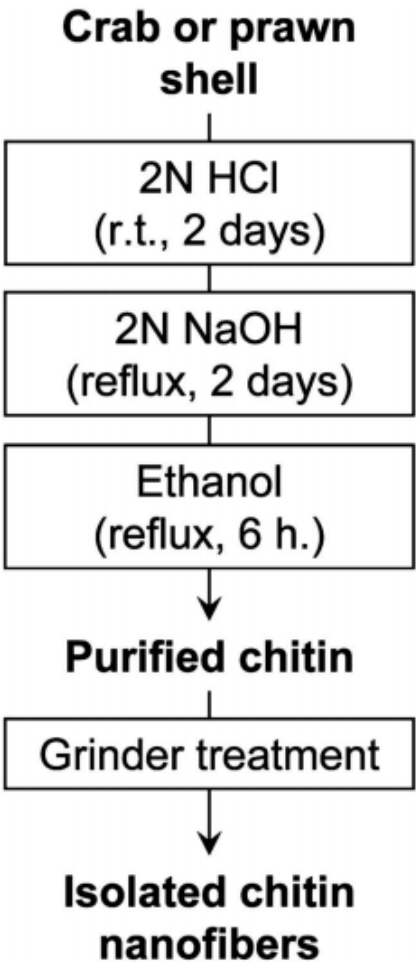

Figure 1.16 General chitin nanofiber preparation process (figure reprinted with permission from reference [59])

In addition to their naturally abundant availability, renewability, and environmentally friendly properties, cellulose and chitin nanofibers were well studied due to their ultra-fine structures in the nanoscale as well as the functional groups on the surface of those nanofibers, such as hydroxyl and amine groups, that can be directly used in medical, immunological, and material sciences, and in water treatment applications [69]. Besides, further modification reactions could also be applied in combination with the abundant functional groups to increase

the fibers functionality. Therefore, both the nanostructure and the diverse functionality make cellulose and chitin nanofibers outstanding candidates for water purification.

1.4 Research objectives

This doctoral thesis focuses on preparation, modification and characterization of ultra-fine (size uniformed nanoscale) cellulose and chitin nanofibers. Carboxylate-rich cellulose and amine-rich chitin fibers were produced for further functionalization by grafting thiol groups for removal of heavy metal ions (such as chromium, lead and arsenic) at different pH values and contact times, as well as with high regeneration efficiency. Also, electrospinning technology was applied to provide high water flux within the interconnected membrane structure. Infusion of functionalized carbohydrate nanofibers into electrospun membranes and further modification with a cross-linked polymer layer enabled the production of functionalized MF and UF membranes for separation and water purification applications.

References

1. Oelkers, E.H., J.G. Hering, and C. Zhu, *Water: Is There a Global Crisis?* Elements, 2011. **7**(3): p. 157-162.
2. Medina, M.A., *Global Water Crisis and Climate Change.* Journal of Hydrologic Engineering, 2010. **15**(3): p. 167-170.
3. *World Water Development Report 4. World Water Assessment Programme (WWAP), March 2012.*

4. Kanae, S., *Global Warming and the Water Crisis.* Journal of Health Science, 2009. **55**(6): p. 860-864.

5. Bridge, G., *Contested terrain: Mining and the environment.* Annual Review of Environment and Resources, 2004. **29**: p. 205-259.

6. Schwarzenbach, R.P., et al., *Global Water Pollution and Human Health.* Annual Review of Environment and Resources, Vol 35, 2010. **35**: p. 109-136.

7. *World Resources Institute: August 2008 Monthly Update: Air Pollution's Causes, Consequences and Solutions Submitted by Matt Kallman on Wed, 2008-08-20 18:22. Retrieved on April 17, 2009.*

8. Kurniawan, T.A., M.E.T. Sillanpaa, and M. Sillanpaa, *Nanoadsorbents for Remediation of Aquatic Environment: Local and Practical Solutions for Global Water Pollution Problems.* Critical Reviews in Environmental Science and Technology, 2012. **42**(12): p. 1233-1295.

9. Kumar, S., et al., *Nanotechnology-Based Water Treatment Strategies.* Journal of Nanoscience and Nanotechnology, 2014. **14**(2): p. 1838-1858.

10. Ying, W.C. and W.J. Weber, *Bio-Physicochemical Adsorption Model Systems for Wastewater-Treatment.* Journal Water Pollution Control Federation, 1979. **51**(11): p. 2661-2677.

11. Rodriguez, A., et al., *Dyes adsorption on low cost adsorbents: inorganic materials.* Desalination and Water Treatment, 2012. **45**(1-3): p. 191-205.

12. Moore, G.T., *Sewage purification by septic tank and chemical precipitation.* Journal of the American Medical Association, 1907. **49**: p. 677-680.

13. Kurhanov, A.M., *Purification of water by ion-exchange method.* Abstracts of Papers of the American Chemical Society, 2003. **226**: p. U495-U495.

14. Ersahin, M.E., et al., *A review on dynamic membrane filtration: Materials, applications and future perspectives.* Bioresource Technology, 2012. **122**: p. 196-206.

15. Li, W.X., et al., *Coagulation-microfiltration for lake water purification using ceramic membranes.* Desalination and Water Treatment, 2010. **18**(1-3): p. 239-244.

16. Pendergast, M.M., et al., *Self-assembled ultrafiltration membranes for enhanced water purification.* Abstracts of Papers of the American Chemical Society, 2012. **243**.

17. Bottino, A., et al., *Water purification from pesticides by spiral wound nanofiltration membrane.* Membrane Water Treatment, 2011. **2**(1): p. 63-74.

18. Rorech, G.J. and S.G. Bond, *Reverse-Osmosis - a Cost-Effective, Versatile Water-Purification Tool.* I&Cs-Instrumentation & Control Systems, 1993. **66**(11): p. 35-37.

19. Reschke, G. and D. Gelbin, *Application of Adsorption for Water-Purification - a Literature-Review.* Chemische Technik, 1982. **34**(3): p. 114-120.

20. Joseph, L., et al., *Removal of natural organic matter from potential drinking water sources by combined coagulation and adsorption using carbon nanomaterials.* Separation and Purification Technology, 2012. **95**: p. 64-72.

21. Mercier, G., et al., *Selective removal of metal impurities from single walled carbon nanotube samples.* New Journal of Chemistry, 2013. **37**(3): p. 790-795.

22. Lu, C.Y. and H.S. Chiu, *Adsorption of zinc(II) from water with purified carbon nanotubes.* Chemical Engineering Science, 2006. **61**(4): p. 1138-1145.

23. Tseng, T. and M. Edwards, *Predicting full-scale TOC removal.* Journal American Water Works Association, 1999. **91**(4): p. 159-170.

24. Liu, P., et al., *Cellulose and chitin nanomaterials for capturing silver ions (Ag+) from water via surface adsorption.* Cellulose, 2014. **21**(1): p. 449-461.

25. Xie, K.L., et al., *Adsorption Removal of Cu2+ and Ni2+ from Waste Water Using Nano-Cellulose Hybrids Containing Reactive Polyhedral Oligomeric Silsesquioxanes.* Journal of Applied Polymer Science, 2011. **122**(5): p. 2864-2868.

26. Monier, M., et al., *Adsorption of Cu(II), Co(II), and Ni(II) ions by modified magnetic chitosan chelating resin.* Journal of Hazardous Materials, 2010. **177**(1-3): p. 962-970.

27. Huang, Z.M., et al., *A review on polymer nanofibers by electrospinning and their applications in nanocomposites.* Composites Science and Technology, 2003. **63**(15): p. 2223-2253.

28. Systems, K.M., *Size of Materials That Are Removed By Various Separation Processes by Koch Membrane Systems* http://www.kochmembrane.com/sep_uf.html

29. Muilenberg, T., *Water management with membrane technologies: The benefits of microfiltration.* Pollution Engineering, 2003. **35**(5): p. 22-25.

30. Yang, Y.Q., R.Z. Chen, and W.H. Xing, *Integration of ceramic membrane microfiltration with powdered activated carbon for advanced treatment of oil-in-water emulsion.* Separation and Purification Technology, 2011. **76**(3): p. 373-377.

31. Wojciech, B., et al., *Cross-flow microfiltration of fermentation broth containing native corn starch.* Journal of Membrane Science, 2013. **427**(0): p. 118-128.

32. Li, L., R. Hashaikeh, and H.A. Arafat, *Development of eco-efficient micro-porous membranes via electrospinning and annealing of poly (lactic acid).* Journal of Membrane Science, 2013. **436**(0): p. 57-67.

33. Liu, Y., et al., *High-flux microfiltration filters based on electrospun polyvinylalcohol nanofibrous membranes.* Polymer, 2013. **54**(2): p. 548-556.

34. Susanto, H., N. Stahra, and M. Ulbricht, *High performance polyethersulfone microfiltration membranes having high flux and stable hydrophilic property.* Journal of Membrane Science, 2009. **342**(1–2): p. 153-164.

35. Mohammad, A.W., et al., *Ultrafiltration in Food Processing Industry: Review on Application, Membrane Fouling, and Fouling Control.* Food and Bioprocess Technology, 2012. **5**(4): p. 1143-1156.

36. Mehta, A. and A.L. Zydney, *Permeability and selectivity analysis for ultrafiltration membranes.* Journal of Membrane Science, 2005. **249**(1–2): p. 245-249.

37. Lee, J. and H.W. Walker, *Mechanisms and factors influencing the removal of microcystin-LR by ultrafiltration membranes.* Journal of Membrane Science, 2008. **320**(1-2): p. 240-247.

38. Yang, R., et al., *Thiol-modified cellulose nanofibrous composite membranes for chromium (VI) and lead (II) adsorption.* Polymer, 2014. **55**(5): p. 1167-1176.

39. Gao, W., et al., *Membrane fouling control in ultrafiltration technology for drinking water production: A review.* Desalination, 2011. **272**(1-3): p. 1-8.

40. Ma, H.Y., B.S. Hsiao, and B. Chu, *Thin-film nanofibrous composite membranes containing cellulose or chitin barrier layers fabricated by ionic liquids.* Polymer, 2011. **52**(12): p. 2594-2599.

41. Hilal, N., et al., *A comprehensive review of nanofiltration membranes: Treatment, pretreatment, modelling, and atomic force microscopy.* Desalination, 2004. **170**(3): p. 281-308.

42. Van der Bruggen, B., *Chemical Modification of Polyethersulfone Nanofiltration Membranes: A Review.* Journal of Applied Polymer Science, 2009. **114**(1): p. 630-642.

43. Luo, J. and Y. Wan, *Effects of pH and salt on nanofiltration—a critical review.* Journal of Membrane Science, 2013. **438**(0): p. 18-28.

44. Potts, D.E., R.C. Ahlert, and S.S. Wang, *A Critical-Review of Fouling of Reverse-Osmosis Membranes.* Desalination, 1981. **36**(3): p. 235-264.

45. Malaeb, L. and G.M. Ayoub, *Reverse osmosis technology for water treatment: State of the art review.* Desalination, 2011. **267**(1): p. 1-8.

46. Pandey, S.R., et al., *Fouling in reverse osmosis (RO) membrane in water recovery from secondary effluent: a review.* Reviews in Environmental Science and Bio-Technology, 2012. **11**(2): p. 125-145.

47. Panda, P.K., *Ceramic nanofibers by electrospinning technique - A review.* Transactions of the Indian Ceramic Society, 2008. **66**(2): p. 65-76.

48. Sonina, A.N., et al., *Production of Nanofibre Materials from Chitosan by Electrospinning (Review).* Fibre Chemistry, 2011. **42**(6): p. 350-358.

49. Wang, Y. and J.J. Santiago-Aviles, *A Review on Synthesis and Characterization of Lead Zirconate Titanate Nanofibers through Electrospinning.* Integrated Ferroelectrics, 2011. **126**: p. 60-76.

50. Pham, Q.P., U. Sharma, and A.G. Mikos, *Electrospinning of polymeric nanofibers for tissue engineering applications: A review.* Tissue Engineering, 2006. **12**(5): p. 1197-1211.

51. Abbas, M.A. and J. Latham, *Disintegration and Electrification of Charged Water Drops Falling in an Electric Field.* Quarterly Journal of the Royal Meteorological Society, 1969. **95**(403): p. 63-&.

52. Yarin, A.L., S. Koombhongse, and D.H. Reneker, *Taylor cone and jetting from liquid droplets in electrospinning of nanofibers.* Journal of Applied Physics, 2001. **90**(9): p. 4836-4846.

53. Burger, C., B.S. Hsiao, and B. Chu, *Nanofibrous materials and their applications.* Annu. Rev. Mater. Res., 2006. **36**: p. 333-368.

54. *In courtesy of Dr. Dufei Fang and Dr. Yang Liu's Ph.D. thesis introduction.*

55. Shen, L. and M.K. Patel, *Life cycle assessment of polysaccharide materials: a review.* Journal of Polymers and the Environment, 2008. **16**(2): p. 154-167.

56. *Global Cellulose Fibers Market is Expected to Reach USD 24.17 Billion in 2018: Transparency Market Research, http://www.transparencymarketresearch.com.*

57. *European Bioplastics (2007) Personal communication with Dr. Harald Kaeb, 16 January 2007.*

58. Cosgrove, J., *The Global Chitosan Market, Increasing application prospects are contributing to a continued positive outlook.* *http://www.nutraceuticalsworld.com/contents/view_online-exclusives/2010-12-02/the-global-chitosan-market-/#sthash.f7WkxdZ3.dpuf.*

59. Ifuku, S. and H. Saimoto, *Chitin nanofibers: preparations, modifications, and applications.* Nanoscale, 2012. **4**(11): p. 3308-3318.

60. Moon, R.J., et al., *Cellulose nanomaterials review: structure, properties and nanocomposites.* Chemical Society Reviews, 2011. **40**(7): p. 3941-3994.

61. Wool, R.P., et al., *Affordable composites and plastics from renewable resources: Part I: Synthesis of monomers and polymers.* Advancing Sustainability through Green Chemistry and Engineering, 2002. **823**: p. 177-204.

62. Oksman, K., et al., *Manufacturing process of cellulose whiskers/polylactic acid nanocomposites.* Composites Science and Technology, 2006. **66**(15): p. 2776-2784.

63. Grunert, M. and W.T. Winter, *Nanocomposites of cellulose acetate butyrate reinforced with cellulose nanocrystals.* Journal of Polymers and the Environment, 2002. **10**(1-2): p. 27-30.

64. Bondeson, D., A. Mathew, and K. Oksman, *Optimization of the isolation of nanocrystals from microcrystalline cellulose by acid hydrolysis.* Cellulose, 2006. **13**(2): p. 171-180.

65. Rodionova, G., O. Eriksen, and O. Gregersen, *TEMPO-oxidized cellulose nanofiber films: effect of surface morphology on water resistance.* Cellulose, 2012. **19**(4): p. 1115-1123.

66. Fukuzumi, H., T. Saito, and A. Isogai, *Properties of TEMPO-oxidized cellulose nanofiber film.* Abstracts of Papers of the American Chemical Society, 2009. **237**.

67. Ravi Kumar, M.N.V., *A review of chitin and chitosan applications.* Reactive and Functional Polymers, 2000. **46**(1): p. 1-27.

68. *R.A.A Muzzarelli (Ed.), Natural Chelating Polymers, Pergamon Press, New York (1973), p. 83.*

69. Harish Prashanth, K.V. and R.N. Tharanathan, *Chitin/chitosan: modifications and their unlimited application potential—an overview.* Trends in Food Science & Technology, 2007. **18**(3): p. 117-131.

Chapter 2 Thiol-modified Cellulose Nanofibrous Composite Membranes for Chromium (VI) and Lead (II) Adsorption

Abstract

Oxidized cellulose nanofibers (CNF), embedded in an electrospun polyacrylonitrile (PAN) nanofibrous scaffold, were grafted with cysteine to increase the adsorption capability for chromium (VI) and lead (II). Thiol-modified cellulose nanofibers (tm-CNF) were characterized by titration, FT-IR, energy dispersive spectroscopy (EDS) and SEM techniques. Static and dynamic Cr(VI) and Pb(II) adsorption studies of tm-CNF nanofibrous composite membranes were carried out as a function of pH and of contact time. The results indicated that these membranes exhibited high adsorption capacities for both Cr(VI) (87.5 mg/g) and Pb(II) (137.7 mg/g) due to the large surface area and high concentration of thiol groups (0.9 mmol of -SH/gram tm-CNF). The morphology and property of tm-CNF nanofibrous composite membranes was found to be stable, and they could be used and regenerated three times with high recovery efficiency. (Copyright of this article to reuse in this thesis was obtained from Elsevier publisher Copyright Clearance Center)

Keywords: cellulose nanofiber, thiol-modification, heavy metal ions removal, nanofibrous membrane

2.1 Introduction

Heavy metal pollution caused by agriculture and manufacturing (e.g., mining and automobile manufacturing) industries is a worldwide problem [1]. The pollutants can contaminate rivers and lakes, and be a major threat to public safety, especially for drinking water. For example, according to the World Health Organization (WHO), the health effects of long term exposure to 0.015 ppm of lead (II) include headache, irritability, abdominal pain and various symptoms related to the nervous system [2], and long-term exposure to chromium (VI) levels over 0.1 ppm can cause respiratory problems, kidney and liver damage [3].

For heavy metal removal, the adsorption method is a cost-effective approach [4-7], which also offers great flexibility in design and operations. In some instances, adsorption can be used together with filtration to yield better efficiency in applications such as drinking water purification. As most sorption processes are reversible, adsorbents can be regenerated by a suitable desorption process. These adsorbents include activated carbon, carbon nanotubes [8] and bioadsorbents (e.g., shrimp and crab shells, dead bacteria, spent yeast) [9, 10]. The application of such adsorbents often requires post-treatment after adsorption. Sometimes the complete separation and removal of adsorbents from water can be difficult and can cause additional environmental problems [11-13]. Heavy metal removal by membrane filtration has also been well demonstrated in the industry. Typically, membrane filtration approaches are not as cost-effective as adsorption because the processes often involve nanofiltration or reverse osmosis, which invariably have high energy costs and can require high pressures [14-18].

It has been recently demonstrated that nanostructured polysaccharide materials can be used for heavy metal adsorption [19]. For example, cellulose nanofibers (cellulose is the most abundant natural polysaccharides on earth), produced by the TEMPO oxidation method, exhibited a high concentration of surface hydroxyl, carboxylic acid (0.05-1.5 mmol/g) and aldehyde groups (0-0.35 mmol/g), depending on the degree of oxidation [20]. These materials can be modified to become effective metal ion absorbents by chemical grafting of suitable functional molecules on the fiber surface [21-23], such as through the formation of amide bonds. Previous studies have demonstrated the efficiency of amine-modified cellulose nanofibers for bacteria, virus and metal ion removal [24]. The objective of this study is to take advantage of the high concentration of available functional groups on the surface of cellulose nanofibers to further increase the capacity for metal ion removal through a new thiol-modification scheme.

In the present study, ultrafine cellulose nanofibers (~5 nm in diameter and a few hundred nanometers in length) were chosen as the base material for absorbent. These nanofibers offer a very large surface to volume ratio, thus providing a great number of active sites for metal ion adsorption after the thiol-modification. Cellulose nanofibers were anchored by thermal cross-linking in an electrospun polyacrylonitrile (PAN) nanofibrous scaffold (fiber diameter about 100 nm), resulting in the formation of nanofibrous composite membranes which contain fibers of two different diameters. The resulting composite membranes with thiol-modified cellulose nanofibers (tm-CNFs) showed large adsorption capacity, fast adsorption efficiency and a superior capacity for regeneration. A hypothetical schematic illustration of the 3D structure for the electrospun PAN nanofibrous scaffold and the tm-CNF infused PAN nanofibrous scaffold is shown schematically in Figure 2.1, where most of the tm-CNFs have been associated with the electrospun PAN nanofibers.

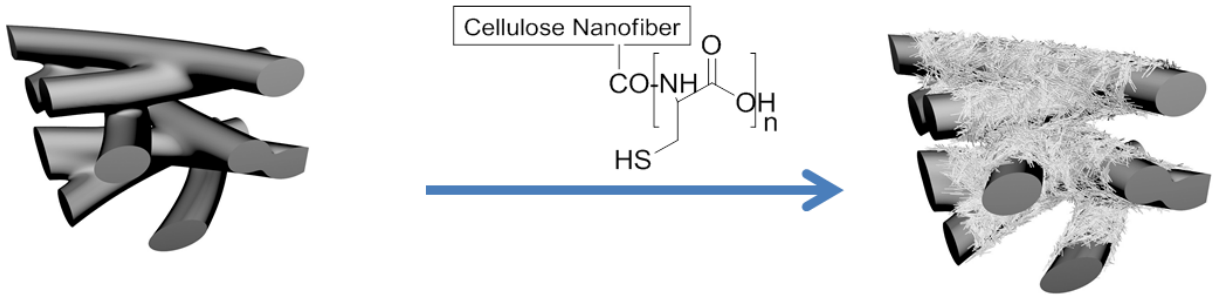

E-spun PAN nanofibers matrix tm-CNFs incorporated PAN matrix

Figure 2.1 A schematic illustration of 3D structure for the electrospun PAN nanofibrous scaffold (left side) and the tm-CNF infused PAN nanofibrous scaffold (right side)

2.2 Materials and Methods

2.2.1 Materials

Polyacrylonitrile (PAN, M_w=150,000 g/mol) was purchased from Scientific Polymer Products, L-cysteine (> 97% purity), dimethylformamide (DMF), *N*-hydroxysuccinimide (NHS), *N*-(3-dimethyl-aminopropyl)-*N*′-ethylcarbodiimide hydrochloride (EDC), 2,2,6,6-tetramethyl-1-piperidinyloxy (TEMPO), sodium hypochlorite (NaClO), sodium chlorite ($NaClO_2$), sodium bromide (NaBr), potassium chromate (K_2CrO_4), lead nitrate ($Pb(NO_3)_2$), 1,5-diphenylcarbazide and 4-(2-pyridylazo)resorcinol (PAR), phosphate buffer were purchased from Sigma-Aldrich. Ellman's Reagent, DTNB (5,5'-dithio-bis-[2-nitrobenzoic acid]) was purchased from Thermo Scientific. Cellulose Biofloc-92 (wood bleached pulp) was provided from Tartas (France). Non-woven poly(ethylene terephthalate) (PET) microfilter substrate (average fiber diameter ~10 μm) for membrane support was provided by Sanko (Japan No. 16-1).

2.2.2 Preparation of thiol-modified cellulose nanofibers

2.2.2.1 Preparation of oxidized cellulose nanofibers by the TEMPO method

Oxidized cellulose nanofibers (CNFs) were produced by the TEMPO method based upon a procedure published elsewhere [25]. In brief, 10.0 g dry wood pulp cellulose was dispersed in water (100 g). Sodium bromide (2.0 g, 19.4 mmol) and TEMPO (0.2 g, 0.13 mmol) were dissolved in the same mixture. Sodium hypochlorite solution (75.0 g, 10–13 % aqueous solution) was then added to the stirred solution at room temperature. The stirring process was continued for 24 h, while the pH value was kept at 10.5-11 (monitored with a pH meter) by adjusting the suspension with 0.5 mol/L sodium hydroxide aqueous solution (approximately 10 ml was used). The resulting cellulose product was separated by centrifugation (5500 rpm with relative centrifugal force of 2706 × g), washed with DI water and separated again by centrifugation several times until the conductivity of the supernatant solution as tested by a conductivity meter, did not change (~ 120 μS/cm). The oxidized cellulose slurry (1.10 g, >90 wt% cellulose) was then dispersed in 100 g of water and sonicated for 15 min with a homogenizer (Cole Parmer, VCX-400). The resulting cellulose nanofiber aqueous suspension had a concentration of ~1 wt%, as determined by a Total Organic Carbon analyzer (TOC-500, Shimadzu Corporation).

2.2.2.2 Preparation of thiol-modified cellulose nanofibers by cysteine

100 g ~1 wt% CNF suspension was mixed with N-hydroxysuccinimide (NHS) (0.18 g, 1.5 mmol), 1-ethyl-3-[3-dimethylaminopropyl]carbodiimide (EDC) (0.27g, 1.4 mmol) and cysteine (0.5 g, 4.1 mmol). The resulting mixture was stirred at room temperature for 24 hours. After reaction, the mixture was centrifuged at 5000 rpm with relative centrifugal force of about

2200 × g to separate the supernatant from the nanofibers. The supernatant was poured off and the nanofibers were re-suspended in water, and the washing and centrifugation process was repeated several times until the conductivity in the centrifugal tube did not change (~ 120 μS/cm), which implied that only cellulose nanofibers (yield of about 70%) remained in the suspension.

2.2.3 Characterization of modified cellulose nanofibers

2.2.3.1 Determination of carboxylate groups by titration

The amount of carboxylate groups could be quantified by using the electric conductivity method [26]. For this test, 3 ml of 0.9 wt% CNF suspension was first diluted into 50 ml DI water. 3 ml of 0.1 M HCl was subsequently added to this suspension to keep the pH value between 2.0 and 3.0. Then, 50 μl aliquots of 0.05 M NaOH were continuously added at the rate of one aliquot every 20 seconds into the suspension to achieve a pH value of 11, while the conductivity of the suspension was measured. The carboxylate content was determined from the conductivity and the pH curves [22]. To determine the amount of aldehyde groups, the same amount of cellulose slurry solution was mixed with $NaClO_2$ (0.5 g) for overnight oxidation [26] and then the mixture was washed with DI water and separated by 5000 rpm (with relative centrifugal force of about 2200 × g) centrifugation for 5 min. The same conductivity titration method was used to determine the concentration of carboxylate groups. The aldehyde group concentration is equal to the carboxylate concentration from this titration minus the carboxylate concentration from the titration carried out prior to $NaClO_2$ oxidation.

2.2.3.2 Quantitative determination of thiol groups with Ellman's Reagent

After the reaction with cysteine, the modified cellulose nanofiber suspensions were purified by dialysis against DI water until no carbon was detectable by TOC analysis of the

solution outside the dialysis bag (molecular weight cut off (MWCO) = 10,000 Daltons). Ellman's Reagent [27], DTNB (5,5'-dithio-bis-[2-nitrobenzoic acid]) were used to determine the amount of thiol groups attached to cellulose nanofibers in the suspension. In this test, DTNB was used to react with thiols to cleave 2-nitro-5-thiobenzoate (NTB^-), which could ionize to the yellow color NTB^{2-} di-anion in aqueous solution at pH = 8.0. Thiol groups were assayed by using the molar adsorption coefficient of NTB^- (14,150 L $mol^{-1}cm^{-1}$ at 412 nm) [28].

DTNB (50 mg) was dissolved in the phosphate buffer (10 ml, pH = 8.0). A cysteine-modified cellulose suspension (3 mL, 0.1 wt% cellulose) was mixed with the phosphate buffer (2.0 mL) and diluted with DI water (5.0 ml). The DTNB/buffer solution (0.02 mL) was then mixed with the modified cellulose/buffer suspension (3.0 mL) in a 1 cm cuvette and the absorbance at 412 nm was measured after 5 min of mixing. A sample of TEMPO oxidized cellulose (0.1 wt% in DI water) was used as the control sample for the same experiment. A series of L-cysteine solutions with concentrations 0.1 mol/L, 0.05 mol/L, 0.01 mol/L, 0.005 mol/L and 0.0001 mol/L in phosphate buffer with Ellman's reagent were used to create a calibration curve. The following equation 2.1 was used to calculate the concentration of thiol groups in the suspension.

$$C_0 = \frac{A}{\varepsilon \cdot b} D \qquad 2.1$$

where C_0 is the original –SH concentration; A is the absorbance at 412 nm; b is the path length of the spectrophotometric cuvette in centimeters (b = 1cm); ε is the extinction coefficient (14150 L $mol^{-1}cm^{-1}$) [29], which is a measure of the amount of light absorbed per unit concentration, based on the phosphate buffer at pH = 8.0; D is the dilution factor (1.007), which is the total volume of the cellulose suspension with DTNB/buffer solution (3.02 ml) divided by the volume of cellulose suspension (3.0 ml). In addition, the functional groups after cellulose modification

were characterized by using Fourier transform infrared spectroscopy (FT-IR) with an attenuated total reflectance (ATR) accessory (Nicolet iS10 spectrophotometer, Thermo Scientific, Inc). Each sample was freeze-dried and tested in the wave number range from 4000 cm^{-1} to 650 cm^{-1}.

2.2.4 Preparation of CNF nanofibrous composite membrane

2.2.4.1 Preparation of electrospun PAN scaffold

3.5 g PAN was stirred in 46.5 g DMF at 60 °C for 2 days in a capped glass container to afford a homogeneous solution with a PAN concentration of 7 wt%. The PAN solution was electrospun onto an aluminum foil or nonwoven PET support at 15 kV by using a laboratory built electrospinning instrument [30]. The chosen flow rate was 20 µl/min and the spinneret diameter was 0.7 mm. The working distance between the collector and the spinneret was 10 cm. In the electrospinning setup, a rotating metal drum (diameter: 9 cm, rotating speed: 300 rpm), covered with aluminum foil or nonwoven PET support was used to collect the deposited nanofibers. A stepping motor was used to control the oscillatory translational motion perpendicular to the drum rotation direction (the oscillation distance was about 12 cm) to ensure the production of more uniform electrospun scaffolds with a sufficiently large membrane size.

2.2.4.2 Preparation of cellulose nanofibrous composite membrane

In order to make a cellulose nanofibrous composite membrane, a cellulose nanofiber suspension (2 mL, 0.03 wt% CNF) was infused at a constant flow rate of 2 ml/min into a 2 inch diameter electrospun PAN scaffold supported by the PET non-woven substrate. The membrane was then dried at 75 °C for 2 min to induce thermal cross-linking of tmCNFs to the electrospun PAN scaffold. The nanofibrous composite membrane was subsequently washed with about 15 ml

DI water until TOC analysis showed no organic content.

2.2.5 Analysis of membrane geometry and porosity

The electrospun PAN scaffold was analyzed by using a scanning electron microscope (SEM, SFEG-SEM LEO1550) with Robinson backscattered electron detector and 10 eV Schottky field emission gun. The instrument was also equipped with an energy-dispersive spectroscopy (EDS) spectrometer (detector from EDAX Inc, NJ USA and software/electronics from automated X-Ray Fluorescence (iXRF), TX, USA) to characterize chemical composition of membrane surfaces. Samples were first cut into 4 mm × 8 mm pieces, peeled off from the PET support, and coated with platinum for 15 s to enhance the surface conductivity. Cross-sectioned specimens were cut from the membranes in 5 mm × 15 mm pieces, treated with liquid nitrogen and cracked before platinum coating. In each SEM image, 40-50 e-spun PAN fibers were randomly selected for the analysis, where the Leica Microscopy Imaging software (Algorithm written by Dr. Dufei Fang from Prof. Chu and Hsiao Lab at Stony Brook University) was used to estimate the average fiber diameter. The electrospun PAN membrane thickness was determined by using a micrometer [31] (Chicago Brand-50073). The porosity of the membrane was calculated using the following equation 2.2, in which ρ_0 was the density of PAN (1.184 g/mL at 25 °C), ρ was the average density of the membrane calculated on the basis of 10 samples of mass over volume.

$$\text{Porosity} = (1-\rho/\rho_0) \times 100\% \qquad 2.2$$

2.2.6 Membrane porometry and pure water flux test

The mean flow pore size and the maximum pore size were determined by using a

Capillary Flow Porometer (Porous Materials Inc (PMI), CFP-1500A, USA). Before the test, a wetting reagent (surface tension 15.9 dynes/cm Galwich, PMI) was used to spontaneously fill the pores of the membrane. During the test, the wetting reagent was gradually removed until the pores became open at differential applied pressures. Flow rates of dry and wet membranes were automatically compared and calculated at different pressures by using the software Capwin (version 6.71.51, PMI), based on the Young-Laplace equation 2.3 [31]:

$$D = \frac{4\gamma}{\Delta p} cos\theta \qquad 2.3$$

The symbol, D, is the maximum diameter of the pore, γ is the surface tension of the wetting reagent, Δp is the differential pressure and θ is the wetting angle. The mean flow pore size was calculated at 50% flow passing through the membrane pores.

The pure water flux was measured by a dead-end filtration cell (Microsyringe Filter Holder-3002500, Millipore) as a function of time and pressure. A one-inch diameter round membrane was cut to fit the membrane holder. Permeability tests were conducted at 2 psi and room temperature by determining the volume of DI water passing through the membrane per unit area, time and pressure. Comparison tests were carried out using both PAN/PET and tm-CNF PAN/PET composite membranes.

2.2.7 Mechanical properties

Samples (30 mm × 50 mm) of the electrospun PAN scaffold layer, with and without the infused tm-CNFs, were pre-cut into a dumbbell-like shape (the cutter was 50 mm × 4 mm) and clamped onto a modified Instron 4410 tensile stretching device to determine the tensile strength. Uniaxial stretching was carried out at room temperature, where the chosen deformation rate was 10 mm/min. The stress was defined as the load divided by the original cross section area; the

strain was defined as the difference of the deformed length and the original length divided by the original length ($(l-l_0)/ l_0$).

2.2.8 Evaluation of heavy metal ion removal

Both static and dynamic adsorption experiments were carried out to evaluate the metal adsorption efficiency of the nanofibrous composite membranes. Stock solutions of potassium chromate (100 ppm K_2CrO_4 in water) and lead nitrate (100 ppm $Pb(NO_3)_2$ in water) were used for this purpose.

For static adsorption experiments, metal ion solutions with concentrations ranging from 10-100 ppm were prepared by diluting the stock solution. Thiol-modified composite membranes (diameter = 2 inches, thickness = 200 μm) adsorbent samples were added to a 50-ml centrifuge tube containing 10 ml of metal ion solution and stirred at room temperature overnight. A series of adsorbents was tested, including tm-CNF nanofibrous composite membrane, CNF nanofibrous composite membrane, pure electrospun PAN membrane, and 450 nm Millipore (SLFH 025NS) commercial microfiltration membrane. The membrane adsorption performance was measured at different initial metal ion concentrations and at solution pH values from 2.0 to 12.0 for Cr (VI) and 2.0 to 6.0 for Pb (II), adjusted by adding solutions of NaOH or HCl.

For dynamic adsorption studies, each adsorbent membrane was placed into a 2-inch diameter cell. Metal ion solutions (50 ppm in water) at the optimum pH determined in the static adsorption studies (pH 4.0 for Cr(VI) and pH 5.0 for Pb(II) were injected through the membrane at the rate of 2.0 ml/min. The adsorption for both static and dynamic measurements was calculated according to the following equation 2.4:

$$Q = \frac{(C_i - C_f)V}{M} \qquad 2.4$$

where Q is the amount of metal adsorbed (mg/g), C_i is the initial metal ion concentration while C_f *is* the final metal ion concentration (mg/L), V is the volume of solution (Liter) and M is the weight of adsorbent.

Membranes were removed from the solution and the residual metal ion concentration was determined by ultraviolet-visible (UV) spectrophotometry after treatment with chromogenic reagents (1,5-diphenylcarbazide and 4-(2-pyridylazo)resorcinol). The calibration curve of Cr(VI) was made by the UV adsorption of 0.5 ml Cr(VI) stock solution at 20 ppm, 40 ppm, 60 ppm, 80 ppm and 100 ppm, separately mixed with 0.5 ml 0.25 wt% 1,5-diphenylcarbazide (DPC) and made up to a total volume of 10 ml with 0.5 N H_2SO_4 in a volumetric flask, The absorption of the Cr-DPC complex was measured at 541 nm [32, 33]. The adsorption peak intensities are proportional to the concentration of the solution. The linear calibration curve of Pb(II) was made by the UV adsorption of 0.5 ml Pb(II) stock solution at 20 ppm, 40 ppm, 60 ppm, 80 ppm and 100 ppm, separately mixed with 0.5 ml 0.024 wt% 4-(2-pyridylazo)resorcinol (PAR) and made up to a total volume of 10 ml with borax buffer (pH = 9.0). The adsorption of the Pb-PAR complex was measured at 523 nm [34]. To measure the residual metal ion concentration, measured 0.5 ml of the solution remaining after membrane exposure was mixed with 0.5 mL of the appropriate chromogenic reagent solution (DPC for Cr(VI) or PAR for Pb(II)) and the total solution volume was made up to 10 mL with the appropriate solution (0.5 N H_2SO_4 for Cr(VI), borax buffer for Pb(II)) before measuring absorption at 541 nm (for Cr(VI)) or 523 nm (for Pb(II)).

2.2.9 Desorption and membrane regeneration experiment

Membrane regeneration studies were carried out after static and dynamic adsorption tests,

by firstly washing the adsorbent membrane with DI water (10 ml). The Cr (VI) adsorbent membrane was subsequently stirred in 50 ml 1 M HCl solution for 1 hour, whereas the Pb (II) adsorbent membrane was treated with 50 ml 0.1M ethylenediaminetetraacetic acid (EDTA) solution for 1 hour [35]. These membranes were then washed by injecting 10 ml water through the membrane body. After this desorption treatment, the membrane was then used for the next cycle of adsorption tests. Desorption and adsorption processes were repeated for three cycles under the same static adsorption test condition at optimum pH to yield the membrane regeneration efficiency using the following equation 2.5:

$$\text{Membrane Regeneration Efficiency} = C_2/C_1 \times 100\% \qquad 2.5$$

where C_1 refers to fresh membrane adsorption capacity, C_2 refers to reused membrane adsorption capacity.

2.3 Results and Discussion

2.3.1 Characterization of thiol-modified cellulose nanofibers

Figure 2.2 shows typical TEM images of TEMPO-oxidized cellulose nanofibers. A typical size of the nanofiber was 5 to 10 nanometers in diameter and a few hundreds nanometers in length. The oxidation reaction breaks up the cellulose wood pulp into smaller fibers and only the surface primary hydroxyl groups of the fiber are oxidized to aldehydes and carboxylates [25]. The negatively charged carboxylate groups interfere with the strong fiber-fiber hydrogen bonding and allow suspension of individual fibers in water.

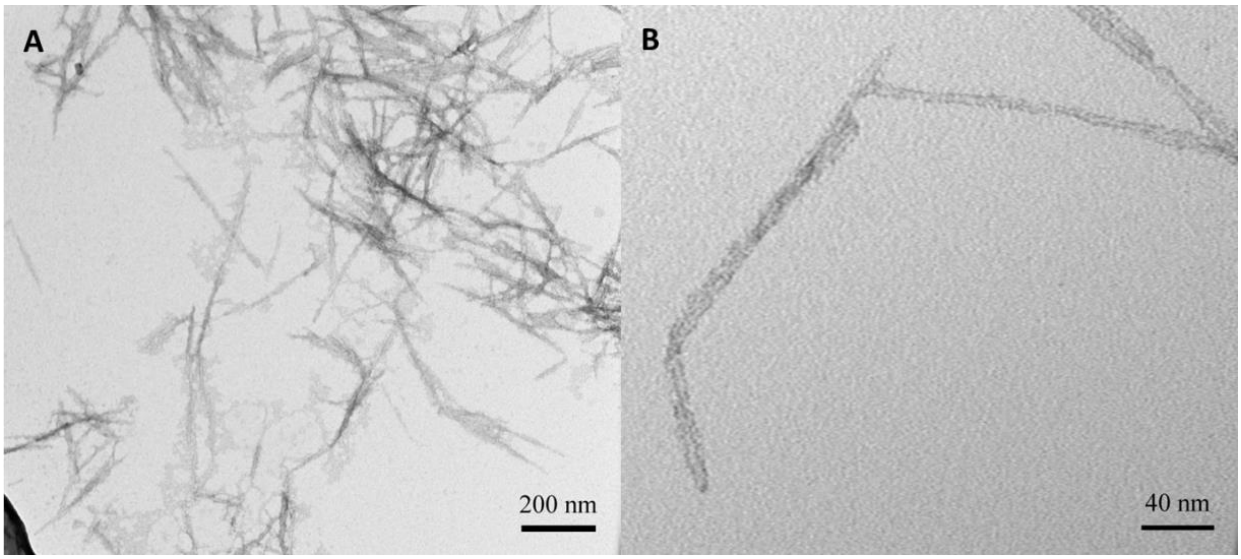

Figure 2.2 TEM images of A: TEMPO oxidized CNF; B: individual CNF. Samples were prepared by dropping a 0.01 wt% CNF suspension on carbon-coated copper grids. All TEM samples were stained with 2.0 wt% uranyl acetate.

The TEMPO oxidation method introduced carboxylate groups to the surface of cellulose nanofibers by converting C6 hydroxyl groups to aldehyde and carboxylate groups [36]. The amount of carboxylate groups could be controlled by changing the amount of NaClO used in the oxidation reaction [24]. The surface concentration of aldehyde could be varied from 0.05-0.2 mmol/g while the surface concentration of carboxylate could be varied from 0.6-1.8 mmol/, as determined by electrical conductivity titration [22], with NaClO concentrations from 0-10 mmol/g cellulose. Higher NaClO concentrations resulted in higher surface concentrations of carboxylate. According to previous studies on the cellulose TEMPO oxidation reaction [37], the chosen oxidation condition (10 mmol/g of added NaClO) could oxidize about one half of surface C6 hydroxyl groups of cellulose nanofibers to carboxylate groups. Aldehyde groups were produced as intermediates in the TEMPO oxidation process and could also result from base-

promoted cleavage of glycosidic bonds [26]. As aldehydes can be oxidized to carboxylate groups, the amount of aldehydes decreases at the highest NaClO concentration, because they are completely oxidized into carboxylates. The relationship of carboxylate generated on the cellulose nanofiber surface and NaClO added is shown in Figure 2.3.

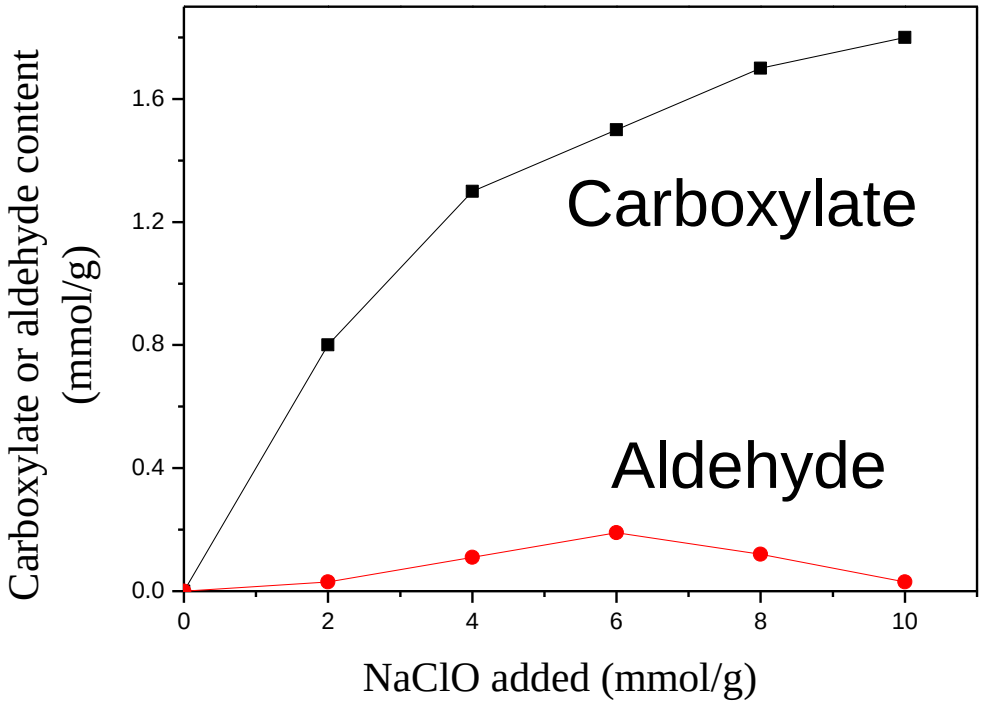

Figure 2.3 Amount of NaClO added in TEMPO oxidized CNF with corresponding amounts of functional groups produced

Thiol-functionalized cellulose nanofibers were created by grafting cysteine onto the surface of CNF through the formation of amide bonds between cysteine amine groups and cellulose carboxylate groups. The reaction was carried out in the presence of NHS and EDC to activate the carboxylate groups for spontaneous reaction with primary amines to form peptide bonds (Scheme 1). Due to the excess amount of cysteine in the reaction, grafted cysteine

oligomers could also result.

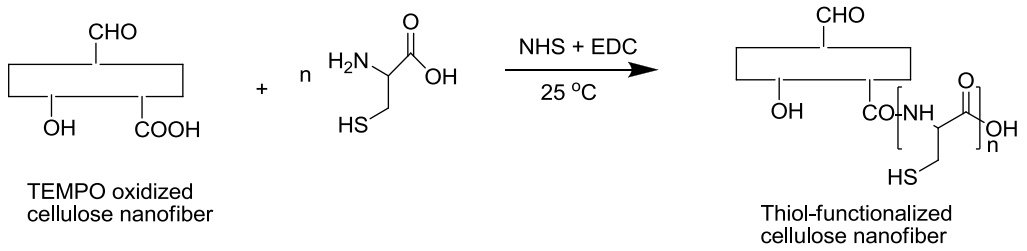

Scheme 2.1 Reaction of cysteine with TEMPO oxidized cellulose nanofiber

After purification by dialysis, both freeze-dried modifed/unmodified CNF were analyzed by FT-IR spectroscopy to show the presence of these functional groups, as shown in Figure 2.4. One carbonyl peak is at 1600 cm^{-1} in the TEMPO-oxidized cellulose. In the cysteine modifed cellulose, the peak around 1640 cm^{-1} is overlapping carbonyl absorptions from cellulose COOH and cysteine COOH. While the peak at 1560 cm^{-1} is the NH bend. In addition, the CONH carbonyl group is between the two peaks but not clearly resolvable. These findings suggest succesful grafting of cysteine onto the cellulose. One possibility for the IR absorbance around 1450 cm^{-1} is the thiazolidine ring from the formation of 2-alkylthiazolidine-4-carboxylic acid groups through reaction of aldehyde groups and cysteine [57].

EDS analysis of cysteine-modified CNF samples showed the presence of sulfur, further supporting the connection of cysteine to the nanofibers (Figure 2.5) when compared with unmodified cellulose nanofibers (Figure 2.5 above). Both Figures 2.4 and 2.5 could be regarded as evidence of the creation of thiol-modified cellulose.

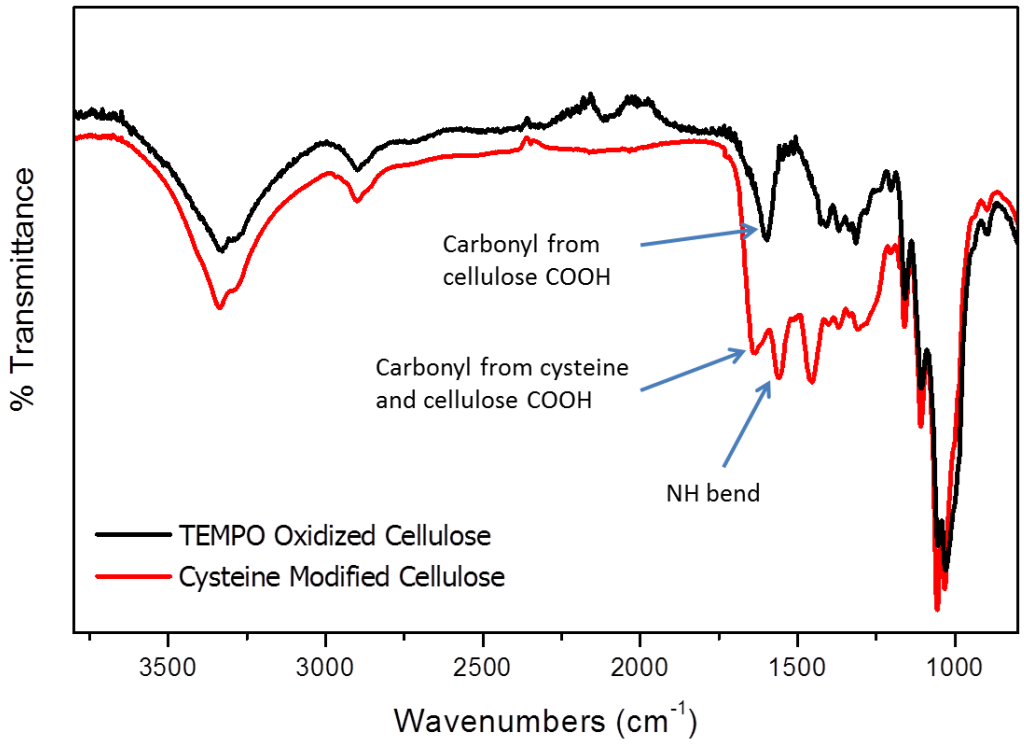

Figure 2.4 FI-IR of TEMPO oxidized cellulose nanofibers (1.6 mmol/g COOH) and thio-modified cellulose nanofibers (0.9 mmol/g -SH)

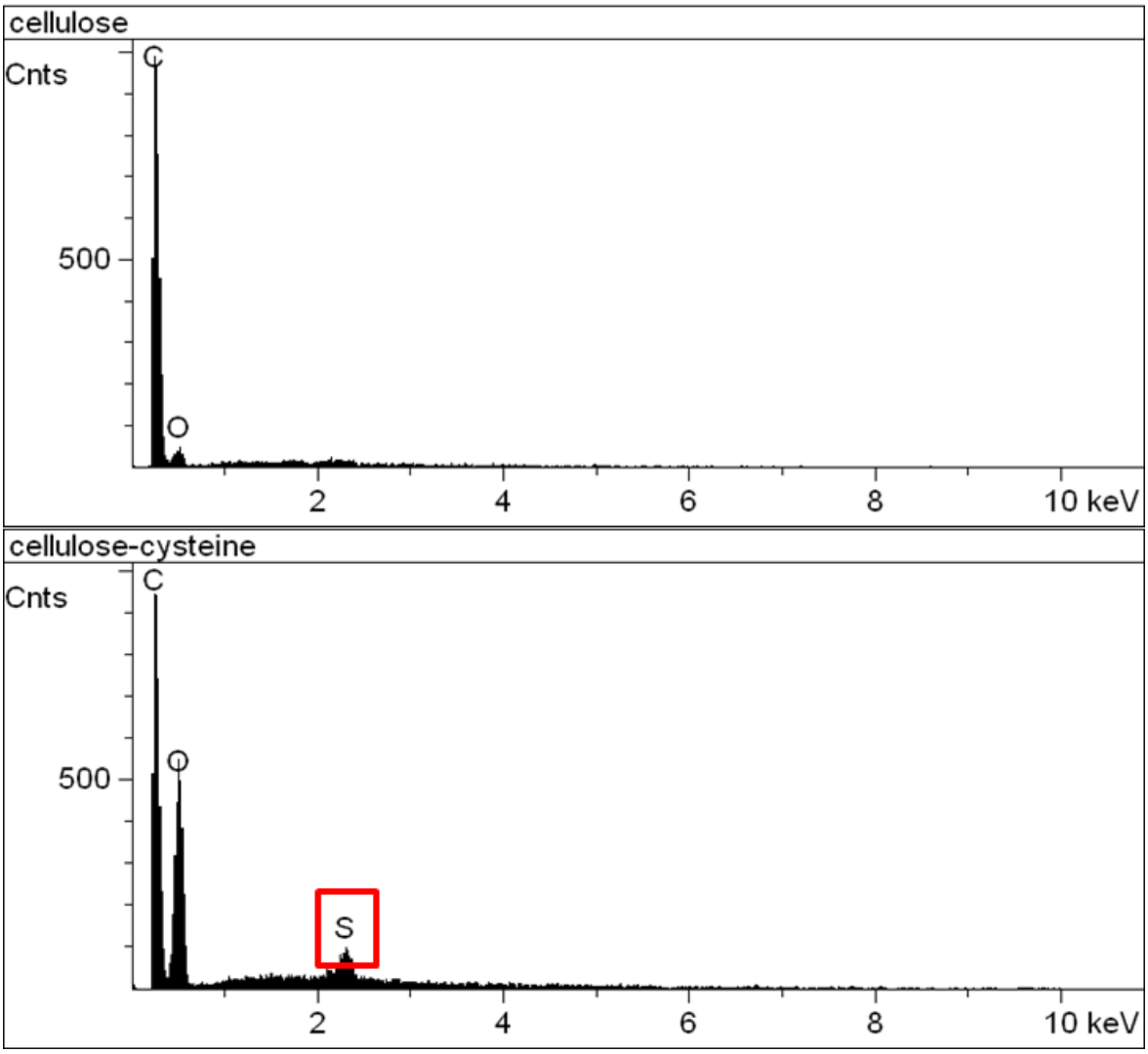

Figure 2.5 Energy Dispersive Spectrum of TEMPO oxidized cellulose nanofibers (1.6 mmol/g -COOH) and thio-modified cellulose nanofibers (0.9 mmol/g -SH)

Modification reactions carried out at different molar ratios of CNF –COOH ([COOH] = 1.6 mmol/g; [CHO] = 0.2 mmol/g) to cysteine, at 1:2, 1:4, 1:6 and 1:8, are listed in Table 2.1. After purification by dialysis, the concentration of thiol groups were determined by mixing the tm-CNF suspension with Ellman's reagent [27]. The concentration of the yellow-colored complex formed could be quantified by measuring absorption at 412 nm. Then, the amount of

thiol groups grafted onto the CNFs could be obtained in terms of the tm-CNF suspension concentration. The highest concentrations of thiol groups (0.9 mmol per gram CNF) were reached at a [cysteine]/[COOH] ratio of greater than 6.

Table 2.1 Molar carboxylate/cysteine reaction ratios and amount of thiol product

Molar Reaction Ratio (-COOH/cysteine)*	tm-CNF thiol concentration
1:2	0.4 ± 0.05 mmol/g
1:4	0.5 ± 0.07 mmol/g
1:6	0.9 ± 0.1 mmol/g
1:8	0.9 ± 0.1 mmol/g

* All cysteine reactions were using 1.6 mmol/g (-COOH) TEMPO oxidized cellulose.

2.3.2 Structural characterization of nanofibrous composite membranes

The electrospun PAN layers used to anchor modified cellulose nanofibers in membranes were characterized by SEM (Figure 4). PAN fibers electrospun from the 7 wt% PAN solution in DMF showed a diameter of 180 ± 20 nm (Figure 4A: top view, 4C: cross-section view). The pores of the electrospun film were interconnected with an average effective pore size of approximately 600 nm. This ratio of average pore size to mean fiber diameter corresponds well with the value of ~3 determined in our previous study [31]. Figure 4 (A top view, C cross-section view) shows SEM micrographs of 7 wt% electrospun PAN nanofibrous scaffold.

Composite membranes were prepared by infusing an aqueous suspension of tm-CNF (0.03 wt %, 5-10 nm diameter, a few hundred nanometers length) through a PAN nanofibrous scaffold. Figure 2.6 (B top view, D cross-section view) shows tm-CNF-coated PAN fibers after infusion at a rate of 2.0 ml/min and subsequent heating at 75 °C for 2 min. In Figures 2.6B and

2.6D, the modified cellulose nanofibers appear to surround the PAN scaffold with tmCFN being associated to the PAN. However, the thermal treatment at 75 °C was a critical step, which created certain association among thiol-CNFs and PAN fibers [38-42]. Since there was no organic carbon detectable by the TOC test in the filtrate after the membrane was subjected to water flow at 30 psi, the results suggested that the infused tm-CNFs were securely immobilized in the electrospun PAN scaffold. When comparing Figure 2.6C with Figure 2.6D, the increases in the apparent surface roughness after tm-CNF infusion clearly indicate association of tm-CNFs with the electrospun PAN nanofibers. It was found that the porosity of the membrane, which was 83% in the original PAN scaffold, was reduced to 78% in the tm-CNF infused PAN scaffold. After the attachment of m-CNF to the PAN nanofibrous scaffold, the pure water flux dropped from 3000 $L/m^2/h/psi$ to 1000 $L/m^2/h/psi$ and the mean flow pore size dropped from 0.60 μm to 0.43 μm, as listed in Table 2.2.

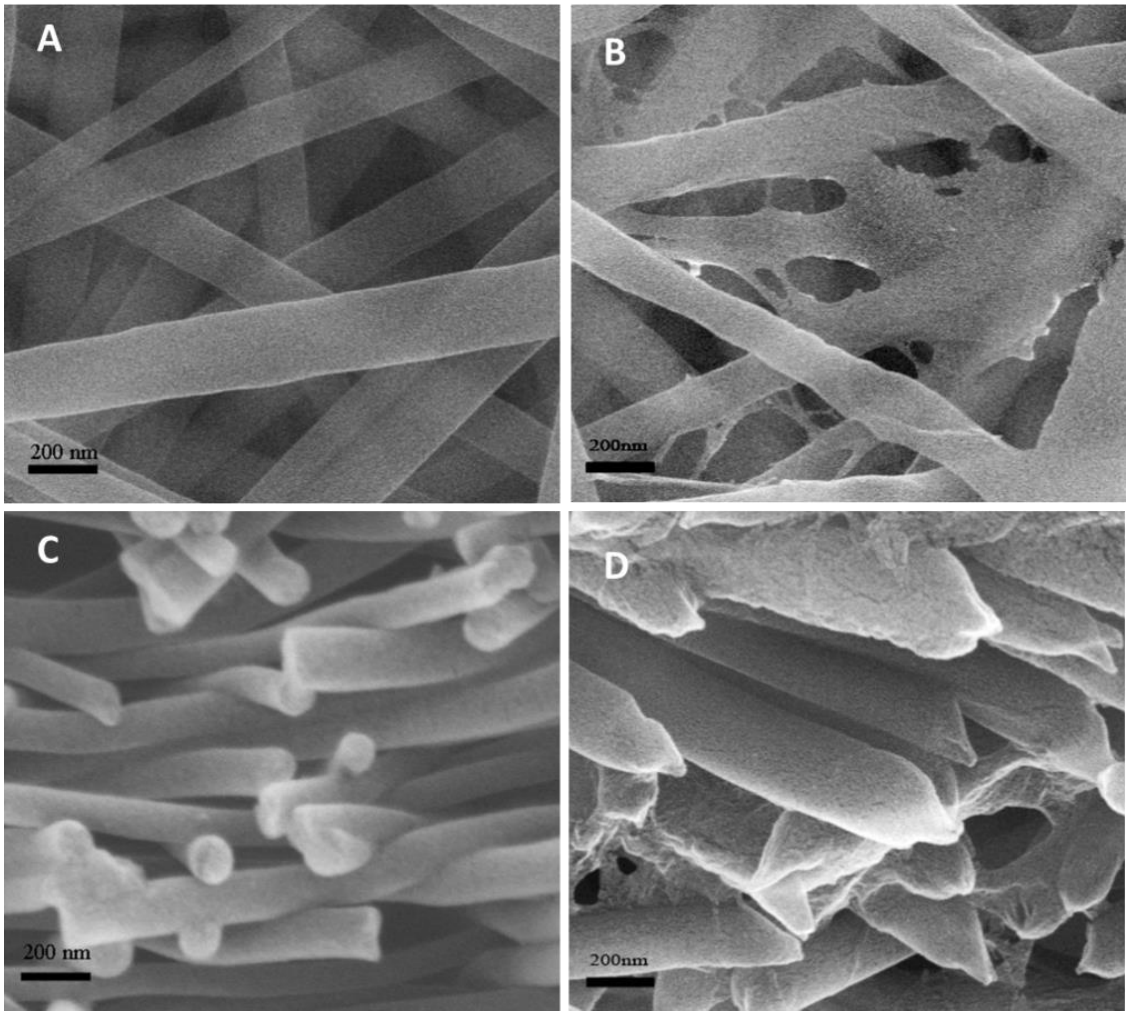

Figure 2.6 SEM images of an electrospun PAN nanofiber scaffold (from 7 wt% PAN solution) with scale bars of 200 nm: (A) top view, (C) cross-sectional view; and an electrospun PAN nanofiber scaffold (with 7 wt% PAN solution) infused with tm-CNF solution (0.03 wt%): (B) top view, (D) cross-sectional view.

Table 2.2 Physical properties of electrospun PAN nanofibrous scaffold (A) and tm-CNF infused PAN nanofibrous scaffold (B)

Membrane	**PAN (A)**	**tm-CNF-PAN (B)**

Fiber Diameter (nm) [a]	180 ± 20	195 ± 30
Porosity [b]	83 ± 1%	78 ± 2%
Maximum Pore Size (μm) [c]	0.91 ± 0.05	0.81 ± 0.05
Mean Flow Pore size(μm) [c]	0.60 ± 0.02	0.43 ± 0.03
Pure Water Flux ($L/m^2/h/psi$) [d]	~3000	~1000

All properties of measurements/calculations have been mentioned in the experimental section.

a. In each SEM image 40-50 fibers were selected for the analysis, where the Leica Microscopy Imaging software was used to estimate the average fiber diameter.

b. Porosity = $(1- \rho/\rho_0) \times 100\%$.

c. Mean flow pore size and maximum pore size were determined by using a capillary flow porometer (PMI, CFP-1500A, USA).

d. Pure water flux was measured by a dead-end filtration cell (Microsyringe Filter Holder-3002500, Millipore) as a function of time and pressure at room temperature.

2.3.3 Mechanical properties of tm-CNF nanofibrous composite membranes

Another way to characterize the stability of the tm-CNF infused PAN scaffold is to test the mechanical property of the nanofibrous composite membranes. The results of tensile strength testing of PAN and tm-CNF infused PAN composite membranes (including the non-woven PET support) are shown in Figure 2.7. It was found that the tm-CNF nanofibrous composite membrane demonstrated an almost doubling of Young's modulus when compared with that of the nanofibrous composite membrane without tm-CNFs. However, the elongation-to-break ratio of

strain was reduced by 20% when compared with that of the unmodified one. Therefore, it is clear that the inclusion of m-CNF fibers in the PAN scaffold led to a stiffening of the membrane. This could also be regarded as evidence that the strong linkage of tm-CNFs with the e-spun matrix.

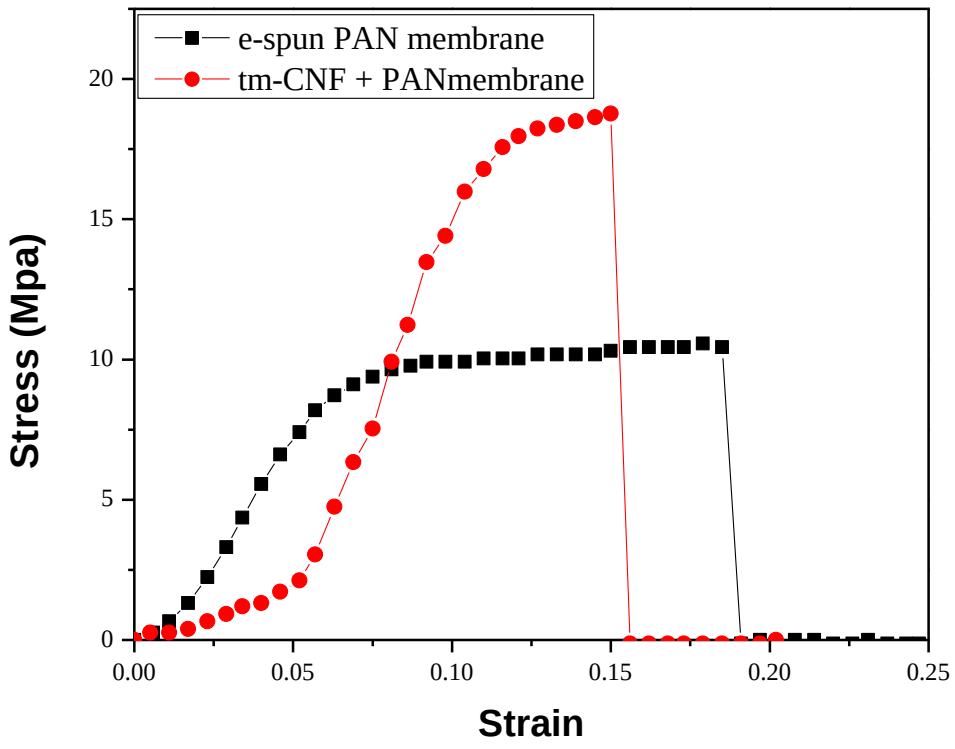

Figure 2.7 Mechanical properties of PAN and tm-CNFs infused PAN nanofibrous composite membranes (including the non-woven PET support).

2.3.4 Effect of pH on static adsorption

The pH level of the solution has a profound impact on metal ion adsorption efficiency because it changes both the form of functional groups on the modified cellulose and also the form of metal ions. For example, chromate ions are in different forms at different pH conditions. Below 100 ppm of chromium ions in aqueous solution, when the pH value increases from1 to 4,

the major species changes from H_2CrO_4 to $HCrO_4^-$. With the pH value increasing from 4 to 14, the major species changes from $HCrO_4^-$ to CrO_4^{2-} [43]. In this study, the initial H_2CrO_4 solution had a pH value of 4, indicating the pH value of a typical chromate contaminated solution. We also studied adsorption of lead under acidic conditions, which reached the optimum adsorption at pH = 5.0.

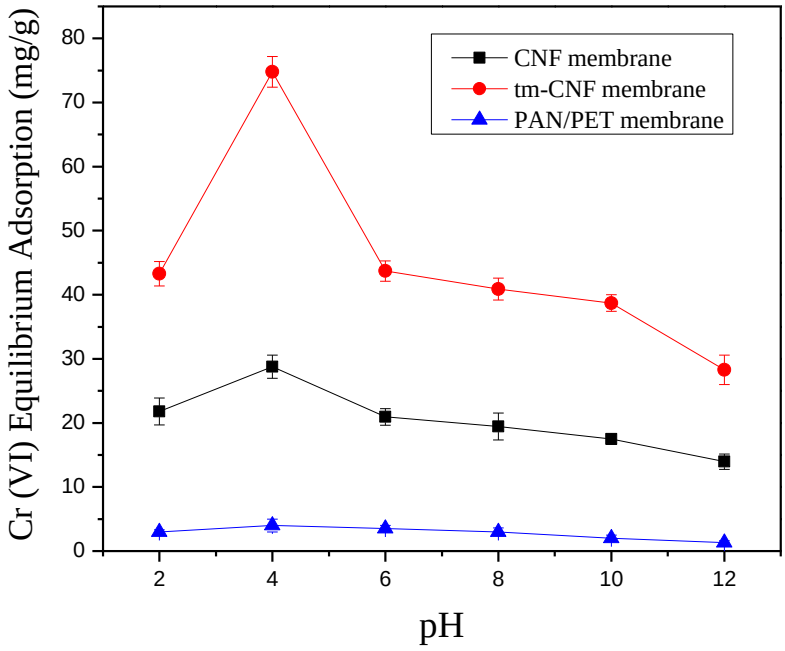

Figure 2.8 Effect of pH on static adsorption of Cr (VI)

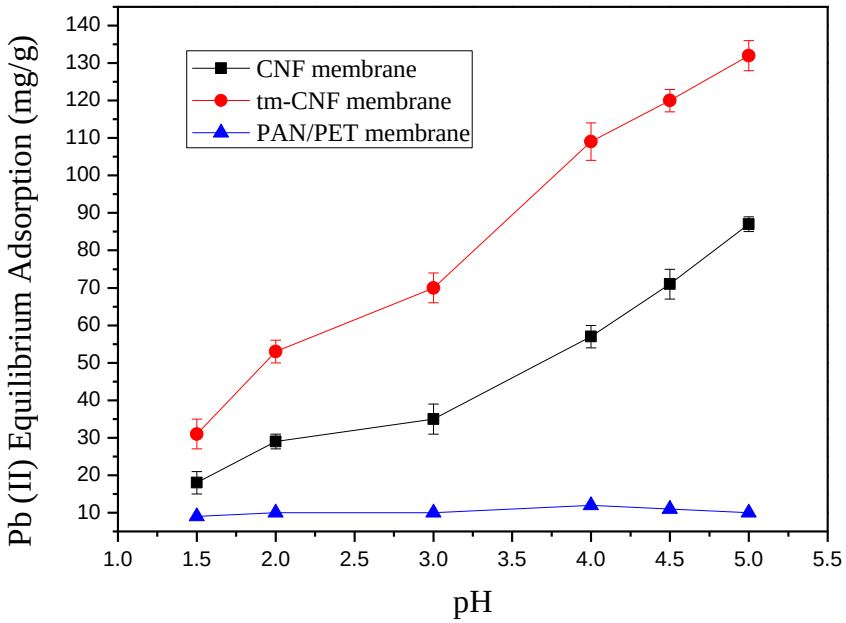

Figure 2.9 Effect of pH on static adsorption of Pb (II)

Adsorption of chromate ($Cr_2O_7^{2-}$) was investigated at pH values ranging from 2.0 to 12.0, and the results are shown in Figure 2.8. Measurements on the amount of adsorption were based on equation (2.4), using the chromate concentration differences before and after adsorption, multiplying by the volume of the solution and divided by the mass of adsorbent. The concentrations are proportional to the intensity of the peak measured by UV at 541 nm. It was found that the highest adsorption amount was 76.5 ± 2.0 mg $Cr_2O_7^{2-}$ metal ions per gram of cellulose nanofiber at pH = 4.0. We also compared the adsorption capacity of the tm-CNF nanofibrous composite membrane with the CNF membrane without the thiol modification. The results show that the tm-CNF membrane exhibited 2 to 3 times higher chromate adsorption capacity than the unmodified CNF membrane. This observation can be explained by the higher concentration of thiol groups in the tm-CNF membrane. The higher adsorption of Cr (VI) in the

tm-CNF membrane can be attributed to the formation of Cr(VI)-thiolate complexion on the surface of tm-CNF. According to a previous study on pH dependence of chromium(VI) thio ester formation [44], there could be several possible formations of $[CrO_3(SR)]^-$. These formations include the coordination of Cr(VI) with the thiolato or amido donors from the cysteine-functionalized cellulose. However, with the increase in pH value, the Cr(VI)-thiolate complex formation is inhibited [44], leading to a lower amount of adsorption.

The Pb (II) adsorption studies were carried out using tm-CNF nanofibrous composite membrane, CNF nanofibrous composite membrane, and an unmodified PAN membrane (Figure 2.9). Only the pH range from 1.5 to 5.5 was examined because lead hydroxides precipitate above pH = 6. Measurements on the amount of Pb (II) adsorption were performed by following the same method as Cr(VI) adsorption, while the concentration was determined by UV optical adsorption at 523 nm. The tm-CNF membrane showed the best adsorption efficiency (133 ± 2.5 mg/g) among the three. The formation of Pb(II) thiolate occured between –SH and Pb (II) [46-49]. This adsorption capacity increased with increasing pH values between 1.0 and 5.5, according to the preference of metal complex formation. As for the CNF membrane without the thiol modification, the system still showed decent adsorption efficiency, likely due to the charge attraction between negatively charged carboxylate groups on the cellulose surface and positively charged Pb (II) ions. At higher pH values, more –COOH groups could be dissociated into COO^- groups, indicating higher adsorption capacity of Pb (II) ions due to charge interactions. In contrast to the above two systems, the control membrane (electrospun PAN scaffold on the PET nonwoven support) exhibited very small adsorption capability (< 8 mg Pb^{2+}/g membrane).

2.3.5 Effect of contact time on adsorption

In typical metal removal practices, the adsorption contact time is an important factor as it directly affects the membrane lifetime and the adsorption time efficiency. Figure 2.10 illustrates the results from experiments carried out under the same conditions as static adsorption at pH = 4.0. A commercial MF membrane (Millipore-SLFH 025NS with 450 nm pore size, which is a hydrophobic fluoropore polytetrafluoroethylene (PTFE) membrane) was also used for comparison. It was found that the tm-CNF nanofibrous composite membrane reached the maximum adsorption of 80 mg/g for Cr (VI) within 15 minutes, due to the fast formation of Cr-thiolate complex [44], whereas the CNF nanofibrous composite showed a moderate Cr(VI) adsorption capacity of about 30 mg/g that could be attributed to some affinity interactions between CNF and metal ions. A residence time of about 30 minutes was required to reach the equilibrium. In contrast, the PAN/PET composite membrane and the chosen Millipore membrane showed very little adsorption (< 3 mg Cr(VI)/g membrane) because of lack of interactions between the membrane and metal ions.

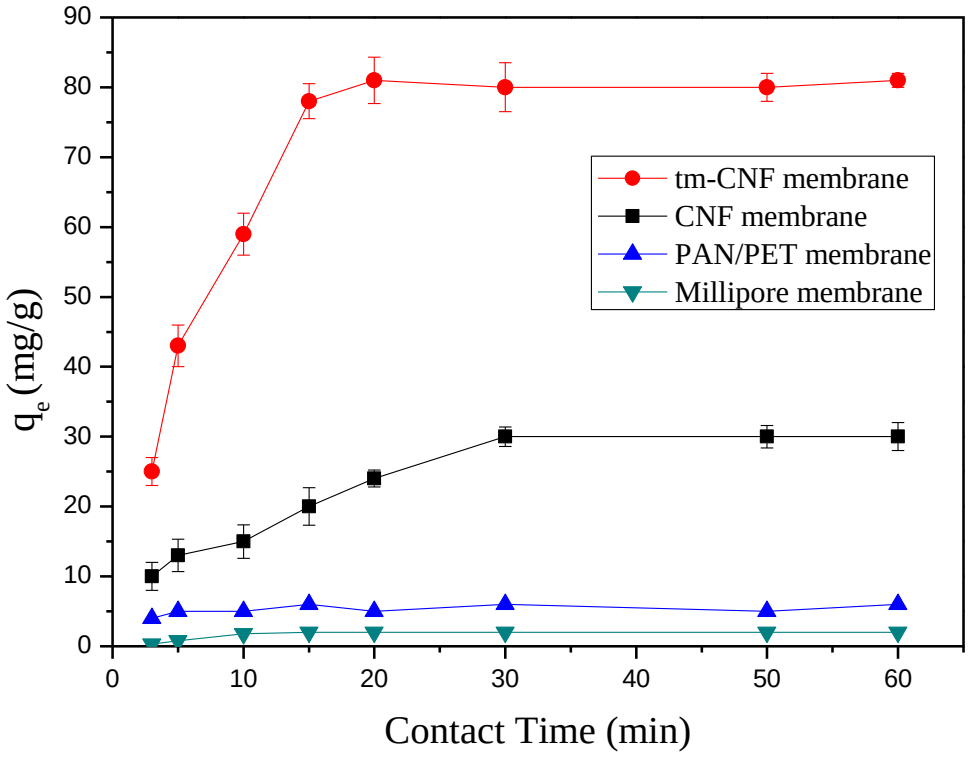

Figure 2.10 Chromium adsorption affected by contact time

Static Pb (II) adsorption measurements as a function of time for tm-CNF and CNF nanofibrous composite membranes were also carried out at pH = 4.0 (Figure 2.11). Two interesting observations were made from this study, i.e., the tm-CNF membrane exhibited a faster adsorption process and higher adsorption capacity over those of the CNF membrane. To be specific, the tm-CNF membrane could adsorb 125 mg/g of Pb (II) within 20 minutes, while it took the unmodified CNF membrane 40 minutes to reach an equilibrium adsorption of 75 mg/g . One possible explanation is that the formation of Pb-thiolate complex through the chelating reaction of –SH and Pb(II) is very fast and strong [50]. In contrast, the charge interactions between the negatively charged $–COO^-$ on CNF and the positively-charged lead ions are

considerably weaker. Neither PAN/PET membranes (without tm-CFN or CFN) nor Millipore microfiltration membranes showed any lead ion adsorption capacity.

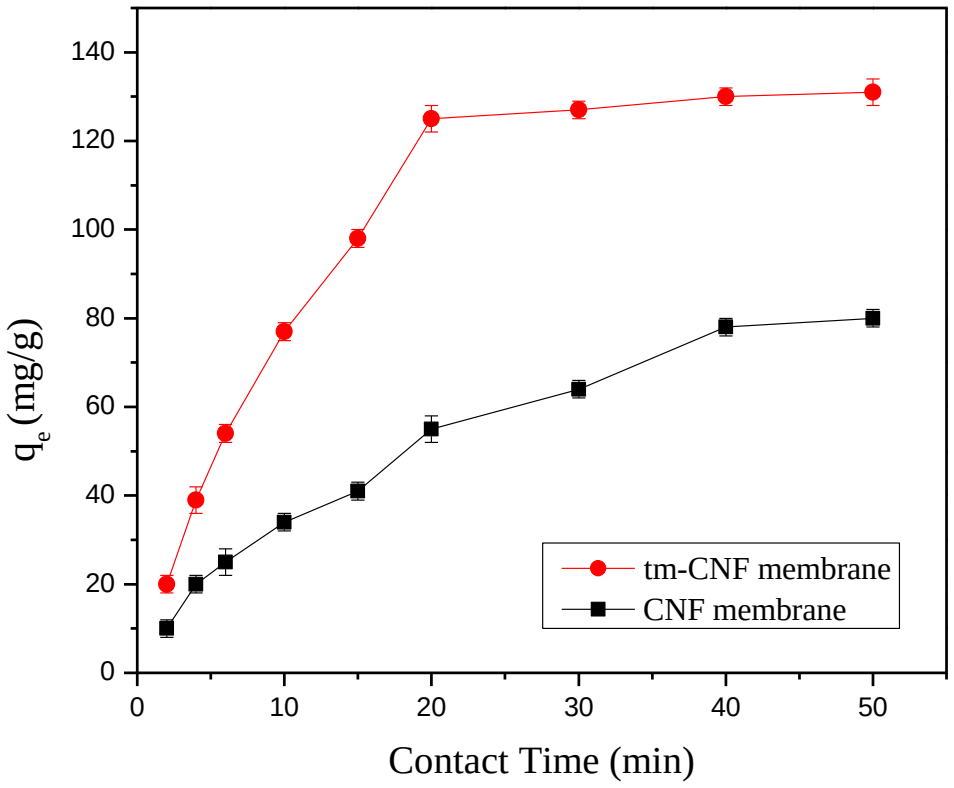

Figure 2.11 Pb(II) adsorption by contact time

2.3.6 Evaluation of dynamic adsorption

Dynamic adsorption experiments involve the quantitative analysis of metal ions adsorbed on the membrane under a constant flow condition at an optimum pH value. In these studies, solutions with 50 ppm of chromate or lead ions were injected through a membrane disc (2-inch diameter) at 2 mL/min. It was found that at pH = 4.0, the most efficient adsorption of Cr(VI) occurred over the first 15 ml for tm-CNF membrane, where 60 mg Cr(VI)/g of membrane was

adsorbed (Figure 2.12). For Pb(II) adsorption at pH = 5.0, the most efficient adsorption occurred over the first 20 ml for tm-CNF membranes, where 115 mg Pb(II)/g membrane was adsorbed, i.e., about 83% of the Pb(II) adsorption capacity in static adsorption was reached. Very low dynamic adsorption values were observed for the PAN/PET composite membrane and the Millipore filter.

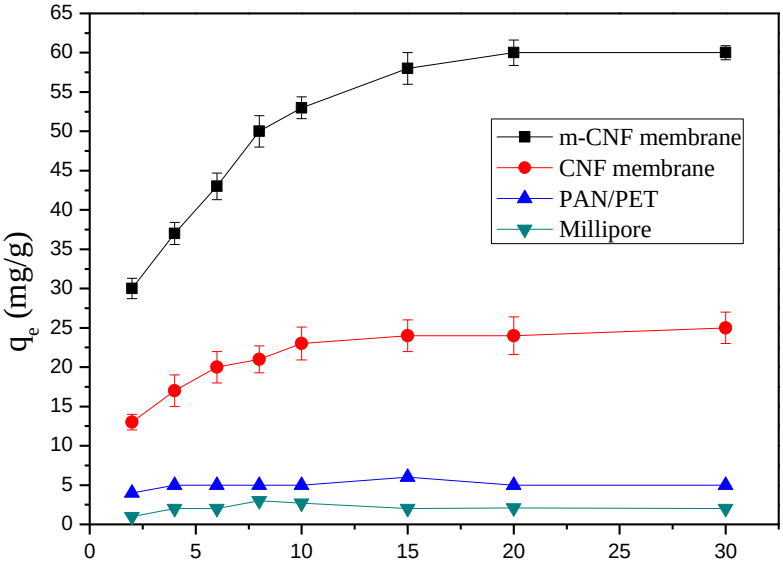

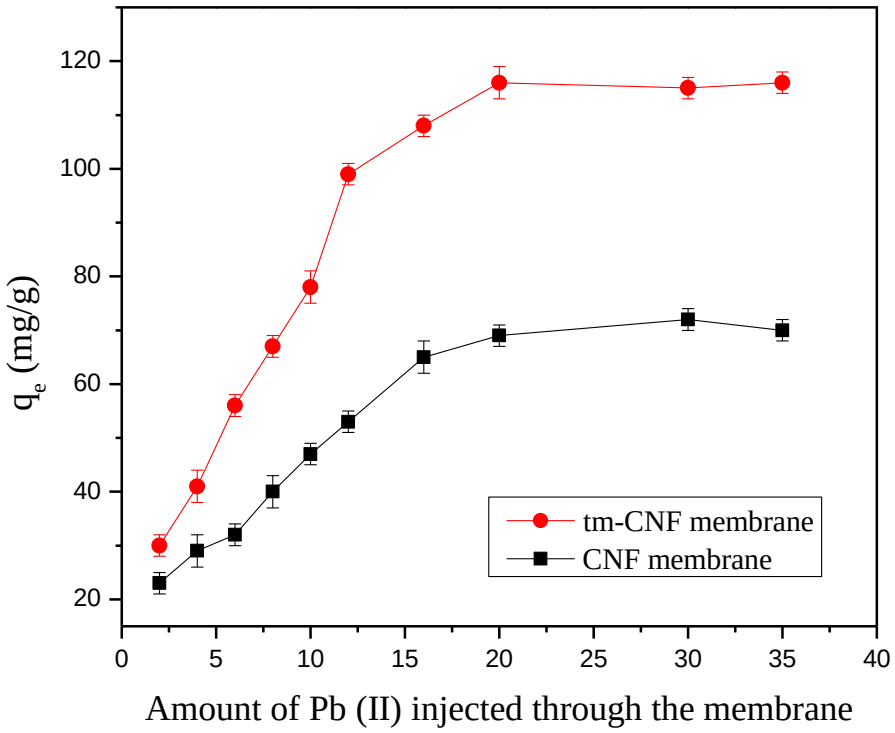

Figure 2.12 Dynamic adsorption of Cr (VI) and Pb (II)

2.3.7 Langmuir adsorption isotherms

Adsorption isotherms can be used to illustrate the interactions between adsorbents and adsorbates, as well as the adsorption capacity of adsorbents. To evaluate the adsorption isotherms for the tm-CNF membrane, we used the Langmuir adsorption model to calculate the adsorption capacity [51]. The adsorption isotherms for both Cr(VI) and Pb(II) ions were evaluated using the following equation:

$$\frac{C_e}{q_e} = \frac{C_e}{q_m} + \frac{1}{bq_m} \qquad 2.6$$

where q_e is the amount of metal ions adsorbed on the membrane at equilibrium (mg/g), C_e is the equilibrium metal ion concentration in solution (mg/L), q_m is the maximum adsorption of the

metal ions (mg/g), and b is the Langmuir constant (L/mg). Based on Equation 2.6, the value of C_e/q_e was plotted against C_e for both Cr(VI) and Pb(II) adsorption isotherms, where the results are illustrated in Figure 2.13. It was seen that both plots exhibited a straight line with the slope representing $1/q_m$ and the intercept representing $1/(bq_m)$. The b value (Langmuir constant) also refers to the corresponding binding energy of adsorption [35], whereby a higher b value means more binding affinity between the adsorbent and the adsorbate. Table 2.3 illustrates the parameters (i.e., the maximum adsorption, Langmuir constant and correlation coefficient) extracted from the adsorption isotherms of Cr(VI) and Pb(II) ions for the tm-CNF membrane. Based on the results in Figure 2.13 and Table 2.3, both lead and chromium adsorption closely followed the Langmuir model with high correlation coefficient of 0.997 and 0.998, respectively and large adsorption capacity (87.5 mg/g for Cr (VI) and 137.7 mg/g for Pb (II) at their optimum adsorption pH values).

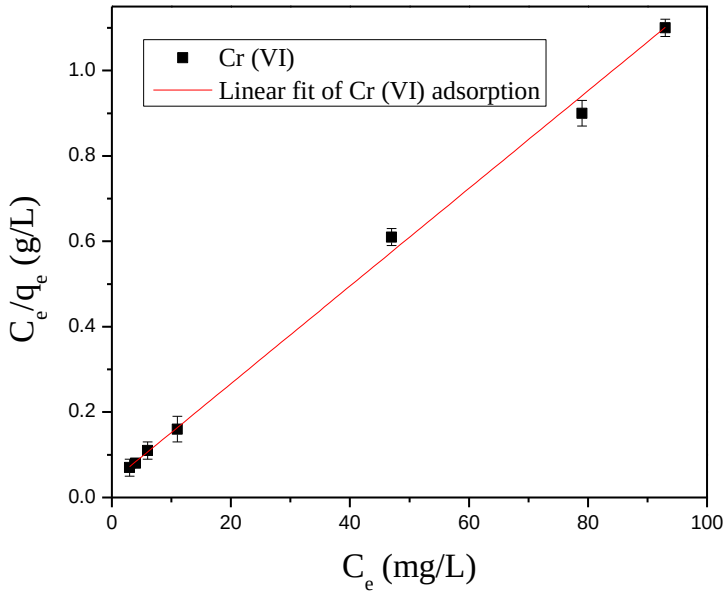

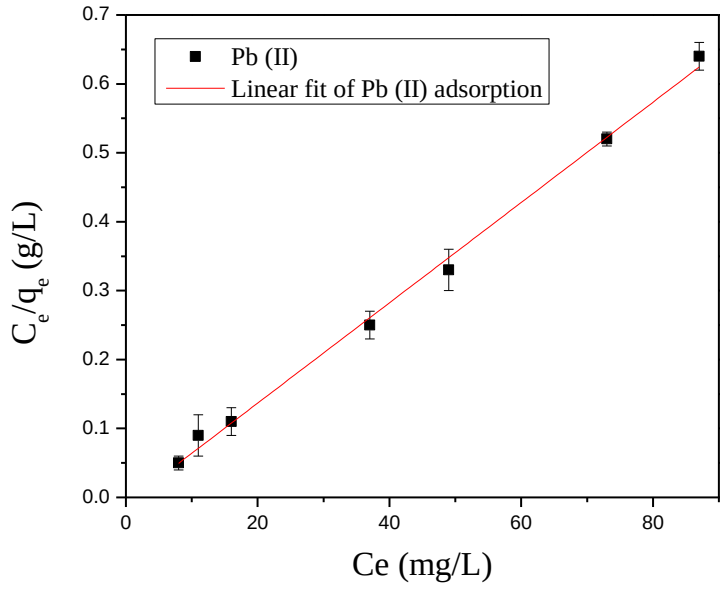

Figure 2.13 Adsorption isotherms of Cr(VI) and Pb(II) for the tm-CNF membrane

Table 2.3 Parameters extracted from adsorption isotherms of Cr(VI) and Pb(II) ions for the tm-CNF membrane

Target Metal	q_m (mg/g)	b (L/mg)	R^2
	Maximum adsorption	Langmuir constant	Correlation coefficient
Cr (VI)	87.5	0.308	0.997
Pb (II)	137.7	0.783	0.998

2.3.8 Comparisons with other adsorbents

The above adsorption results were compared with other modified cellulose-based adsorbents (Table 2.4). Under similar test conditions in terms of optimum pH, room temperature,

the tm-CNF membranes demonstrated higher adsorption capacity than the chosen adsorbents. It is interesting to note that the format of tm-CNF membranes is also designed to be a separation system. As most of the chosen adsorbents were designed to adsorb metal ions prior to filtration, they required an additional adsorbent filtration separation step for water purification.

Table 2.4 Comparisons of Cellulose based Adsorbents

Metal Ions	Adsorbents	Adsorption Capacity(mg/g)	Initial Metal Conc.(ppm)	Optimum pH	Temperature (°C)	Adsorption Model
Cr(VI)	tm-CNF Membrane	87.5	50	4.0	22 ± 2	Langmuir
	Cellulose Microsphere-based Adsorbent [52]	78	100	3.5	Room Temperature	Langmuir
	Sulfamate-Bacterial Cellulose [53]	22.73	100	2.3	20	Langmuir
Pb(II)	tm-CNF Membrane	131	50	5.0	22 ± 2	Langmuir
	Diethylenetriamine-bacterial Cellulose [54]	31.41	100	4.5	Room Temperature	Langmuir/ Freundlich
	Ethylenediamine Modified Cellulose [55]	50.0	200	6.0	Room Temperature	Langmuir/ Freundlich

2.3.9 Desorption and reuse

As high regeneration efficiency is an important parameter in membrane performance, the thiol modified CNF membrane was subjected to a desorption and reuse test. In this study, aqueous solutions of EDTA (0.05 M) were selected to remove lead ions from the used

membrane, as EDTA ligands have a very strong affinity binding with lead ions [56]. For Cr(VI) desorption, HCl (2 M) was applied to release the metal ions from the tm-CNF membrane surface. This is because at very low pH conditions, the membrane uptake of Cr(VI) ions is low. The results of this study is shown in Table 2.5, where the tm-CNF membrane could retain greater than 93% of their initial adsorption capacity after three use/regeneration cycles. In other words, even after being used and regenerated for 3 cycles, the tm-CNF membrane still possessed 93% of the original Cr(VI) adsorption capacity and 95% of the original Pb(II) adsorption capacity. It is important to note that as the fabrication cost for this membrane system is relatively low, the membrane may be treated as disposable under certain practical conditions when the regeneration cost is high or not accessible.

Table 2.5 Membrane regenerate efficiency

Recycled Times	Regenerate Efficiency	
	Cr(VI)	Pb(II)
1st	96 ± 3%	97 ± 1%
2nd	93 ± 2%	95 ± 3%
3rd	93 ± 3%	95 ± 2%

2.4 Conclusions

In conclusion, ultra-fine oxidized cellulose nanofibers (diameter about 5 nm) with substantial amounts of carboxylate groups (1.6 mmol/g) were prepared by using the TEMPO oxidation method. These oxidized cellulose nanofibers (CNF) were subsequently coupled with cysteine to afford thiol-functionalized fibers (surface thiol concentration ≈ 0.9 mmol/g). Due to

the small size of tm-CNF fibers, the resulting nanofibrous composite membrane structure could provide a very large surface-to-volume ratio with many active sites for heavy metal ion adsorption. We have successfully demonstrated a high flux microfiltration filter (1000 $L/m^2h/psi$), which could simultaneously achieve a high metal adsorption capacity (the Cr (VI) adsorption capacity is 87.5 mg/g and the Pb (II) adsorption capacity is 137.7 mg/g) after a relatively short adsorption time (15 to 20 min). Furthermore, the adsorption results could be described by the Langmuir model. In addition, the demonstrated tm-CNF membranes could be regenerated up to three times with high adsorption efficiency retention (> 93%), indicating that this membrane system may be a promising candidate for water purification applications involving the removal of heavy metal ions.

References

1. Weber, O., et al., *Risk perception of heavy metal soil contamination and attitudes toward decontamination strategies.* Risk Analysis, 2001. **21**(5): p. 967-977.
2. Jarup, L., *Hazards of heavy metal contamination.* British Medical Bulletin, 2003. **68**(1): p. 167-182.
3. Morello-Frosch, R.A., et al., *Air toxics and health risks in California: The public health implications of outdoor concentrations.* Risk Analysis, 2000. **20**(2): p. 273-291.
4. Peng, X.W., et al., *Highly Effective Adsorption of Heavy Metal Ions from Aqueous Solutions by Macroporous Xylan-Rich Hemicelluloses-Based Hydrogel.* Journal of Agricultural and Food Chemistry, 2012. **60**(15): p. 3909-3916.
5. Pang, Y., et al., *PEI-grafted magnetic porous powder for highly effective adsorption of heavy metal ions.* Desalination, 2011. **281**: p. 278-284.

6. Zhao, Y.L., et al., *Effective NH2-grafting on mesoporous SBA-15 surface for adsorption of heavy metal ions.* Materials Letters, 2011. **65**(6): p. 1045-1047.

7. Lagadic, I.L., M.K. Mitchell, and B.D. Payne, *Highly effective adsorption of heavy metal tons by a thiol-functionalized magnesium phyllosilicate clay.* Environmental Science & Technology, 2001. **35**(5): p. 984-990.

8. Salam, M.A., G. Al-Zhrani, and S.A. Kosa, *Simultaneous removal of copper(II), lead(II), zinc(II) and cadmium(II) from aqueous solutions by multi-walled carbon nanotubes.* Comptes Rendus Chimie, 2012. **15**(5): p. 398-408.

9. Thirumavalavan, M., et al., *Cellulose-Based Native and Surface Modified Fruit Peels for the Adsorption of Heavy Metal Ions from Aqueous Solution: Langmuir Adsorption Isotherms.* Journal of Chemical and Engineering Data, 2010. **55**(3): p. 1186-1192.

10. Zhou, Y.F. and R.J. Haynes, *A comparison of organic wastes as bioadsorbents of heavy metal cations in aqueous solution and their capacity for desorption and regeneration.* Environmental Earth Sciences, 2012. **66**(4): p. 1137-1148.

11. Reddad, Z., et al., *Adsorption of several metal ions onto a low-cost biosorbent: Kinetic and equilibrium studies.* Environmental Science & Technology, 2002. **36**(9): p. 2067-2073.

12. Kratochvil, D., P. Pimentel, and B. Volesky, *Removal of trivalent and hexavalent chromium by seaweed biosorbent.* Environmental Science & Technology, 1998. **32**(18): p. 2693-2698.

13. Yan, G.Y. and T. Viraraghavan, *Heavy-metal removal from aqueous solution by fungus Mucor rouxii.* Water Research, 2003. **37**(18): p. 4486-4496.

14. Religa, P., A. Kowalik, and P. Gierycz, *Effect of membrane properties on chromium(III)*

recirculation from concentrate salt mixture solution by nanofiltration. Desalination, 2011. **274**(1-3): p. 164-170.

15. Muthukrishnan, M. and B.K. Guha, *Effect of pH on rejection of hexavalent chromium by nanofiltration.* Desalination, 2008. **219**(1-3): p. 171-178.
16. Ahmed, M.T., et al., *Nanofiltration process applied to the tannery solutions.* Desalination, 2006. **200**(1-3): p. 419-420.
17. Taleb-Ahmed, M., et al., *The influence of physico-chemistry on the retention of chromium ions during nanofiltration.* Desalination, 2002. **145**(1-3): p. 103-108.
18. Hafiane, A., D. Lemordant, and M. Dhahbi, *Removal of hexavalent chromium by nanofiltration.* Desalination, 2000. **130**(3): p. 305-312.
19. Kim, S.K., C.G. Lee, and H.S. Yun, *Heavy metal adsorption characteristics of extracellular polysaccharide produced by Zoogloea ramigera grown on various carbon sources.* Journal of Microbiology and Biotechnology, 2003. **13**(5): p. 745-750.
20. Ishii, D., T. Saito, and A. Isogai, *Viscoelastic Evaluation of Average Length of Cellulose Nanofibers Prepared by TEMPO-Mediated Oxidation.* Biomacromolecules, 2011. **12**(3): p. 548-550.
21. Ruhaak, L.R., et al., *2-Picoline-borane: A non-toxic reducing agent for oligosaccharide labeling by reductive amination.* Proteomics, 2010. **10**(12): p. 2330-2336.
22. Araki, J., M. Wada, and S. Kuga, *Steric stabilization of a cellulose microcrystal suspension by poly(ethylene glycol) grafting.* Langmuir, 2001. **17**(1): p. 21-27.
23. Lemieux, G.A. and C.R. Bertozzi, *Chemoselective ligation reactions with proteins, oligosaccharides and cells.* Trends in Biotechnology, 1998. **16**(12): p. 506-513.
24. Wang, R., et al., *Nanofibrous Microfiltration Membranes Capable of Removing Bacteria,*

Viruses and Heavy Metal Ions. Journal of Membrane Science, 2013.

25. Saito, T., et al., *Cellulose nanofibers prepared by TEMPO-mediated oxidation of native cellulose.* Biomacromolecules, 2007. **8**(8): p. 2485-2491.
26. Saito, T. and A. Isogai, *TEMPO-mediated oxidation of native cellulose. The effect of oxidation conditions on chemical and crystal structures of the water-insoluble fractions.* Biomacromolecules, 2004. **5**(5): p. 1983-1989.
27. Ellman, G.L., *Tissue Sulfhydryl Groups.* Archives of Biochemistry and Biophysics, 1959. **82**(1): p. 70-77.
28. Riddles, P.W., R.L. Blakeley, and B. Zerner, *Ellman's reagent: 5, 5′-dithiobis (2-nitrobenzoic acid)—a reexamination.* Analytical biochemistry, 1979. **94**(1): p. 75-81.
29. Riddles, P.W., R.L. Blakeley, and B. Zerner, *Reassessment of Ellman Reagent.* Methods in Enzymology, 1983. **91**: p. 49-60.
30. Wang, R., et al., *Electrospun nanofibrous membranes for high flux microfiltration.* Journal of Membrane Science, 2012. **392**: p. 167-174.
31. Liu, Y., et al., *High-flux microfiltration filters based on electrospun polyvinylalcohol nanofibrous membranes.* Polymer, 2013. **54**(2): p. 548-556.
32. Milacic, R., et al., *Critical-Evaluation of 3 Analytical Techniques for the Determination of Chromium(Vi) in Soil Extracts.* Analyst, 1992. **117**(2): p. 125-130.
33. Pflaum, R.T. and L.C. Howick, *The Chromium-Diphenylcarbazide Reaction.* Journal of the American Chemical Society, 1956. **78**(19): p. 4862-4866.
34. Basta, N.T. and M.A. Tabatabai, *Determination of Total Metals in Sewage Sludges by Ion Chromatography.* Journal of Environmental Quality, 1991. **20**(1): p. 79-88.
35. Min, M.H., et al., *Micro-nano structure poly(ether sulfones)/poly(ethyleneimine)*

nanofibrous affinity membranes for adsorption of anionic dyes and heavy metal ions in aqueous solution. Chemical Engineering Journal, 2012. **197**: p. 88-100.

36. Saito, T., et al., *Homogeneous suspensions of individualized microfibrils from TEMPO-catalyzed oxidation of native cellulose.* Biomacromolecules, 2006. **7**(6): p. 1687-1691.
37. Isogai, A., T. Saito, and H. Fukuzumi, *TEMPO-oxidized cellulose nanofibers.* Nanoscale, 2011. **3**(1): p. 71-85.
38. Ma, H.Y., et al., *Nanofibrous Microfiltration Membrane Based on Cellulose Nanowhiskers.* Biomacromolecules, 2012. **13**(1): p. 180-186.
39. Back, E.L., et al., *Ultrasonic Measurements of Thermal Softening of Paper Products and Influence of Thermal Auto-Cross-Linking Reactions.* Tappi, 1967. **50**(11P1): p. 542-&.
40. Back, E.L., et al., *Effect of Auto Cross-Linking Reactions on Thermal Softening of Cellulose.* Textile Research Journal, 1967. **37**(5): p. 432-&.
41. *Sun et al. Patent US 6962608 B1.*
42. B.V., B.I., *US Patent No: 6586588 Polysaccharide aldehydes prepared by oxidation method and used as strength additives in papermaking*
43. Kotas, J. and Z. Stasicka, *Chromium occurrence in the environment and methods of its speciation.* Environmental Pollution, 2000. **107**(3): p. 263-283.
44. Connett, P.H. and K.E. Wetterhahn, *Reaction of Chromium(Vi) with Thiols - Ph-Dependence of Chromium(Vi) Thio Ester Formation.* Journal of the American Chemical Society, 1986. **108**(8): p. 1842-1847.
45. Lay, P.A. and A. Levina, *Kinetics and mechanism of chromium(VI) reduction to chromium(III) by L-cysteine in neutral aqueous solutions.* Inorganic Chemistry, 1996. **35**(26): p. 7709-7717.

46. Gajendragad, M.R. and U. Agarwala, *Complexing Behavior of 5-Amino-2-Thiol-1,3,4-Thiadiazole .3. Complexes of Cu(I), Zn(Ii), Ag(I), Cd(Ii), Tl(I), Pb(Ii), Pd(O) and Pt(O).* Indian Journal of Chemistry, 1975. **13**(12): p. 1331-1334.

47. Gupta, B.K., et al., *Complexes of Zn(Ii), Cd(Ii), Hg(Ii), Pb(Ii), Ti(I) and Ag(I) with 1,2,4-Triazole-3(5)-Thiol.* Indian Journal of Chemistry Section a-Inorganic Bio-Inorganic Physical Theoretical & Analytical Chemistry, 1977. **15**(7): p. 624-626.

48. Wu, Z.M., Z.H. Cheng, and W. Ma, *Adsorption of Pb(II) from glucose solution on thiol-functionalized cellulosic biomass.* Bioresource Technology, 2012. **104**: p. 807-809.

49. Payne, J.C., M.A. ter Horst, and H.A. Godwin, *Lead fingers: Pb2+ binding to structural zinc-binding domains determined directly by monitoring lead-thiolate charge-transfer bands.* Journal of the American Chemical Society, 1999. **121**(29): p. 6850-6855.

50. Mah, V. and F. Jalilehvand, *Lead(II) Complex Formation with Glutathione.* Inorganic Chemistry, 2012. **51**(11): p. 6285-6298.

51. Chen, S.Y., et al., *Carboxymethylated-bacterial cellulose for copper and lead ion removal.* Journal of Hazardous Materials, 2009. **161**(2-3): p. 1355-1359.

52. Li, C.C., et al., *Adsorption of Cr(VI) using cellulose microsphere-based adsorbent prepared by radiation-induced grafting.* Radiation Physics and Chemistry, 2012. **81**(8): p. 967-970.

53. Lu, M., et al., *Characteristic and mechanism of Cr(VI) adsorption by ammonium sulfamate-bacterial cellulose in aqueous solutions.* Chinese Chemical Letters, 2013. **24**(3): p. 253-256.

54. Shen, W., et al., *Adsorption of Cu(II) and Pb(II) onto diethylenetriamine-bacterial cellulose.* Carbohydrate Polymers, 2009. **75**(1): p. 110-114.

55. Musyoka, S.M., et al., *Synthesis, Characterization, and Adsorption Kinetic Studies of Ethylenediamine Modified Cellulose for Removal of Cd and Pb.* Analytical Letters, 2011. **44**(11): p. 1925-1936.

56. Chrastny, V., et al., *A critical evaluation of the 0.05M EDTA extraction of Pb from forest soils.* International Journal of Environmental Analytical Chemistry, 2008. **88**(6): p. 385-396.

57. Soloway, H., Kipnis, F., *2-Substituted-thiazolidine-4-carboxylic acid.* J. Am. Chem. Soc. 1948, 70(4), p.1667-1668

Chapter 3 Surface Thiol-Functionalized Ultra-fine Chitin Nanofibrous Adsorbents in As (III) Removal

Abstract

A natural polysaccharide, chitin, was treated with a series of chemical treatments and mechanical disintegration to produce ultra-fine nanofibers. The dimensions of the chitin nanofibers were 5 nm to 20 nm wide and a few hundred nanometers in length, which could allow them to be well dispersed in aqueous solution at neutral pH. The large amount of surface amine groups of nanofibers (1.7 mmol/g) can provide opportunities for selective modifications and a strong linkage modification could be made by the formation of amide bonds. In this study, the grafting of cysteine has provided sites for arsenic metal ions adsorption. Functionalized adsorbents were characterized by titration, FT-IR, Energy Dispersive Spectroscopy (EDS) and SEM. The arsenic adsorption performance of thiol-modified chitin nanofibers was tested under different pH conditions and for different metal ion concentrations, in order to ascertain the best adsorption capacity. The cysteine-modified chitin nanofibers achieved a maximum AsO_2^- adsorption capacity of 138 mg/g at pH = 6.5. Due to the ultra-fine nanofibrous scaffold's large surface–to-volume ratio combined with a tremendous amount surface functional groups directly exposed to arsenic ions, it demonstrated better adsorption capacity than other chitin/chitosan-based hydrogels or beads.

Key Words: Thiol modification, chitin nanofibers, As (III) removal, water purification

3.1 Introduction

3.1.1 Arsenic contamination regions and health effects

Arsenic contamination has been a serious global problem for groundwater sourcing lakes and rivers worldwide. It is a problem in many countries such as India [1, 2], China [3-5], Canada [6] and the USA [7]. Arsenic is an element that naturally exists in different forms, such as orpiment (As_2S_3), realgar (AS) and arsenopyrite (FeAsS), which are mostly abundant in the environment [8]. It is very likely that, in some regions, the natural element or compound goes into the groundwater and soil through rainfall, but it can also be introduced through anthropogenic behaviors [9]. According to the latest World Health Organization (WHO) report [10], the standard arsenic levels in water should not exceed 10 µg/L. However, for example, in Vaishali of India, over 95% of the ground water was found to contain arsenic above the limit for drinkable water and reaching as high as 143 µg/L. Some other regions can reach up to 2 mg/L (ppm), while the pH values of the corresponding contaminated water in those areas range from 6.6 to 7.7 [10].

Both short term and long term intake of arsenic contaminated water would cause severe health problems, such as spontaneous pregnancy loss, respiratory complications, immunological system disorders and the blackfoot disease [11]. Recent studies since 2003 have revealed that there is a very high risk of assessing cancer from exposure to inorganic arsenic (As) from water, these include possibilities of getting bladder cancer [7], lung cancer [12] and skin cancer [13].

3.1.2 Fundamental chemistry of arsenic compounds

There are two dominant oxidation states of arsenic naturally found in aqueous solutions in the environment, As (III) and As (V), though other oxidation forms also exist, for example -3 as in

arsine gas, -1 as in alkyl arsenic and 0 as in the arsenic element, as is shown in Figure 3.1a [14]. The solubility of arsenic compound in water is affected by pH and oxidation and reduction potential (Eh). Figure 3.1b shows that when Eh is between 0 mV and 200 mV, As (III) is the major form and As (V) is dominate when the Eh goes between 200 mV and 500 mV.

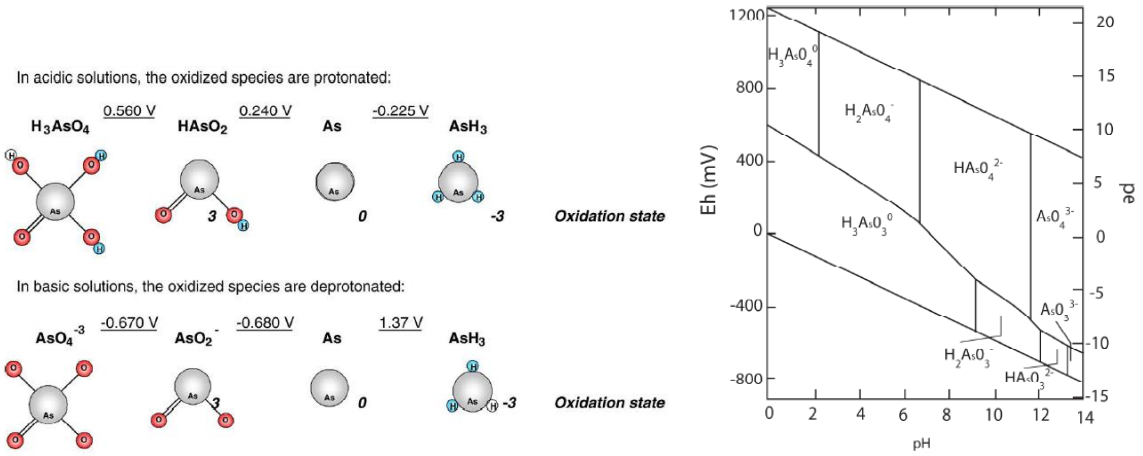

Figure 3.1 (a) Oxidation state of arsenic species in both acid and base solution [14] (b) Eh – pH relation in As (III) and As (V) compounds[15] (Figures reprinted with permission)

3.1.3 Arsenic removal methods review

Over the years, scientists and engineers have been making an effort to develop materials and methods for arsenic removal from aqueous solution by chemical precipitation [16, 17], ion exchange [18, 19], membrane filtration [20] and adsorption [21].

3.1.3.1 Physical-chemical precipitation

One of the most common methods to remove arsenic is to mix metal hydroxide ions with the arsenic contaminated water; species such as iron [22] and calcium hydroxide [23] are widely used. When water-dissolvable iron ions mix with arsenate ions, they bind with each other with a

ratio of 1:3 iron ions to arsenic ions. The optimum removal performance pH falls in the range between 7 and 8.5.

3.1.3.2 Ion exchange method

Ion exchange resins are another popular material for metal ion removal in water purification. The general mechanism, as in its self-explained name, is that certain functional groups of the resin with some charges will carry out an exchange reaction with competitive ions in the aqueous solution. Specifically, to remove arsenic ions, resins can be pre-treated with chloride ions to increase the exchange efficiency [24]. In the exchange resins, the chloride anion is associated with an alkylammonium group, while ion exchange occurs through association of the arsenate species with the ammonium ions to replace chloride ions. In addition, The resins can be regenerated by treated with strong acid such as HCl efficiently [25].

3.1.3.3 Membrane filtration method

Membrane filtration is another widely applied technology that is used to remove bacteria, viruses and heavy metal ions, based on size exclusion of the membrane pore size and feed solution particle size, charge exclusions of the surface charge of membrane, and charge of the particles or specific chelating effects between membrane surface and targets in the feed. Among those, Reverse Osmosis (RO) [26] and Nanofiltration (NF) [27] are two popular ways to efficiently remove toxic arsenic compounds from aqueous solution. There are many factors that could influence the filtration performance, such as solution pH and concentration of filtrate. Some scientists have also found that nanofiltration membranes have a limitation in removing arsenic at different oxidation states. For example, at low feed concentration in the range of 20 and 90 ppb, the removal efficiency of As (V) is over 90%, while As (III) removal efficiency is only around 10%, as shown in the Figure 3.2. However, the limitation is that both NF and RO

usually require very high operation pressures and are very energy consuming. In addition, membranes have to be disposable in industry in terms of validation purposes, therefore leading to various environmental problems.

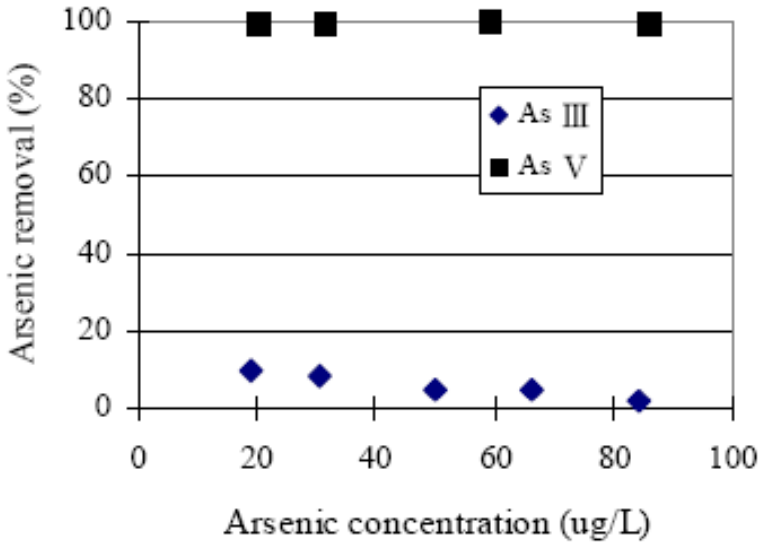

Figure 3.2 Arsenic (III) and (V) removal by nanofiltration at different feed concentration (figure reprinted with permission from reference [28])

3.1.3.4 Adsorption method

A variety of natural inorganic and organic materials, for instance, alum species and active carbon, have been studied for the purpose of arsenic removal. There are two forms of alum that demonstrate arsenic adsorption capability. One is aluminum hydroxide $Al(OH)_3$, which is a sludge in aqueous solution at neutral pH. Being in a sludge state provides an extremely large surface area; therefore, arsenic species can easily be trapped in the alum sludge and precipitate. Another form is alumina oxide (Al_2O_3), which is known as active alumina and can demonstrate up to an adsorption capacity of 87% As(V) at the optimum pH = 6.5 with concentration of 10

ppm [29]. However, the limitation is that active alumina is a poor adsorbent for As (III), which means that in order to remove arsenic species from water, an oxidative pre-treatment is required, thereby introducing more difficulty, although the active alumina itself is inexpensive and accessible [30].

Active carbon is regarded as a versatile adsorbent due to its unique porous structures and large surface area, which provides a tremendous number of sites for adsorption via Van der Waals interactions. The origin of active carbon can be from wood, leaves, coconut shells, sawdust, natural fruit peals, nuts hulls and so forth. Previous studies have also demonstrated the successful removal capability of both bacteria and different metals ions from aqueous solution. Specifically, in some studies, the best performance of arsenic removal by active carbon was when pH = 2.4 and the corresponding adsorption capability could reach up to 3.09 mg/g of arsenic versus active carbon; while with the pH value increasing to neutral, the adsorption amount dropped by 50% [31].

In addition to the all the natural adsorbents above, there are also a number of inorganic material candidates such as titanium dioxide [32] and iron oxide minerals [33], which adsorb arsenic ions either by large active surface area or metal ions through some chelating binding effect. However, one of the biggest adsorption limitations of natural materials without modification is the lack of a great number of sites for adsorption. The morphology and structure of the original natural adsorbents are highly condensed, aggregated or overlapped, which does not provide enough space for adsorption.

3.1.3.5 ECAR and ARUBA methods breakthroughs

Among the numerous methods and technologies for solving the arsenic contamination issues, scientists in Professor Gadgil's group from Lawrence Berkeley National Lab developed

two novel methods providing cost-effective and efficient approaches to remove the arsenic from water; one is called Arsenic Removal Using Bottom Ash (ARUBA)[34] and the other is called Electro-Chemical Arsenic Remediation (ECAR) [35].

In the ARUBA method [34], bottom ash from an Indian coal-fired energy plant comprised the raw starting materials. As shown in Figure 3.3 (A), the bottom ash was treated with ferric hydroxide to coat on the surface, which binds arsenic effectively. Figures 3.3 (B) and 3.3 (C) show the difference of the ash before and after $Fe(OH)_3$ coating, which increases the ash diameters up to 15 μm. The water treatment process is as simple as mixing with water and filtration. The researchers claim about 8 U.S. cents for 10 L up to 1000 ppb water purification to meet the WHO standard (10 ppb).

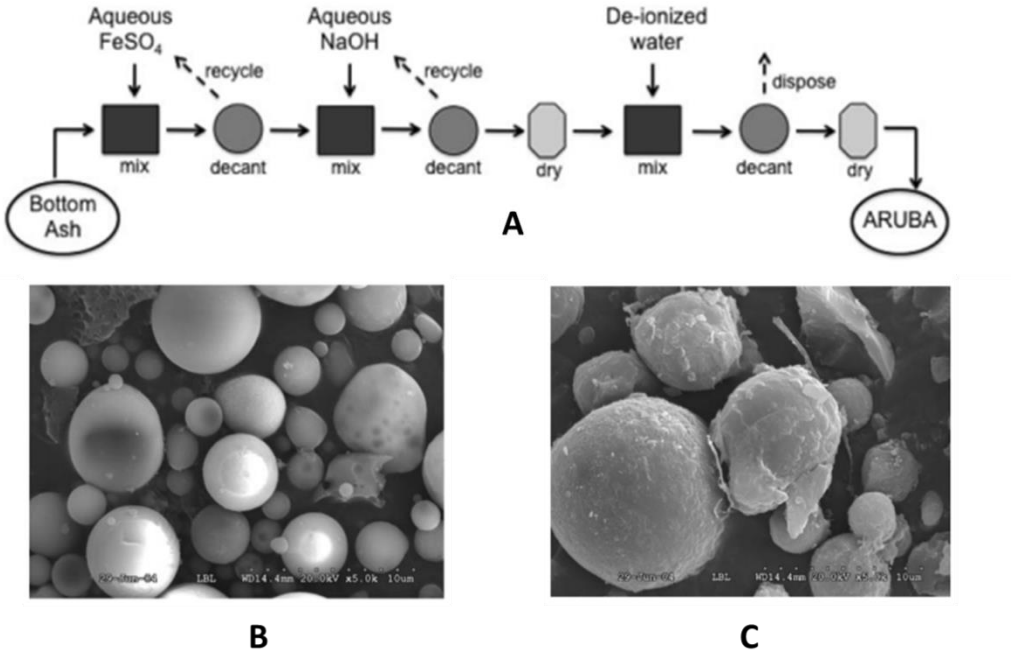

Figure 3.3 (A) ARUBA preparation protocol, (B) SEM image of raw bottom ash and (C) SEM image of $Fe(OH)_3$ modified bottom ash (figure reprinted with permission from reference [34])

In the ECAR method [35], iron (Fe) from an iron anode dissolves into solution, forming $Fe(OH)_3$ rust. The rust forms complexes with arsenic in solution through adsorption to the rust surface, or precipitation into a new iron-arsenic solid. The arsenic-rust complexes are then filtered or settle out of the water. The key part of the experiment is to oxidize As (III) to As (V) prior to the ECAR process, because trivalent arsenite does not bind as strongly as pentavalent arsenate to the mineral surface. In addition, the researchers estimated the operating costs of this treatment, claiming that it can provide up to 1000 L of WHO required safe standard water from arsenic contaminated groundwater at the cost of 22 U.S. cents.

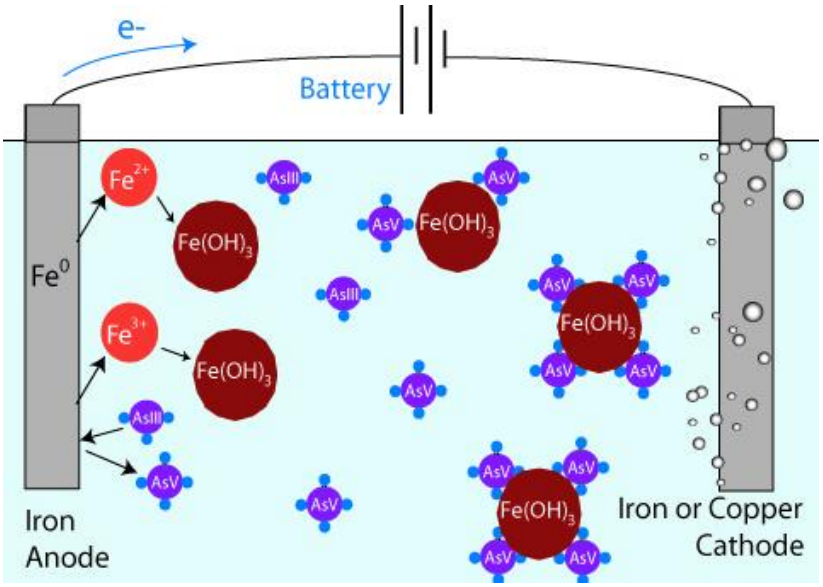

Figure 3.4 ECAR arsenic removal mechanisms(figure reprinted with permission from reference [35])

Therefore, it can be concluded that both of the methods are taking advantage of the high binding affinity between $Fe(OH)_3$ and As (V). Adsorption is carried out on the ferric hydroxide, which both can provide large surface area down to a few microns. However, though the bottom

ash sizes are quite small (1μm to 10 μm), they do not have a uniform morphology and cannot be further broken down, which limits the adsorption performance. In addition, these two methods may be also limited to As (V) removal; hence, creating ultra-fine size-uniformed particles that can efficiently remove As (III) becomes a challenging problem.

3.1.4 Natural polysaccharide chitin as adsorbent

Chitin is the second most abundant, non-toxic, biodegradable, and biocompatible natural polysaccharide behind cellulose. Chitin can be obtained from shellfish exoskeletons, such as shrimp and crab shells or from plants, such as mushrooms [36]. There were about 10^{11} tons per year of chitin produced by industrial processes as of 2003 and a large amount of chitin resources are thrown away without utilization [37]. Figure 3.5 reveals a representative chitin fiber production process from the original source. Individual molecules are naturally connected to form the crystalline structure; the molecular chains are imbedded in proteins forming bundles of larger fibers; those bundles aggregate and connect to each other through branched woven networks to constitute larger nanofiber bundles; furthermore, the large fiber bundles are the actual skeletons which are wrapped by different proteins and minerals, such as calcium carbonates; the woven network are twisted in a hierarchically structural sequence, which is named as the “Bouligand Structure”. In addition, there is no strict definition between chitin and chitosan, when the degree of deacetylation is over 50%, it can be defined as chitosan, otherwise chitin. [38]

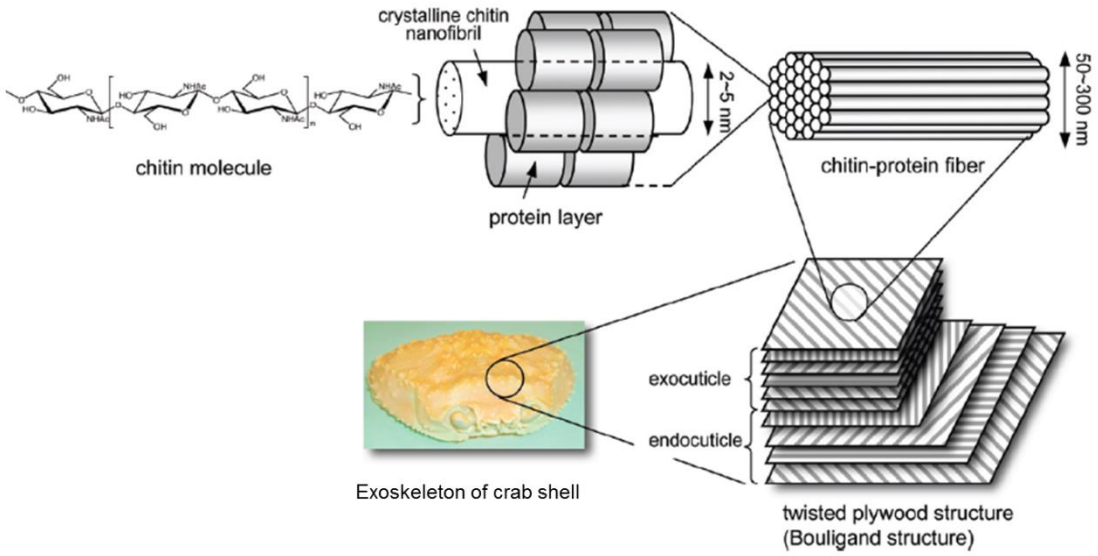

Figure 3.5 Schematic representation of the organization of chitin chains and fibers to form hierarchical structures supporting living bodies (figure reprinted with permission from reference [39])

In this research, we aimed to extract ultra-fine (nanoscale size-uniform) nanofibers from the shrimp shell chitin by a series of chemical and mechanical treatments and then modify it with different functional molecules to demonstrate arsenic adsorption performance from water due to the tremendous nanofiber surface area and large functionality.

3.2 Materials and Methods

3.2.1 Materials

L-Cysteine (> 97% purity), *N*-hydroxysuccinimide (NHS), *N*-(3-dimethyl-aminopropyl)-*N*′-ethylcarbodiimide hydrochloride (EDC), 2,2,6,6-tetramethyl-1-piperidinyloxy (TEMPO), sodium

hydroxide (NaOH), sodium hypochlorite (NaClO), sodium chlorite ($NaClO_2$), sodium arsenite ($NaAsO_2$), phosphate buffer, practical grade powder chitin from crab shell and shrimp shell (Poly-(1-4)-β-N-acetyl-D-glucosamine) and chitosan (Medium molecular weight 103kDa; degree of deacetylation 85%) were purchased from Sigma-Aldrich. Ellman's Reagent, DTNB (5,5'-dithio-bis-[2-nitrobenzoic acid]) was purchased from Thermo Scientific. Dialysis tubing 44 mm × 28 mm with molecular weight cut off (MWCO) = 14,000 Daltons was purchased from Fisher Science Education.

3.2.2 Preparation of thiol-modified chitin nanofibers

3.2.2.1 Preparation of chitin nanofibers Step 1: Acid / Base Treatment

One way to prepare chitin nanofibers is through a series of acid, base and mechanical treatments as previously published [39, 40]. 10.0 g of dried powder of chitin from shrimp shell was dispersed in 500 ml 2 M HCl and stirred at room temperature for 6 h to remove mineral salts, such as calcium carbonate. The slurry was separated by vacuum filtration and then washed with water to remove HCl until the pH value was neutral. Next, the chitin was dispersed and refluxed in 500 ml 30% NaOH at 80 °C for 10 hours to remove proteins and deacetylate the fibers. Then the slurry was separated by vacuum filtration. Finally, it was washed with DI water until the pH value of the filtrate was close to 7, tested by a pH meter, indicating that all NaOH was being removed. 1.0 g chitin slurry (>90 wt% chitin) was dispersed in 100 g of water and sonicated for 15 min with a homogenizer (Cole Parmer, VCX-400). The resulting chitin nanofiber aqueous suspension had a concentration of ~1 wt%, determined by a Total Organic Carbon analyzer (TOC-500, Shimadzu Corporation). Part of the insoluble portion of solution was freeze-dried for further analysis.

3.2.2.2 Preparation of chitin nanofibers by Step 2: Oxidant Treatment

In addition to step 1, previous literatures also reported fiber surface oxidation to produce ultra-fine fibers [41, 42]. Specifically, the product from step 1 was continuously treated by adding a certain amount of NaClO (~5 mmol of NaClO per gram of chitin nanofiber), stirring overnight and then separating the slurry by vacuum filtration and washing by DI water until the pH value reached 7. Next, the slurry was treated with 30 wt% NaOH, boiled at 80 °C again to remove left-over protein and allowed the deacylation reaction to occur. The final product was purified by using a dialysis bag (MWCO 140k) in a 5 L water tank. DI water was changed every 2 hours until the conductivity of the solution was equal to water (~ 120 μS/cm). 2.0 g chitin slurry (> 60 wt% chitin) purified from the dialysis bag was dispersed in 100 g of water to sonicate with the homogenizer for 15 min, then confirmed the concentration of chitin stock solution ~1 wt%, as determined by TOC-500. Part of the solution was freeze-dried for further analysis.

3.2.2.3 Preparation of thiol-modified chitin nanofibers with cysteine

100 g of (~ 0.5 wt%) chitin nanofiber suspension (from the oxidant treatment) was mixed with N-hydroxysuccinimide (NHS) (0.16 g, 1.4 mmol), 1-ethyl-3-[3-dimethylaminopropyl] carbo-diimide hydrochloride (EDC) (0.24g, 1.3 mmol) and cysteine (0.5 g, 4.1 mmol). The reaction was allowed to proceed for 24 hours at room temperature, then the mixture was centrifuged at a speed of 5000 rpm (with a relative centrifugal force of about 2200 × g) and the supernatant was poured off. Then the slurry of modified nanofibers was re-suspended in DI water and the washing and centrifugation process was repeated several times until the conductivity in the centrifuge tube remained the same (~ 120 μS/cm), which indicated that only chitin nanofibers remained in the solution which was about 75 wt% (~ 400 mg) yield confirmed by TOC-500.

3.2.3 Characterization of modified chitin nanofibers

3.2.3.1 Determination of amine groups by conductivity titration

The amount of amine groups on the surface of chitin nanofibers could be quantified by using the electric conductivity method [43, 44]. During the test, 6 ml of 0.9 wt% chitin suspension was first diluted with DI water into 50 ml suspension. 3 ml of 0.1 M HCl was subsequently added to this suspension to keep the pH value between 2.0 and 3.0. Then, 50 µl aliquots of 0.1 M NaOH were added continuously at the rate of one aliquot every 20 seconds into the suspension to achieve a pH value of 11, while the conductivity of the suspension was measured. The amine content was determined from the conductivity and the pH curves [44].

3.2.3.2 Quantitative determination of thiol groups with Ellman's Reagent

After the chitin nanofiber reaction with cysteine, the thiol-modified chitin nanofiber suspensions were purified by dialysis against DI water until no carbon was detectable by TOC analysis of the solution outside the dialysis bag (MWCO = 140,000 Daltons). Previous studies [45] have demonstrated using Ellman's Reagent, DTNB (5,5'-dithio-bis-[2-nitrobenzoic acid]), to determine the amount of thiol groups on the surface of cellulose nanofibers in aqueous suspension. The same method was applied to determine the thiol groups on the surface of chitin nanofibers in aqueous suspension. During the testing process, the DTNB was used to react with thiols to release 2-nitro-5-thiobenzoate (NTB^-) and was ionized to the yellow color NTB^{2-} di-anion at pH = 8.0 aqueous solution. Thiol groups were assayed by using the molar adsorption coefficient of NTB^- (14,150 L $mol^{-1}cm^{-1}$ at 412 nm) [46]. Detail preparation, testing and calculation were included previously in 2.2.3.2 Quantitative determination of thiol groups with Ellman's Reagent.

3.2.3.3 Fourier Transform Infrared (FT-IR) spectroscopy

Fourier transform infrared (FT-IR) spectroscopy with attenuated total reflectance (ATR) accessory (Nicolet iS10 spectrophotometer, Thermo Scientific, Inc) is one way to provide chemical functionality of chitin nanofibers and thiol-modified chitin nanofibers. Each sample was freeze-dried and analyzed in the range from 4000 cm^{-1} to 650 cm^{-1}.

3.2.3.4 Scanning Electron Microscopy (SEM)

The morphology of raw chitin and chitin after chemical treatment were investigated by SEM (LEO 1550 with a Robinson backscatter detector and a 20 kV Schottky filed emission gun). All the dried samples were carried through a sputter coating process for 45 seconds with platinum in vacuum. The SEM was equipped with an Energy Dispersive Spectrophotometer (EDS) (EDAX Sapphire PV7715/89-ME). EDS data were analyzed with Iridium Ultra software (iXRF).

3.2.3.5 Transmission Electron Microscopy (TEM)

The chitin nanofiber (and thiol-modified chitin) suspension was diluted to 0.01wt% aqueous suspension, then sonicated by using a homogenizer and cast on a carbon-coated electron microscopy TEM grid, then stained by dropping (~ 0.5 ml) 2.0 wt% uranyl acetate. The TEM applied to conduct the image acquisition was FEI Bio $TwinG^2$ with an accelerating voltage of 120 kV.

3.2.3.6 Small Angle X-ray Scattering (SAXS) experiment

A series of 0.05 wt% to 0.7 wt% chitin nanofiber suspensions were measured by simultaneous SAXS on the X-9 beam line at National Synchrotron Light Source (NSLS) at Brookhaven National Lab (BNL). Experiment procedures followed the previous study on cellulose nanofiber

morphology characterization in aqueous suspensions [48]. A 20 µl chitin nanofiber aqueous suspension was automatically injected into a glass capillary with a diameter of 1 mm in vacuum. The X-ray wavelength was 0.0918 nm and the PILATUS 300K detector was set at 3.2 meters away to collect the SAXS data. During the data collection process, samples were continuously passed through the capillary to minimize the radiation damage. A Python-based software package was applied to process the preliminary data, converting the two-dimensional images into one-dimensional scattering, blocking unnecessary pixels and subtracting buffers and background information.

3.2.4 Evaluation of arsenic removal by thiol-modified chitin nanofibers

The As (III) adsorption experiment was performed to evaluate the adsorption maximum efficiency of chitin nanofibers (in suspension) before and after thiol modification. 100 ppm sodium arsenite (Na_3AsO_3) in DI water was applied as stock solution for the series of adsorption tests. The concentrations of arsenite ion solutions were prepared by diluting stock solution from 10 to 100 ppm. 0.5 wt% chitin nanofibers before and after modification were separately applied for the adsorption testing at different initial arsenite concentrations and at a solution pH ranging from 4.0 to 11.0 adjusted by adding NaOH or HCl solutions and left overnight.

$$Q = \frac{(C_i - C_f)V}{M} \qquad 3.1$$

In Equation (3.1), Q refers to the amount of metal adsorbed (mg/g), C_i means the initial metal ion concentration while C_f means the final metal ion concentration (mg/L), V refers to the volume of solution (L) and M is the weight of adsorbent.

An Atomic Absorption Spectrophotometer (AAS) from Perkin Elmer was used to determine the arsenic concentration in the solution. Graphite Furnace model with ionization temperature:

2850°C was selected for the testing. In addition, diluent was 0.2 wt % HNO_3 as background and matrix modifier was 0.1wt % $Mg(NO_3)_2$ for sample stabilization from evaporation.

3.3 Results and Discussions

3.3.1 Analysis of chitin nanofibers

It is known that shrimp shells are composed of hierarchical structures. In order to extract chitin nanofibers from the raw chitin powder, a certain process of chemical and mechanical treatments were applied. As has been described in the experimental section, HCl was used to remove the minerals, mainly calcium carbonate and $NaClO_2$ was applied to bleach the pigment buried in the woven networks structure. The protein layers wrapping around the nanofibers could be removed by strong NaOH solution. Figure 3.6 shows the raw chitin powder from shrimp shell Figure 3.6(A). The surface was quite uniform and it was impossible to see any fiber network due to the coverage of proteins on the surface. In addition, EDS also detected a high amount of calcium, indicating the existence of some minerals, like calcium carbonate. In Figure 3.6 (B), the fibrous network structure was quite visible after a series of chemical treatment and there was no metal peak detectable in the EDS analysis.

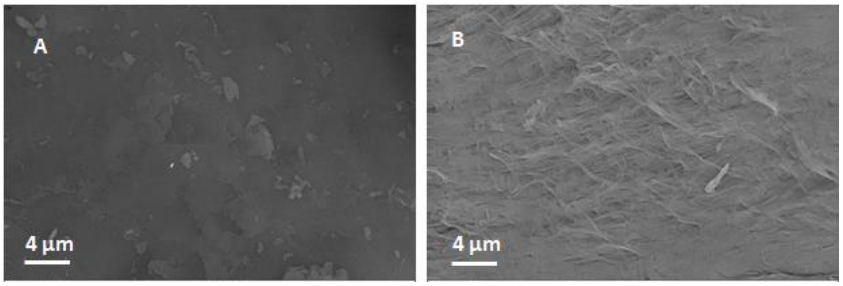

Figure 3.6 SEM images of (A) raw chitin and (B) chitin fiber network with scale bars of 4 µm.

However, the chitin fibrous network we purified from vacuum filtration could not be well dispersed in aqueous solution at neutral pH. In Figure 3.7, sample (1) was the chitin nanofiber suspension dispersed in the aqueous solution, and the photograph revealed that chitin nanofibers modified only by the acid/base treatment were not well suspended in water, but rather formed a gel-like precipitate. The aggregation could be due to the large portion of the hydrophobic part of the chitin nanofibers arising from strong inter-fibrillar hydrogen bonding effects among the surface of the chitin fibers. When the pH of the suspension was decreased, the deacylated C2 amine groups on the surface of the fiber could be cationized and the electrostatic repulsion among the positive charge groups could help to disperse the fibers in the aqueous solution. However, after the NaClO treatment and dialysis purification, and under neutral pH conditions, sample (2) chitin fibers became much better dispersed in the aqueous solution. It is very likely that the hydroxyl groups at the C6 positions could be partially oxidized to carboxylate, creating a water soluble fraction of polyuronic acid Na salts on the surface of chitin nanofibers. Sample (3) was after the NaOH deacetylation treatment; more hydrophilic amine groups were exposed and these groups facilitated the dispersion of the fibers in the solution. The concentration of the homogenous suspension of sample (3) was 0.5 wt%, as confirmed by TOC. Though the final suspension was only partially transparent, when compared with sample (1) and (2), the chitin fibers could most likely be converted into individual nanofibers, were highly crystalline and appeared to be well dispersed in DI water after mechanical disintegration [41].

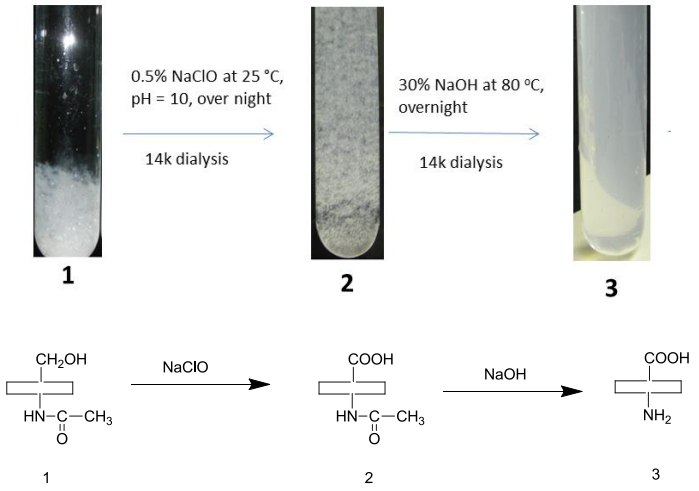

Figure 3.7 Photographs and mechanism of chitin at different chemical treatment stages: (1) chitin nanofiber suspension by acid/base treatment, (2) chitin nanofiber suspension by NaClO treatment (3) chitin nanofiber suspension (concentration 0.5 wt%) by NaOH treatment

After the series of chemical treatments and the mechanical disintegration, the surface of chitin nanofibers should have certain functional groups, as shown in Figure 3.8. At C2 position, a certain amount of amino groups were generated during the deacetylation process by NaOH. If there were a sufficiently large amount of primary amines created, then the chitin fibers could be well dispersed in the aqueous solution due to the cation formation of amine under acidic conditions. As mentioned above, the oxidation reaction by NaClO at C6 positions could convert hydroxyl groups to carboxylates, which might also play a significant role in separating the nanofibers from one another due to electrostatic repulsions between negatively charged ions. In this case, this well-separated natural polysaccharide nanofibers with different functional groups can be further modified for various applications, such as biomedical and life science technologies and for additional applications to water purification.

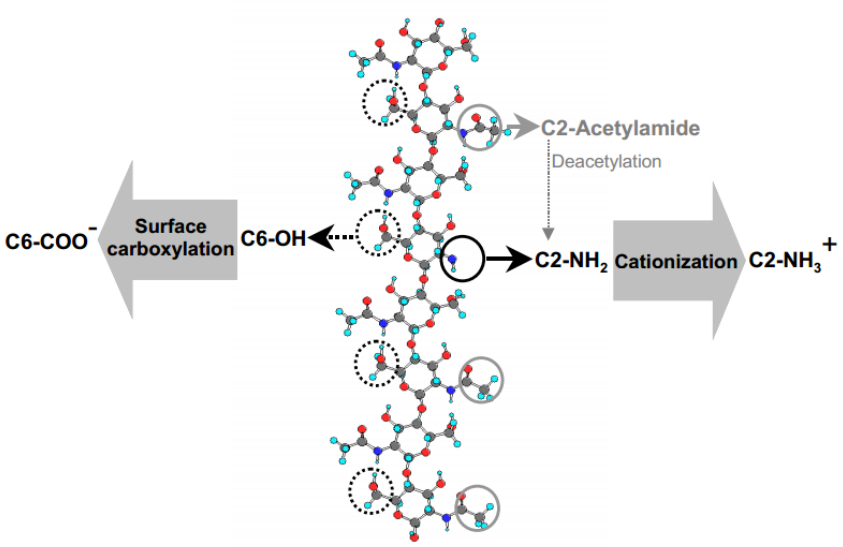

Figure 3.8 Possible sketch map of chitin nanofiber functional surface after chemical treatments [49].

Moreover, the series of chemical treatments and mechanical disintegration can produce ultra-fine and size-uniform nanofibers. In Figure 3.9 (A), it is clear to see that the fiber length is from a few hundred nanometers to a few microns. It also shows some fiber aggregation. It could be possible that after casting the 0.01 wt% chitin nanofiber suspension and removal of the extra liquid from the grid, the concentration of the suspension was increased, leading to a higher concentration and induced fiber aggregation and overlaps among the fibers. In Figure 3.9 (B), the ultra-fine chitin nanofibers were 5 – 20 nm in width and could be easily observed. In addition, some regions of twisted fibers can be seen on both of the TEM images indicating a ribbon-like structure. Furthermore, the morphology analysis of chitin nanofibers by small-angle X-ray scattering (SAXS) also confirmed a ribbon-like structure [48].

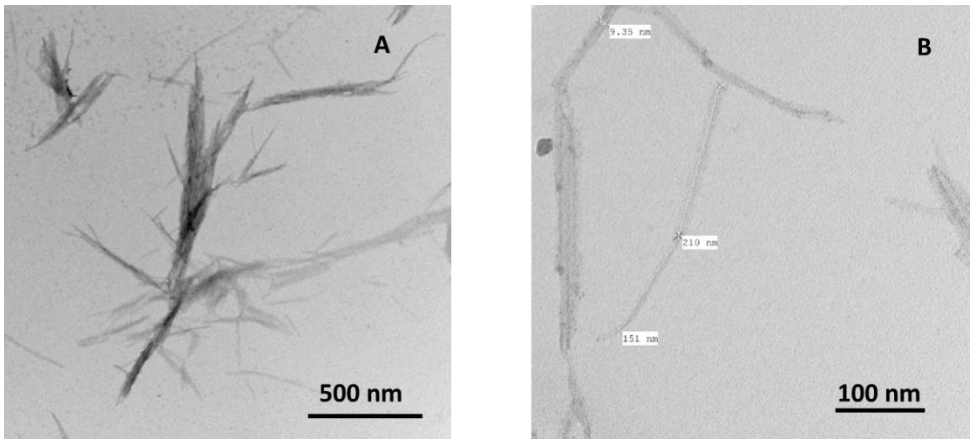

Figure 3.9 TEM images of the same chitin nanofibers after acid/base and oxidant treatment with scale bar of (A) 500 nm and (B) 100 nm, stained with 2.0 wt% uranyl acetate solution before imaging

3.3.2 Chitin nanofiber characterization by SAXS

Previous studies [48] in our research group have utilized SAXS to characterize cellulose nanofibers (3 nm to 13 nm width and a few hundred nanometers in length) in aqueous suspension, similar in size dimension to chitin nanofiber dimension found from TEM in this study. A ribbon model, which assumes that the cross-section of the fiber was more rectangular in shape, was established to characterize the nanofibers and an equation (3.6) [48] was developed as follows. With the lengths of nanofibers ranging from hundreds of nanometers to more than one micron, far exceeding the normal SAXS size investigation range (0.5 – 500 nm), the length of the ribbon was taken as infinitely long in this model. Based on the previously published model, the ribbon-like chitin nanofiber had an average diameter of 18 nm, which matched TEM observed fiber sizes.

3.3.3 Quantitative analysis of chitin nanofiber functional groups

In the aforementioned chitin nanofiber preparations, several different functional groups were generated, serving as potential sites for direct applications or further modification reactions. Hence, quantitative analysis of functional groups on the surface of chitin nanofibers is of great importance.

In the chitin nanofiber preparation, the protein wrapping around the fiber and the minerals buried in the network have been removed by NaOH and HCl, respectively. After isolation and purification, though not well dispersed in water, a small amount of C2 amino groups was detectable with approximately 0.8 mmol per gram of chitin. Furthermore, C6 hydroxyl groups could be oxidized by NaClO and the carboxylate conductivity titration [45] yielded a surface carboxylate concentration of 0.05 to 0.1 mmol/g. In addition, after the strong base (30 wt% NaOH) had been boiled with chitin fibers, the C2 acetylamide deacetalytion reaction could provide a large amount of primary amine groups, about 1.7 mmol/g. The increasing amount of amine groups detected could be due to a better dispersion of the fibers in the solution rather than the fiber aggregation after NaClO oxidant treatment. Therefore, more C2-amino groups were exposed. It is also likely that the second long term treatment of NaOH can release more nanofibers from the residual protein matrix and meanwhile deacetylate more of the C2-acetylamide.

In addition, since amine groups on the surface of the chitin fiber are the key in the following grafting reaction and adsorption performance studies, understanding the degree of deacetylation of fiber surface is crucial. As is shown in the Figure 3.11, the surface molecular chain of chitin has a composition of n moles of N-acetyl glucosamine (GlcNAC) and m moles of glucosamine ($GlcNH_2$). The difference between chitin and chitosan relies on the m and n ratios. When n >>

m, the polymer is consider as chitin, while n ≪ m, the polymer is consider as chitosan [50].

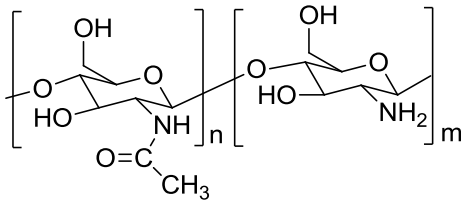

Figure 3.10 Chemical structure of chitin/chitosan chain

The degree of deacetylation ratio of chitosan (f_D) is given in the following equation:

$$f_D = \frac{m}{m+n} \tag{3.2}$$

The chitosan monomer average weight ($M_{cs,mon}$) is given in the following equation:

$$M_{cs,mon} = MW_n \times (1 - f_D) + MW_m \times f_D \tag{3.3}$$

The concentration (mol/g) of primary amine groups on the chitosan is calculated in the following equation.

$$C_{NH2} = \frac{f_D}{M_{cs,mon}} = \frac{f_D}{MW_n \times (1 - f_D) + MW_m \times f_D} \tag{3.4}$$

Therefore, the molar amine concentration on the 100%-deacetylated chitosan is 6.2 mmol/g based on equation (3.4). There are 1.7 mmol of amine per gram of chitin, as determined by the electrical conductivity titration [51-53], and shown in Table 3.1. The number of amine groups on the 100% deacetylated chitosan is much larger than the number of amine groups determined by titration. The reason for this is that the chitin fiber is an aggregation of chitin chains up to 5 nm – 20 nm diameter in dimension. Thus, even though the surface of the chitin nanofibers was

deacetylated by a series of NaOH treatments, there is still a large amount of chitin molecular chains being bundled together and not exposed. Therefore, these internal sites cannot be detected by conductivity titration.

Table 3.1 Determination of amine groups on the ultra-fine chitin nanofibers

Amine Determination Method	Amount of Amine Groups
Theoretical amine in chitosan *[1]	6.2 mmol/g
Primary active amine on chitin fiber by titration *[2]	1.7 ± 0.03 mmol/g

*1. Data was calculated according to equation (3), on the assumption of 100%-deacetylated chitosan

*2. Data was generated by conductivity titration measurement in the experimental section

3.3.4 Characterizations of thiol-modified chitin nanofibers

Thiol-functionalized chitin nanofibers were created by grafting cysteine molecules onto the fiber surface by forming amide bonds between cysteine carboxylate groups and amine groups from chitin. The reaction happened in the presence of NHS and EDC to activate the carboxylate groups and to react with amine forming amide bonds (Scheme 3.1). Specifically, the modification reactions carried out at different molar ratio of chitin – amine ([NH_2]= 1.7 mmol/g) to cysteine at 1:2, 1:6, 1:10. The maxium chitin nanofiber surface thiol concentration was obtained equally at 1:6 and 1:10 with 1.1 ± 0.1 mmol/g determined by Ellman's reagent method.

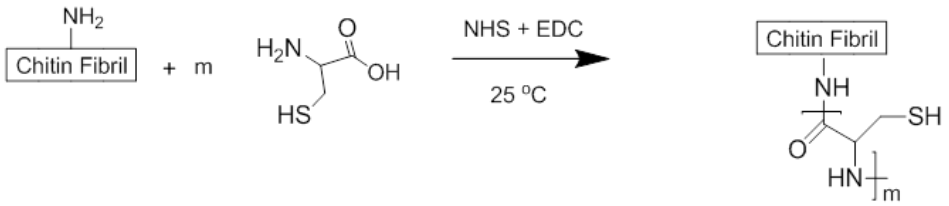

Scheme 3.1 Reaction of cysteine with chitin nanofiber

FT-IR spectroscopy was applied to demonstrate the presence of functional groups in the modification reaction (Figure 3.12). Both unmodified/modified chitin nanofibers were freeze-dried after dialysis for analysis. The IR spectrum of cysteine modified chitosan is compared with raw chitosan samples, as shown in Figure 3.12. The broad band at 1650 cm^{-1} could be the carbonyl adsorption from modified chitin surface COOH overlapping amide I band [54]. The primary amine adsorption at 1590 cm^{-1} on chitin was found as amide II signals at 1550 cm^{-1} on chitin-cysteine [54]. The peaks in the IR indicate the success of cysteine grafted onto the chitin nanofiber. One possibility for the IR absorbance around 1400 cm^{-1} is the thiazolidine ring from the formation of alkylthiazolidine through reaction of aldehyde groups and cysteine.

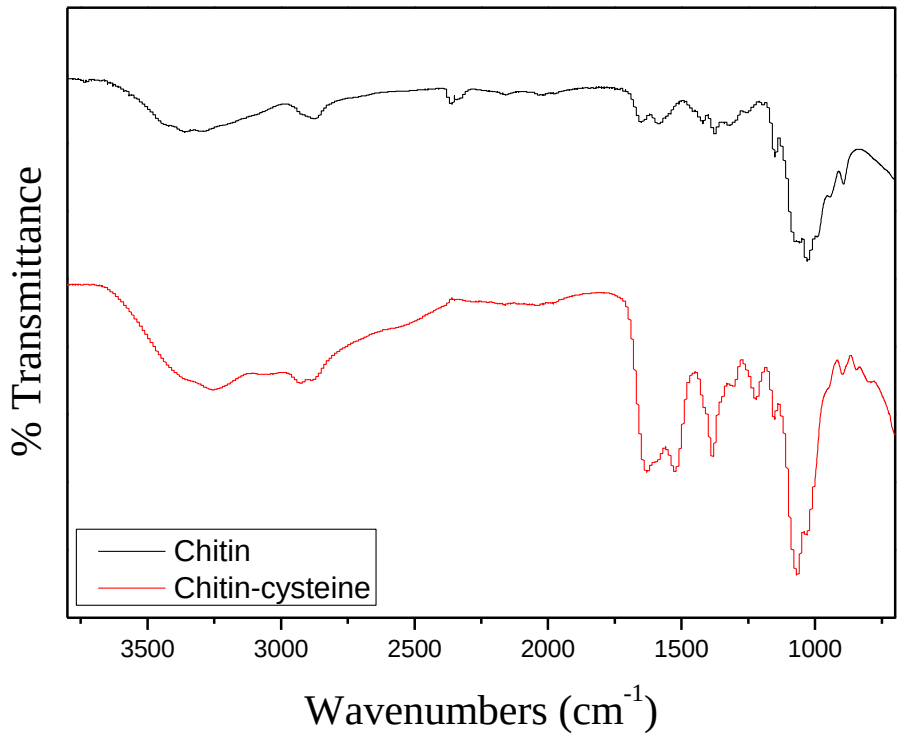

Figure 3.11 FTIR of chitin nanofibers and thiol-modified chitin nanofibers

The EDS analysis of freeze-dried cysteine-modified chitin nanofibers can be regarded as a proof of the presence of sulfur (Figure 3.13), which supports the argument of cysteine being connected to the nanofibers. In addition, it also yields a weight percentage of each element composition, which provides a quantitative analysis of the amount of functional groups. Based on the chemical molecular structure of thiol-modified chitin, the thiol amount was 2.0 ± 0.2 mmol/g of chitin nanofiber, as listed in Table 3.2.

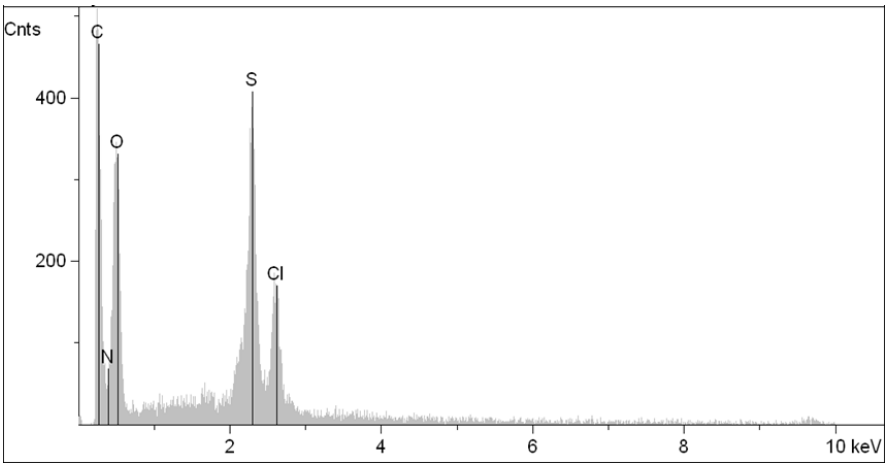

Element	C	O	N	S
Weight Percentage (%)	34.3 ± 0.7	38.3 ± 1.0	17.8 ± 0.5	6.3 ± 0.7

Figure 3.12 EDS with quantitative analysis of thiol-modified chitin nanofibers

After dialysis purification, the thiol concentration on the chitin nanofiber could also be detected in the suspension formed by Ellman's reagent. This method has already been successfully used in previous studies to demonstrate the amount of thiol grafting on the surface of cellulose nanofibers [45]. The concentration of the yellow compound formed was quantified by measuring the UV adsorption at 412 nm wavelength. As listed in Table 3.2, the highest concentration of thiol obtained on the surface of chitin nanofiber was 1.1 mmol per gram of chitin, where the maximum primary amine was 1.7 mmol/g of chitin. It suggested the possibility of about 65% amine groups on the chitin were grafted with cysteine, or it is also possible that less than 65% amine reaction with cysteine oligomers formed.

Table 3.2 Determination of thiol groups on ultra-fine chitin nanofibers

Thiol Groups Amount Determination Method	Amount of Thiol Groups
Thiol groups on the surface of chitin by EDS analysis [*1]	2.0 ± 0.2 mmol/g
Thiol groups on the surface of chitin by Ellman's Reagent [*2]	1.1 ± 0.1 mmol/g

*1 Calculation based on the S weight percentage and chitin molecular structure

*2 Calculation based on Ellman's Reagent equation described in the experimental part

3.3.5 Adsorption performance evaluation

3.3.5.1 pH effect on static adsorption

The pH of the solution has a marked influence on both amine and thiol functionalized chitin nanofibers. When the pH is below pKa of chitosan (6.5), all the amine groups can be completely positively ionized [55]. When the pH value is above the pKa value of cysteine (8 to 9), the groups will be mostly negatively charged in aqueous solution [56, 57]. In addition, the pH also has an effect on arsenic ion species that is present in aqueous solution. For instance, when pH < 4, neutral H_3AsO_3 is the dominate species; when pH is over 4, negatively charged $H_2AsO_3^-$, $HAsO^{2-}$ and AsO_3^{3-} start to appear[58, 59].

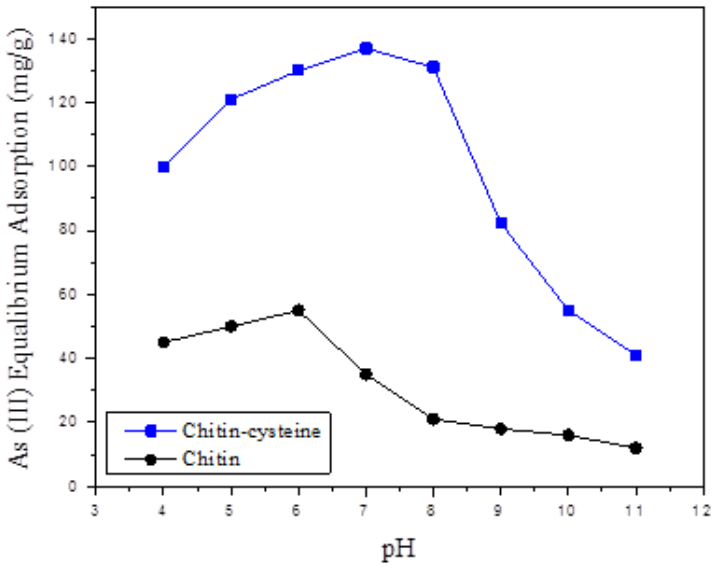

Figure 3.13 As (III) adsorption by chitin and thiol-chitin nanofibers

As shown in Figure 3.14, the adsorption of arsenite ions (AsO_3^{3-}) was investigated at pH values from 4.0 to 11.0, while as mentioned in the introduction, most arsenic pollution in rivers and lakes is within a pH range of 5.0 to 8.0. The adsorption amount was tested by AAS and calculated using the arsenite concentration differences before and after adsorption, multiplied by the volume of solution and then divided by the mass of the adsorbent. It was found that the highest adsorption amount was 138 mg arsenite per gram of thiol-modified chitin nanofibers at a pH = 7.0. In comparison, the maximum adsorption of unmodified chitin nanofibers was 58 mg/g, which is less than half of that of the modified ones. This could be explained by the higher concentration of thiol (1.1 mmol per gram of chitin) forming an As (III)–thiolate complex on the surface of the chitin nanofiber [60]. If the thiol-arsenite is 1:1 ratio coordination, the theoretical As(III) adsorption is 118 mmol/g, but protonated amine can also have interactions with arsenite as in unmodified chitin nanofiber (58mg/g), leading to a total theoretical arsenite adsorption by

thiol-chitin could be 176 mg/g .When the pH value was between 4.0 and 7.0, the dominate arsenic ions were negatively charged, and the protonated amine could adsorb arsenic on to the surface due to an electrostatic attraction for the oppositely-charged species and a Van der Waals attraction for the neutral species [59]. However, when the pH value was increased, the As-thiolate complex formation was inhibited and charge attraction adsorption started to dissociate due to the deprotonation of amines.

3.3.5.2 Langmuir adsorption isotherms

Adsorption isotherms are commonly used to calculate the maximum adsorption capacity by studying the interactions between adsorbents and adsorbates. The calculation of arsenic ion adsorption capacity by chitin nanofibers using Langmuir Adsorption Model could be referred to 2.3.7 Langmuir adsorption isotherms section in Chapter 2.

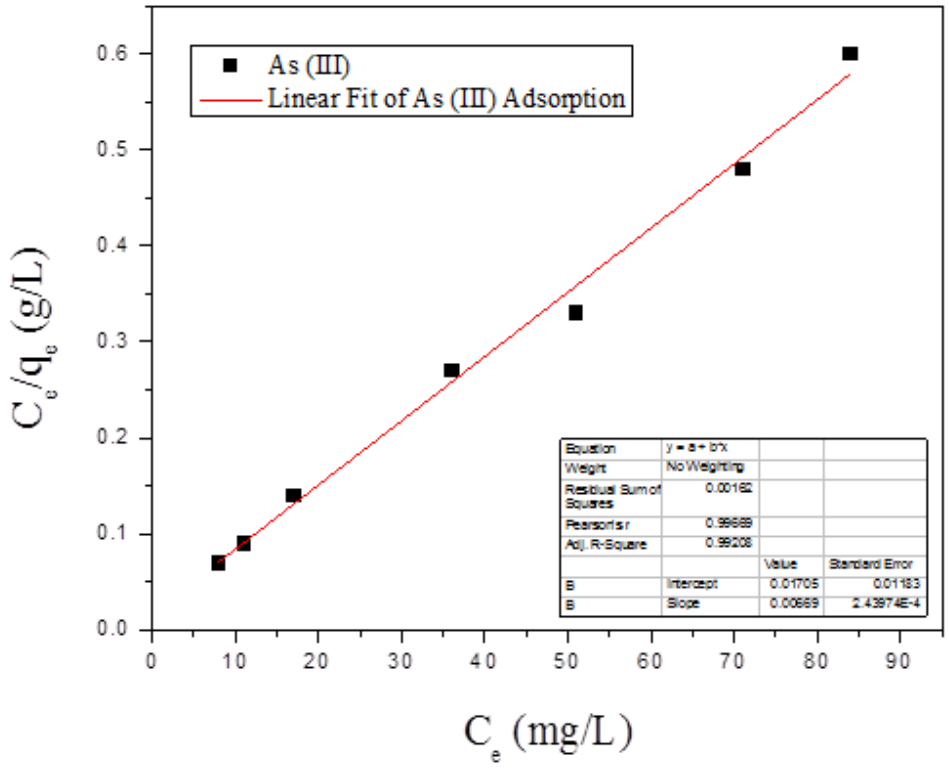

Figure 3.14 Langmuir Adsorption isotherm of As (III) adsorption by thiol-chitin nanofibers

Table 3.3 illustrates the parameters (i.e., the maximum adsorption capacity, Langmuir constant and correlation coefficient) extracted from the adsorption isotherms of As (III) ions for thiol-chitin nanofibers. Based on the results in Figure 3.17 and Table 3.3, As (III) adsorption closely fits the Langmuir Model with high a correlation coefficient of 0.997 and large adsorption capacity 149 mg/g at its optimum adsorption pH values).

Table 3.3 Parameters extracted from adsorption isotherms of As (III)

Heavy Metal Ions	q_m (mg/g)	b (L/mg)	R^2
	Maximum adsorption	Langmuir constant	Correlation coefficient

As (III)	149	0.392	0.997

3.3.6 Comparison with other thiol-modified adsorbents

The above thiol-modified chitin nanofiber adsorption results were compared with other competitive adsorbents at their optimal adsorption capacity, as listed in Table 3.4. Ferrihydrite has the highest adsorption at 266.5 mg/g at pH = 9. Previous studies showed the strong binding affinity between ferrihydrite and arsenic ions [62, 63]. In addition, the ferrihydrite sample listed in the table was freeze-dried after synthesis, which had a very large surface area exposed to the metal ion solution. It is also clear that all the adsorbents listed in the table might not have a large adsorption capacity due to their adsorption format, which was in powder form. These adsorbent powders had particle sites larger than a few millimeters and had a relatively low surface area, meaning that they already lost many potential adsorption sites. However, our thiol-modified chitin nanofibers had a nanoscale dimension that could provide hundreds of times higher active surface areas for adsorption than most of the listed materials. Besides, as mentioned above, the thiol groups had a strong affinity to arsenic ions that could also contribute to the adsorption capacity.

Table 3.4 Comparison of different adsorbents in arsenic adsorption

	Adsorbents	As (III) adsorption (mg/g)	Optimum adsorption pH	Initial Concentration (ppm)
1*	Thiol-resin dry powder [64]	30	8	10 ppm
2*	Thiol-chitosan bead [21]	2.5	7.0	10 ppm
3*	Chitosan powder [65]	58	4.0	400 ppm
4*	Active carbon (coconut husk)[66]	146.3	12.0	50 – 600 ppm
5*	Bead cellulose loaded with iron	99.6	7.0	1 -100 mmol/L

	oxyhydroxide (BCF) [67]			
6*	Ferrihydrite[63]	266.5	9	0.267 – 26.7 mmol/L
7	Chitin nanofiber	56	6.0	50 ppm
8	Thiol-chitin nanofiber	149	7.0	50 ppm

3.4 Conclusions

In conclusion, ultra-fine chitin nanofibers (diameter about 5 nm to 20 nm) with substantial amounts of amine groups (1.7 mmol/g) were formed by a series of chemical and mechanical treatments. These chitin nanofibers were subsequently coupled with cysteine to afford thiol-functionalized fibers (surface thiol concentration ≈ 1.1 mmol/g). The small size of tm-CNF fibers provided a very large surface-to-volume ratio with many active sites for arsenic ions adsorption. The fibers had a maximum capacity of 149 mg/g as generated by the Langmuir Adsorption Model. Furthermore, the nanofibers can be cross-linked to form an aerogel or hydrogel that could be a promising candidate to be commercialized for water purification applications involving the removal of heavy metal ions.

References

1. Acharyya, S.K. and B.A. Shah, *Groundwater arsenic contamination affecting different geologic domains in India - a review: influence of geological setting, fluvial geomorphology and Quaternary stratigraphy.* Journal of Environmental Science and

Health Part a-Toxic/Hazardous Substances & Environmental Engineering, 2007. **42**(12): p. 1795-1805.

2. Paul, K., *Groundwater arsenic contamination and human sufferings in West Bengal, India and Bangladesh: A review.* Abstracts of Papers of the American Chemical Society, 2006. **231**.

3. Rodriguez-Lado, L., et al., *Groundwater Arsenic Contamination Throughout China.* Science, 2013. **341**(6148): p. 866-868.

4. Liu, C.P., et al., *Arsenic contamination and potential health risk implications at an abandoned tungsten mine, southern China.* Environmental Pollution, 2010. **158**(3): p. 820-826.

5. Wang, Y.X., et al., *Model for the formation of arsenic contamination in groundwater. 1. Datong Basin, China.* Geochemistry International, 2009. **47**(7): p. 713-724.

6. McGuigan, C.F., et al., *A review on arsenic concentrations in Canadian drinking water.* Environmental Reviews, 2010. **18**: p. 291-307.

7. Christoforidou, E.P., et al., *Bladder cancer and arsenic through drinking water: A systematic review of epidemiologic evidence.* Journal of Environmental Science and Health Part a-Toxic/Hazardous Substances & Environmental Engineering, 2013. **48**(14): p. 1764-1775.

8. He, J. and L. Charlet, *A review of arsenic presence in China drinking water.* Journal of Hydrology, 2013. **492**: p. 79-88.

9. *Predicting Arsenic Contamination in Groundwater.* Jama-Journal of the American Medical Association, 2013. **310**(15): p. 1551-1551.

10. Singh, S.K., et al., *Groundwater Arsenic Contamination and Associated Health Risks in*

Bihar, India. International Journal of Environmental Research, 2014. **8**(1): p. 49-60.

11. Wai, C.M., J.S. Wang, and M.H. Yang, *Arsenic contamination of groundwater, Blackfoot disease, and other related health problems.* Biogeochemistry of Environmentally Important Trace Elements, 2003. **835**: p. 210-231.
12. Celik, I., et al., *Arsenic in drinking water and lung cancer: A systematic review.* Environmental Research, 2008. **108**(1): p. 48-55.
13. Yoshida, T., H. Yamauchi, and G.F. Sun, *Chronic health effects in people exposed to arsenic via the drinking water: dose-response relationships in review.* Toxicology and Applied Pharmacology, 2004. **198**(3): p. 243-252.
14. Sullivan, C., et al., *Disposal of water treatment wastes containing arsenic - A review.* Science of the Total Environment, 2010. **408**(8): p. 1770-1778.
15. Masscheleyn, P.H., R.D. Delaune, and W.H. Patrick, *Effect of Redox Potential and Ph on Arsenic Speciation and Solubility in a Contaminated Soil.* Environmental Science & Technology, 1991. **25**(8): p. 1414-1419.
16. Pal, P., et al., *Removal of arsenic from drinking water by chemical precipitation - A modeling and simulation study of the physical-chemical processes.* Water Environment Research, 2007. **79**(4): p. 357-366.
17. Pinisakul, A., et al., *Arsenic removal efficiency and mechanisms by electro-chemical precipitation process.* Water Science and Technology, 2002. **46**(9): p. 247-254.
18. Oehmen, A., et al., *Arsenic removal from drinking water through a hybrid ion exchange membrane - Coagulation process.* Separation and Purification Technology, 2011. **83**: p. 137-143.
19. Zhang, X.Z., et al., *Removal of Arsenic in Water by an Ion-Exchange Fiber with Amino*

Groups. Journal of Applied Polymer Science, 2008. **110**(6): p. 3934-3940.

20. Nguyen, V.T., et al., *Arsenic removal by a membrane hybrid filtration system.* Desalination, 2009. **236**(1-3): p. 363-369.
21. Mohan, D. and C.U. Pittman, *Arsenic removal from water/wastewater using adsorbents - A critical review.* Journal of Hazardous Materials, 2007. **142**(1-2): p. 1-53.
22. Driehaus, W., M. Jekel, and U. Hildebrandt, *Granular ferric hydroxide - a new adsorbent for the removal of arsenic from natural water.* Journal of Water Services Research and Technology-Aqua, 1998. **47**(1): p. 30-35.
23. Nishimura, T. and K. Tozawa, *Removal of Arsenic from Waste-Water by Addition of Calcium Hydroxide and Stabilization of Arsenic-Bearing Precipitate by Calcination.* Cim Bulletin, 1985. **78**(878): p. 75-75.
24. Ben Issa, N., et al., *Determination of inorganic arsenic species in natural waters-Benefits of separation and preconcentration on ion exchange and hybrid resins.* Analytica Chimica Acta, 2010. **673**(2): p. 185-193.
25. Visoottiviseth, P.A., F. In Reviews of Environmental Contamination Volume 197; Springer New York: 2009; Vol. 197, p 77.
26. Gholami, M.M., et al., *Application of reverse osmosis technology for arsenic removal from drinking water.* Desalination, 2006. **200**(1-3): p. 725-727.
27. Seidel, A., J.J. Waypa, and M. Elimelech, *Role of charge (Donnan) exclusion in removal of arsenic from water by a negatively charged porous nanofiltration membrane.* Environmental Engineering Science, 2001. **18**(2): p. 105-113.
28. Xia, S.J., et al., *Study of arsenic removal by nanofiltration and its application in China.* Desalination, 2007. **204**(1-3): p. 374-379.

29. Bang, S., et al., *Removal of arsenate from water by adsorbents: a comparative case study*. Environmental Geochemistry and Health, 2011. **33**: p. 133-141.

30. Maliyekkal, S.M., L. Philip, and T. Pradeep, *As(III) removal from drinking water using manganese oxide-coated-alumina: Performance evaluation and mechanistic details of surface binding.* Chemical Engineering Journal, 2009. **153**(1-3): p. 101-107.

31. Chuang, C.L., et al., *Adsorption of arsenic(V) by activated carbon prepared from oat hulls.* Chemosphere, 2005. **61**(4): p. 478-483.

32. Guan, X.H., et al., *Application of titanium dioxide in arsenic removal from water: A review*. Journal of Hazardous Materials, 2012. **215**: p. 1-16.

33. Gallegos-Garcia, M., K. Ramirez-Muniz, and S.X. Song, *Arsenic Removal from Water by Adsorption Using Iron Oxide Minerals as Adsorbents: A Review.* Mineral Processing and Extractive Metallurgy Review, 2012. **33**(5): p. 301-315.

34. Mathieu, J.L., et al., *Arsenic remediation of drinking water using iron-oxide coated coal bottom ash.* Journal of Environmental Science and Health Part a-Toxic/Hazardous Substances & Environmental Engineering, 2010. **45**(11): p. 1446-1460.

35. Wang, J.W.J., D. Bejan, and N.J. Bunce, *Electrochemical method for remediation of arsenic-contaminated nickel electrorefining baths.* Industrial & Engineering Chemistry Research, 2005. **44**(10): p. 3384-3388.

36. Mincea, M., A. Negrulescu, and V. Ostafe, *Preparation, Modification, and Applications of Chitin Nanowhiskers: A Review.* Reviews on Advanced Materials Science, 2012. **30**(3): p. 225-242.

37. Nair, K.G. and A. Dufresne, *Crab shell chitin whisker reinforced natural rubber nanocomposites. 1. Processing and swelling behavior*. Biomacromolecules, 2003. **4**(3): p.

657-665.

38. Ifuku, S. and H. Saimoto, *Chitin nanofibers: preparations, modifications, and applications.* Nanoscale, 2012. **4**(11): p. 3308-3318.

39. Ifuku, S., et al., *Preparation of Chitin Nanofibers with a Uniform Width as alpha-Chitin from Crab Shells.* Biomacromolecules, 2009. **10**(6): p. 1584-1588.

40. Ifuku, S., et al., *Simple preparation method of chitin nanofibers with a uniform width of 10-20 nm from prawn shell under neutral conditions.* Carbohydrate Polymers, 2011. **84**(2): p. 762-764.

41. Fan, Y.M., T. Saito, and A. Isogai, *TEMPO-mediated oxidation of beta-chitin to prepare individual nanofibrils.* Carbohydrate Polymers, 2009. **77**(4): p. 832-838.

42. Fan, Y., T. Saito, and A. Isogai, *Chitin nanocrystals prepared by TEMPO-mediated oxidation of alpha-chitin.* Biomacromolecules, 2008. **9**(1): p. 192-198.

43. Wang, L.C., et al., *Dissociation behaviors of carboxyl and amine groups on carboxymethyl-chitosan in aqueous system.* Journal of Polymer Science Part B-Polymer Physics, 2008. **46**(14): p. 1419-1429.

44. Sorlier, P., et al., *Relation between the degree of acetylation and the electrostatic properties of chitin and chitosan.* Biomacromolecules, 2001. **2**(3): p. 765-772.

45. Yang, R., et al., *Thiol-modified cellulose nanofibrous composite membranes for chromium (VI) and lead (II) adsorption.* Polymer, 2014. **55**(5): p. 1167-1176.

46. Riddles, P.W., R.L. Blakeley, and B. Zerner, *Ellman's reagent: 5, 5′-dithiobis (2-nitrobenzoic acid)—a reexamination.* Analytical biochemistry, 1979. **94**(1): p. 75-81.

47. Riddles, P.W., R.L. Blakeley, and B. Zerner, *Reassessment of Ellman Reagent.* Methods in Enzymology, 1983. **91**: p. 49-60.

48. Su, Y., et al., *Characterization of TEMPO-oxidized cellulose nanofibers in aqueous suspension by small-angle X-ray scattering.* Journal of Applied Crystallography, 2014. **47**(2): p. 788-798.

49. Fan, Y., *Studies on Preparation and Structural Characterization of Nano-Disperse Chitins.* Ph.D. Thesis, 2009.

50. Chatterjee, T., S. Chatterjee, and S.H. Woo, *Enhanced coagulation of bentonite particles in water by a modified chitosan biopolymer.* Chemical Engineering Journal, 2009. **148**(2-3): p. 414-419.

51. Jia, Z.S. and X.L. Li, *Determination of the deacetylation degree of chitosan by acid-base conductometric titration.* Chinese Journal of Analytical Chemistry, 2002. **30**(7): p. 846-848.

52. Raymond, L., F.G. Morin, and R.H. Marchessault, *Degree of Deacetylation of Chitosan Using Conductometric Titration and Solid-State Nmr.* Carbohydrate Research, 1993. **246**: p. 331-336.

53. dos Santos, Z.M., et al., *Determination of deacetylation degree of chitosan: a comparison between conductometric titration and CHN elemental analysis.* Carbohydrate Research, 2009. **344**(18): p. 2591-2595.

54. Cathell, M.D., et al., *Structurally colored thiol chitosan thin films as a platform for aqueous heavy metal ion detection.* Biomacromolecules, 2008. **9**(1): p. 289-295.

55. Liu, W., et al., *An investigation on the physicochemical properties of chitosan/DNA polyelectrolyte complexes.* Biomaterials, 2005. **26**(15): p. 2705-2711.

56. Tajc, S.G., et al., *Direct determination of thiol pK(a) by isothermal titration microcalorimetry.* Journal of the American Chemical Society, 2004. **126**(34): p. 10508-

10509.

57. Tang, S.S. and G.G. Chang, *Kinetic characterization of the endogenous glutathione transferase activity of octopus lens S-crystallin.* Journal of Biochemistry, 1996. **119**(6): p. 1182-1188.

58. *Bangladesh Consortium For Arsenic Management*

59. Kwok, K.C.M., et al., *Mechanism of arsenic removal using chitosan and nanochitosan.* Journal of Colloid and Interface Science, 2014. **416**(0): p. 1-10.

60. Hao, J.M., et al., *Enhanced removal of arsenite from water by a mesoporous hybrid material - Thiol-functionalized silica coated activated alumina.* Microporous and Mesoporous Materials, 2009. **124**(1-3): p. 1-7.

61. Min, M.H., et al., *Micro-nano structure poly(ether sulfones)/poly(ethyleneimine) nanofibrous affinity membranes for adsorption of anionic dyes and heavy metal ions in aqueous solution.* Chemical Engineering Journal, 2012. **197**: p. 88-100.

62. Jain, A. and R.H. Loeppert, *Effect of competing anions on the adsorption of arsenate and arsenite by ferrihydrite.* Journal of Environmental Quality, 2000. **29**(5): p. 1422-1430.

63. Raven, K.P., A. Jain, and R.H. Loeppert, *Arsenite and arsenate adsorption on ferrihydrite: Kinetics, equilibrium, and adsorption envelopes.* Environmental Science & Technology, 1998. **32**(3): p. 344-349.

64. Styles, P.M., M. Chanda, and G.L. Rempel, *Sorption of arsenic anions onto poly(ethylene mercaptoacetimide).* Reactive & Functional Polymers, 1996. **31**(2): p. 89-102.

65. Mcafee, B.J., et al., *Biosorption of metal ions using chitosan, chitin, and biomass of Rhizopus oryzae.* Separation Science and Technology, 2001. **36**(14): p. 3207-3222.

66. Eguez, H.E. and E.H. Cho, *Adsorption of Arsenic on Activated-Charcoal.* Journal of

Metals, 1987. **39**(7): p. 38-41.

67. Guo, X.J. and F.H. Chen, *Removal of arsenic by bead cellulose loaded with iron oxyhydroxide from groundwater.* Environmental Science & Technology, 2005. **39**(17): p. 6808-6818.

Chapter 4 Radical Polymerized Cellulose Composite Ultrafiltration Membranes

Abstract

An ultrafiltration membrane with a hydrophobic surface was made by radical polymerization of styrene and divinylbenzene (DVB) at different composition ratios at the membrane surface. The surface of the composite membrane layer-by-layer structure (from bottom to top: PET, e-spun PAN, Cellulose nanofiber layer, radical polymerization of DVB and styrene) was characterized by SEM, atomic force microscopy (AFM) and water contact angle measurement. In addition, porometry studies, molecular weight cutoff (MWCO), and filtration performance was tested. A series of chemical treatments: acid, base, toluene, and methyl ethyl ketone (MEK), were applied to test the chemical resistance of the membrane. Based on runs of testing and experiments, optimum membrane fabrication conditions were achieved, resulting in a highly cross-linked membrane with maximum pore size of 12 nm which was toluene and MEK resistant.

Key words: styrene, divinylbenzene, polymerization, cellulose, ultrafiltration membrane

4.1 Introduction

As previously discussed in the introduction to Chapter 1, membrane filtration plays an important role in separation and purification, both in academic research and in various industries. Microfiltration (MF) membrane usually refers to a membrane with pore sizes ranging from 0.1 μm to 10 μm that filters away particles, such as bacteria and pathogens [1]. Ultrafiltration (UF) membranes with pore sizes in the range of 10 nm to 100 nm can block smaller units, such as proteins and gelatin [2]. The common commercialized MF membrane production varies from ceramic membrane fabrication, polymeric membrane fabrication by phase inversion [3, 4] or electrospinning [5-7]. Despite the hollow fiber-based ultrafiltration[8] or nanoporous carbon membrane [9], a common method of ultrafiltration fabrication is by thin-film/chemical coating or deposition on top of the MF or equivalent filter substrate to minimize the pore size and functionalize the membrane surface [10-12].

Previous research in our group has been successful in producing e-spun nanofibrous MF membranes (made of polyacrylonitrile, polyvinylalcohol) with high pure water flux, uniform pore size, and a high rejection ratio for bacteria (e.g. Escherichia coli, > 99.9999%) [13, 14]. In addition, ultra-fine cellulose nanofibers have also been produced and coated on the top of e-spun membranes to generate cellulose cross-linked barrier layer UF membranes with a smaller pore size while retaining a high water flux and allowing adsorption of positively charged dyes and UO_2^{2+} [15, 16]. A schematic representation of the three layer membrane can be found in the following Figure 4.1, a hydrophilic, cellulose nanofiber top layer coated on a non-woven e-spun nanofibrous middle layer, supported by a micron-scale pore nonwoven bottom layer. In this research, we introduce a novel method of barrier layer fabrication with cellulose nanofibers incorporated to minimize the membrane pore size to filter away smaller particle sizes.

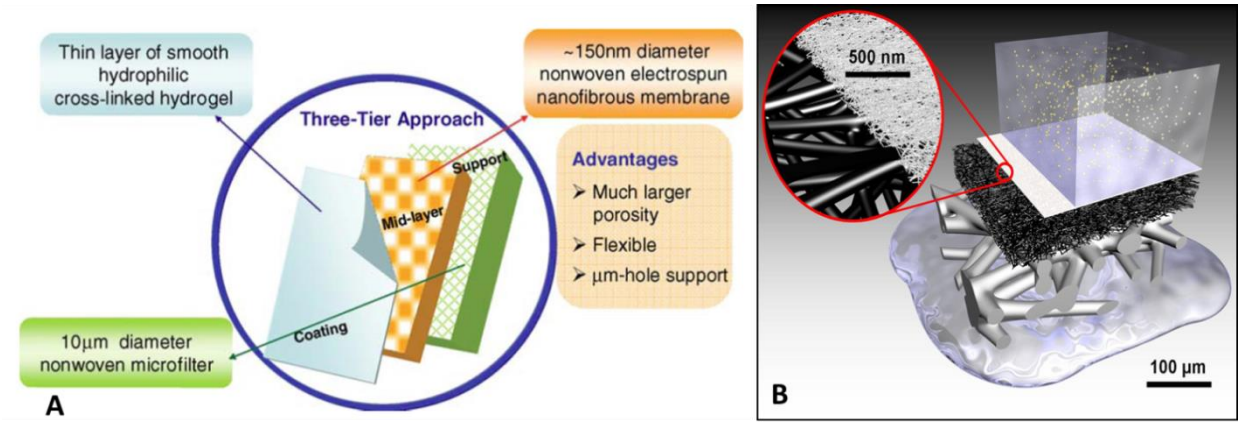

Figure 4.1 Schematic representation of novel composite membrane structure, (A) layer by layer structure with corresponding layer properties (figure reprinted with permission from reference [17]), (B) demonstration of cellulose/PAN/PET 3-layer composite membrane in water filtration (figure reprinted with permission from reference [18]).

4.2 Materials and Methods

4. 2.1 Materials

Styrene (contains 4-tert-butylcatechol as stabilizer, ≥ 99%), divinylbenzene (DVB) (technical grade ≥ 80 %), 2,2,6,6-tetramethyl-1-piperidinyloxy (TEMPO), sodium hypochlorite (NaClO), 98% 2,2'-Azobis(2-methylpropionitrile) (AIBN) (recrystallized twice from methanol to purify before reaction), and dextran (from *Leuconstoc mesenteroides*) were purchased from Sigma Aldrich. Polyacrylonitrile (PAN, Mw=150,000 g/mol) was purchased from Scientific Polymer Products. Cellulose Biofloc-92 (wood bleached pulp) was provided from Tartas, France.

Non-woven poly (ethylene terephthalate) (PET) microfilter substrate with an average fiber diameter ~10 μm for membrane support was provided by Sanko (Japan No. 16-1).

4.2.2 Preparation of e-spun PAN nanofiber

PAN was dissolved in DMF to form a solution by stirring for 2 days at 60 °C in a sealed glass container to obtain 7 wt% homogeneous solutions. The PAN solution was electrospun onto a PET nonwoven support at 15 kV by the electrospinning apparatus described previously. More detailed information could be found in the Chapter 2 experimental section of electrospinning.

4.2.3 Preparation of TEMPO oxidized cellulose nanofiber

A cellulose nanofiber suspension was prepared by the TEMPO oxidation method and purified by dialysis. The concentration was confirmed by TOC. More detailed information could be found in the Chapter 2 experimental section of TEMPO-oxidized cellulose preparation.

4.2.4 Preparation of cellulose coated UF membrane

After PAN was e-spun onto PET, the PAN/PET composite membrane was dipped into pH = 1.2 HCl aqueous solution until saturated (~ 30 seconds). A rubber roller was used to remove bubbles below the membrane substrate as well as excess solution. A 0.35 wt% cellulose nanofiber suspension was cast on the top of the substrate and the coating process was applied by using a draw-down machine (Gardco DP-8301), as shown in Figure 4.2 (left). Figure 4.2 (right) is a schematic representation of a draw-down machine. It controls the coating thickness of the cellulose to about 200 μm by the thickness of the tape around the membrane. After coating, the membrane was dried in an oven at 75 °C for 20 min.

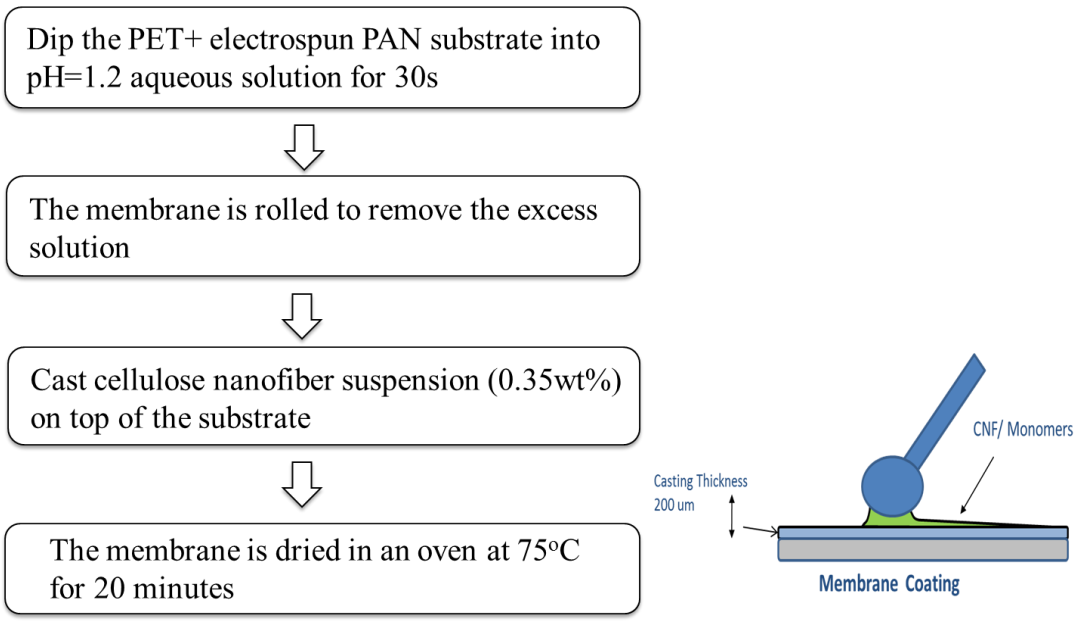

Figure 4.2 Cellulose nanofiber coating steps (left) and draw-down coating machine demonstration (right)

4.2.5 Preparation of radical polymerized UF membrane

Radical polymerization of styrene and DVB on the surface of a cellulose-coated UF membrane was conducted in the following way, as shown in Figure 4.3. A 10 cm × 10 cm substrate was sprayed with DI water (~ 5 mL) and the membrane top layer was partially dried (no liquid flow) with a heat-gun (~ 60 ºC) for ~ 1 min . Then, the wet membrane was fixed onto a 20 cm × 20 cm glass plate with the four edges sealed with chemical-resistant polyamide tape. After that, 10 mL organic solution (containing styrene, DVB, AIBN) was cast on the top of the wet membrane. A steel roller was used to remove excess organic solution. Then, the membrane, being stabilized on the plate, was put in the oven at 95 ºC for 0.1 h to 2 hours for polymerization. The AIBN added was from 1 wt% to 5 wt% for different trials.

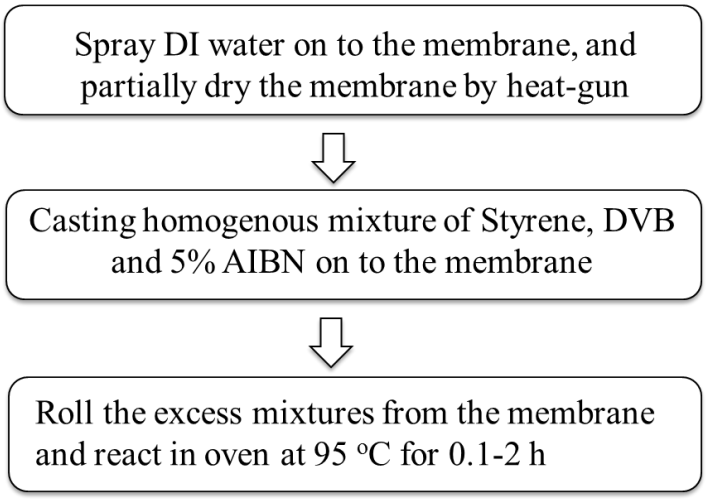

Figure 4.3 Radical polymerized barrier layer UF membrane

4.2.6 Membrane morphology characterization

The e-spun MF membrane, cellulose coated UF membrane, and radical polymerized UF membrane top view and cross-section morphology structures were analyzed by SEM (LEO 1550, Carl Zeiss). More detailed information can be found in the Chapter 2 analysis of membrane geometrical studies experimental section. Specifically, the membrane cross-section was prepared by instant fracturing the water-wet membrane in liquid nitrogen. Then all samples were coated with gold for 45s in vacuum.

The pore size and distribution studies were carried out by Capillary Flow Porometer (Porous Materials Inc., CFP-1500A, USA). More detailed information regarding the test can be found in Chapter 2 experimental section of membrane porometry test.

Atomic Force Microscopy (AFM) measurements were conducted through a Nanoscope III AFM (Digital Instrument 3000) in the contact mode. The root mean square measurement in the

scale was 5 μm × 5 μm. The measurement included surface roughness of the cellulose-coated UF membrane and radical polymerized UF membrane at different monomer compositions.

The water contact angle test of membrane hydrophobicity was conducted by a CAM200 Optical Contact Angle Meter (KSV Instrument, LTD) to measure the water droplet contact angle. During the test, the membrane was taped on to a glass slide, followed by dropping a 5 μL drop of water for 5 seconds while capturing the image by CAM software. Then, the water contact angle was calculated by a curve fitting method.

4.2.7 Membrane filtration performance

The water flux was measured by a dead-end filtration cell (Microsyringe Filter Holder – 3002500, Millipore) as a function of time and pressure. The flux test was conducted at 2 psi to 30 psi based on different membranes at room temperature by determination of the water volume passing through the membrane per unit area, time, and pressure. The rejection test was conducted in the same equipment as the flux test; the feed solution was 500 ppm dextran at different molecular weight. Rejection was determined by testing the dextran concentration difference between the feed and permeate solutions, as confirmed by TOC. Calculation of flux (4.1) and rejection (4.2) are shown in both equations below.

$$\text{Permeate flux} \quad P = \Delta V/(S \bullet \Delta t) \tag{4.1}$$

$$\text{Rejection rate (\%)} = 100\% \times (1 - C_p/C_f) \tag{4.2}$$

In both equation 4.1 and 4.2, ΔV is volume of water though the membrane in a given time Δt; S is the membrane effective area; and C_f and C_p are the concentrations of the feed and permeate, respectively, as determined by TOC.

4.3 Results and Discussions

4.3.1 Characterization of E-spun MF membranes

The composite membrane consists of the following layers, from bottom to top: nonwoven PET layer, electrospun PAN layer, cellulose coating layer, and radical polymerized barrier layer. Characterization of each layer was conducted in the following manner.

The bottom layer was nonwoven PET, which has excellent mechanical strength as a supporting layer, as has been demonstrated in previous studies of our group [19]. A typical thickness of the PET membrane we used was about 110 µm, with fiber diameters of around 30 µm, measured by a micrometer. PET was used as a substrate to collect e-spun nanofibers generated by the electrospinning machine. Specifically, the (7 wt% PAN solution) e-spun nanofibrous membrane collected on the PET was about 40 µm (can be 30 µm to 50 µm depending on the electrospinning process time). Figure 4.4 (A) shows an SEM image of a (7 wt%) PAN nanofibrous membrane with fiber diameters of 200 nm ± 30 nm. Figure 4.4 (B) was determine by capillary flow porometry explained in Chapter 2 experimental section 2.2.6 and it shows the distribution of pore size diameters of the e-spun nanofibrous MF membrane with mean flow pore size of 690 nm ± 10 nm. The relationship between the pore size and e-spun fiber diameter was roughly 3:1, which corresponded to the previous studies [5, 6], showing that the mean pore size was about 3 times larger than the mean e-spun fiber diameter. The pure water flux of this MF membrane was about 3000 $L \cdot m^{-2} \cdot h^{-1} \cdot psi^{-1}$.

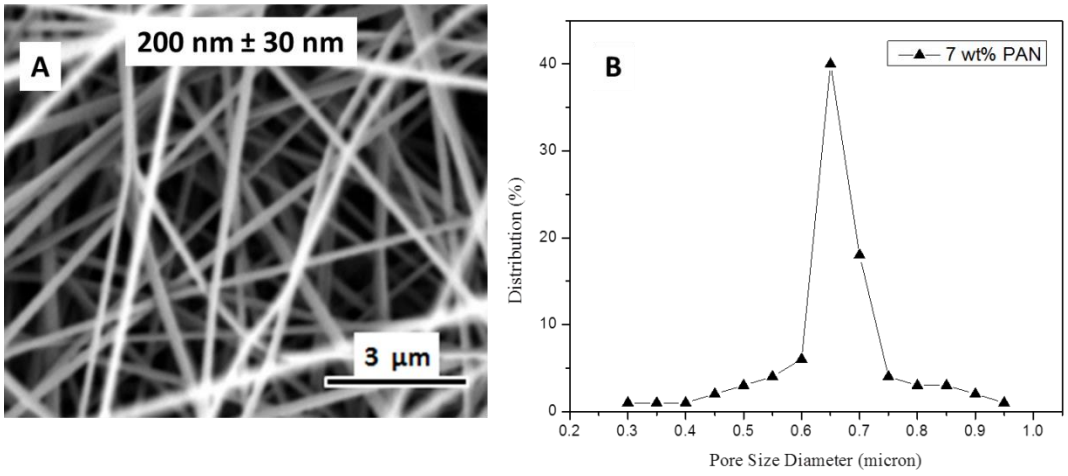

Figure 4.4 (A) SEM images of 7 wt% e-spun nanofibrous membrane, (B) pore size distribution of e-spun membrane as determined by Capillary Flow Porometry

4.3.2 Characterization of cellulose nanofibers coated UF Membranes

Specifically, the cellulose nanofiber for the membrane-coating purpose was produced by adding 6 mmol of NaClO per gram of cellulose in the TEMPO oxidation process. It resulted in around 1.5 mmol/g of carboxylate and 0.2 mmol/g of aldehyde groups being functionalized on the surface of cellulose nanofibers. Figure 4.5 (A) & (B) show the cross-section & the top view of the cellulose nanofiber-coated membrane. In Figure 4.5 (A), it can be seen that the bottom layer is a matrix of e-spun PAN nanofibers, on top of which is a cellulose nanofiber-coated ultra-thin layer with a thickness of 250 nm ± 30 nm. In Figure 4.5 (B), the top view of this UF membrane surface, a uniform and semitransparent thin film can be observed and the e-spun nanofibers substrate is also observable.

The cellulose nanofibrous thin film generating process involves 75 °C heating for 20 min. Due to the large amount of cellulose nanofiber surface functional groups, including hydroxyl, carboxylate and aldehyde, as well as the nanoscale fiber structures, several physical and chemical reactions could happen during this process [20] [21].

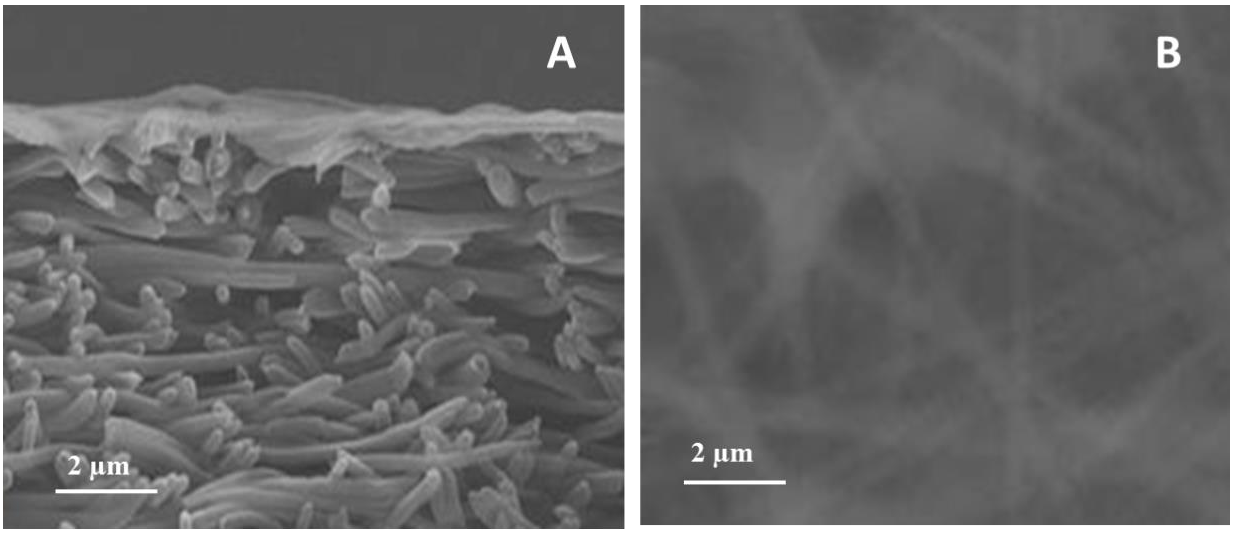

Figure 4.5 SEM images of cellulose nanofiber layer, cross-section (A) and top view (B)

The molecular weight cutoff (MWCO) studies were applied to evaluate the pore size of the cellulose nanofiber-coated UF membrane. The pore size could not be observed by SEM due to the nanoscale pore size. During the studies, the concentrations of dextran with different molecular weights were tested before and after membrane filtration as in feed solution and in permeate solution. The average pore size of the membrane could be calculated as a Stokes-Einstein radius (r_s in Å) in the following empirical equation 4.3 [19, 21, 22]:

$$r_s = 0.33 \times (MW)^{0.463} \quad 4.3$$

In the equation above, the molecular weight (MW) refers to the molecular weight of dextran in Da. Therefore, the diameter of 5000 KDa dextran has a diameter of 83.4 nm, according to the equation calculation. Figure 4.6 shows the MWCO of cellulose-coated UF membrane. It can be seen that the cellulose nanofibrous membrane has an over 90% rejection ratio of 5000 KDa dextran, indicating that more than 90% of the pores of the cellulose-coated top layer were smaller than 83 nm in diameter. The corresponding direct filtration pure water flux (tested by dead-end cell) was about 16 $L \cdot m^{-2} \cdot h^{-1} \cdot psi^{-1}$.

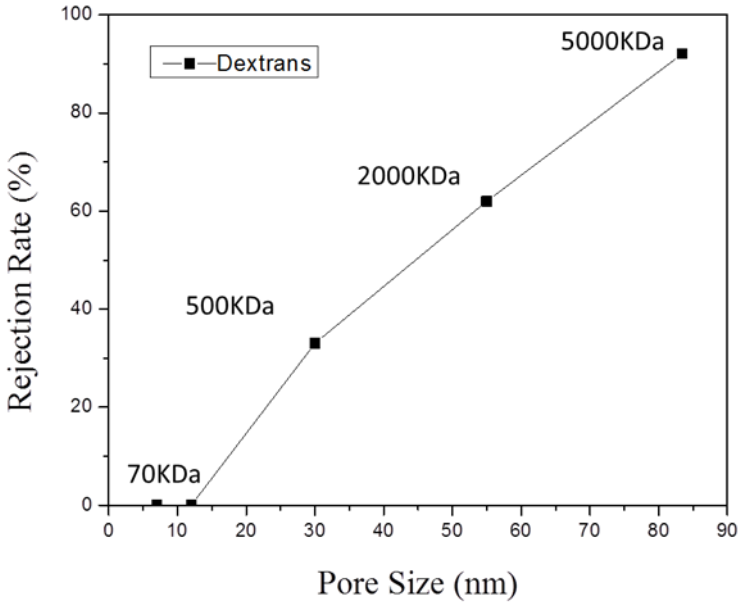

Figure 4.6 Molecular weight cut off (MWCO) of cellulose coated UF membrane

4.3.3 Surface characterization of radical polymerized UF membranes

Based on the UF membrane, radical polymerization was carried out at different ratios of styrene and divinylbenzene (DVB) in the presence of thermo-initiator AIBN on top of and within

the cellulose barrier layer. The reaction temperatures ranging from 60 °C to 120 ºC were tested to obtain the optimum condition. The AIBN half-life was also taken into consideration. It is 10 hours at 64 ºC, 1.0 hour at 85 °C, and 0.1 h at 101 ºC [23-25]. Based on preliminary results of membrane filtration performance, a 95 °C reaction temperature was selected. One crucial step was to ensure that the polymerization reaction was only carried out in the cellulose barrier layer. In order to achieve this, the cellulose UF membrane was saturated with water first since both monomers were insoluble in water. A schematic representation of polymerization in the cellulose barrier layer is shown in Figure 4.7. In addition, since this reaction was carried out on the membrane surface, many limiting processes could happen during the reaction, such as evaporation of the reactant which could prevent further polymerization.

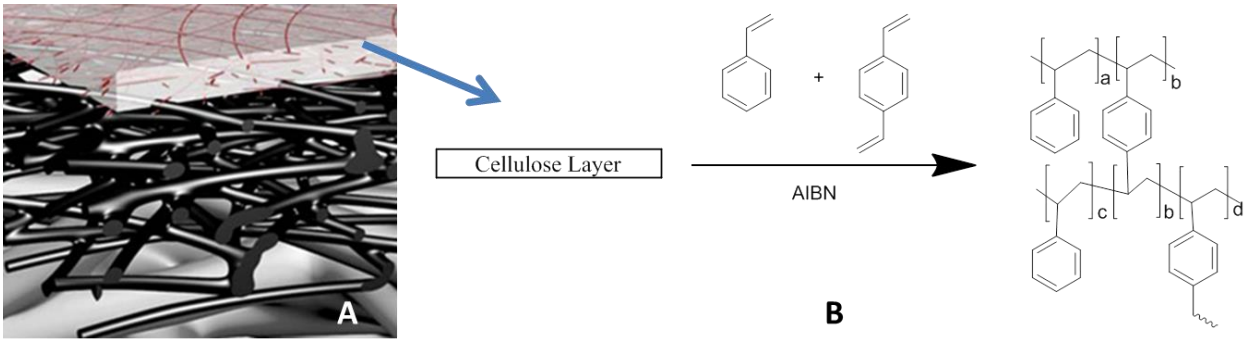

Figure 4.7 Schematic representation of cellulose coated UF membrane (A) [31] with representation of styrene and DVB polymerization reaction in the barrier layer (B)

After the polymerization reaction, the membrane top barrier layer was analyzed by SEM as shown in Figure 4.8; (A) is a cross-section of polymerized membrane and Figure 4.8 (B) is the top view of the image. We can see that there is no penetration after the polymerization reaction, in which the styrene and DVB ratio was well controlled on the top cellulose barrier layer. In

addition, it can also be seen from the AFM image below that with different membrane top layer composition, the surface roughness changes. Figure 4.9 (A) is cellulose-coated UF membrane with surface roughness of 12 ± 3 nm; Figure 4.9 (B) is 20 wt% styrene to 80 wt% DVB barrier layer with a surface roughness 17 ± 5 nm; and Figure 4.9 (C) is 100 wt% DVB polymerization giving a surface roughness of 27 ± 4 nm.

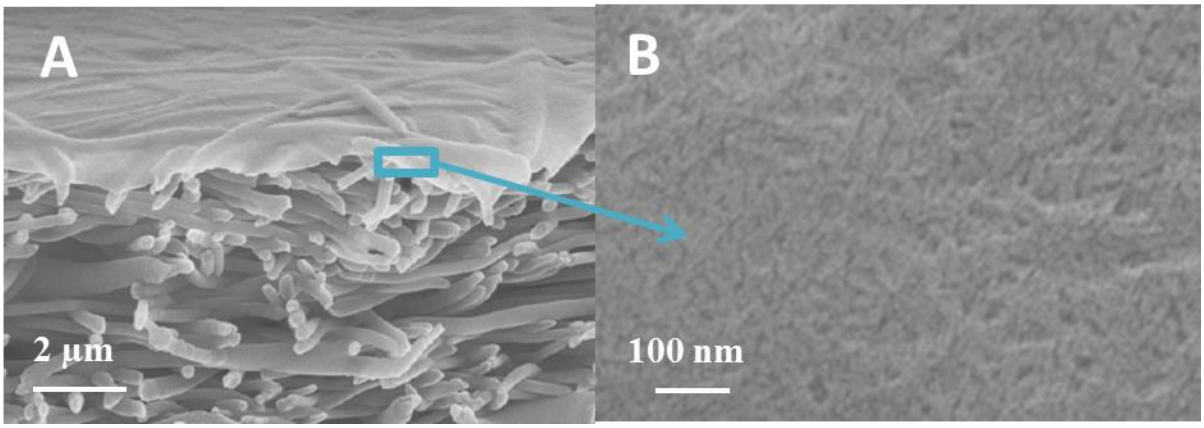

Figure 4.8 cross-section and top view of radical polymerized UF membrane

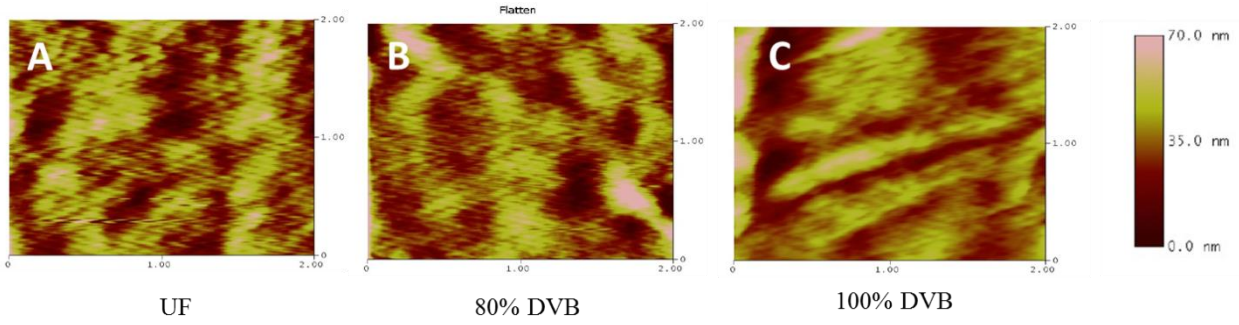

Figure 4.9 AFM image of membrane surface roughness of different barrier layer composition.

The cellulose-coated UF membrane is hydrophilic on the surface due to the hydrophilic property of cellulose nanofibers on the surface. We can see from the Figure 4.10 that the 0 min reaction time refers to the cellulose-coated UF membrane, the water contact angle was 20° ± 1°. Both styrene and DVB are hydrophobic monomers and the copolymerization results in a hydrophobic surface. Specifically, the polymerization was carried out at styrene to DVB ratio of 1:4 (by weight) with 5 wt % AIBN at 95 °C from 0 min to 60 min. It can be seen from the same figure that the 15 min reaction time led to the contact angle of 44º ± 1º. When the polymerization time was increased, the hydrophobicity was also increased. After 30 min reaction, the membrane surface hydrophobicity remained at 96º ± 1º.

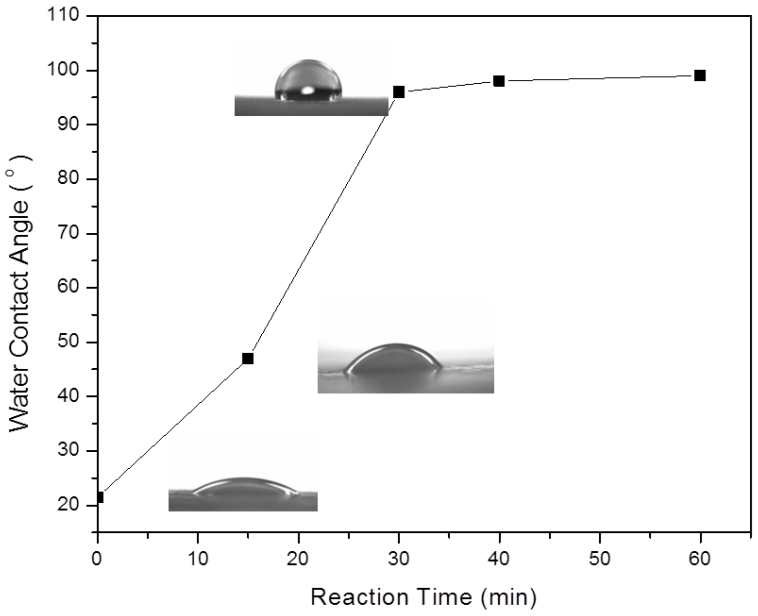

Figure 4.10 Relationship of water contact angle and membrane surface polymerization time

4.3.4 Radical polymerized barrier layer membrane filtration performance

Both the flux and rejection membrane filtration tests were conducted through a dead-end filtration cell at 30 psi. A series of monomer ratios by weight of styrene and DVB was analyzed. The reaction condition for all ratios was 95 °C for 60 min. Figure 4.11 (left) below gives the pure water flux of this radical polymerized membrane at different DVB compositions and Figure 4.11 (right) is rejection ratio of 500 ppm 70 kDa dextran. The trade-off relationship between the flux and rejection is clearly seen; a high flux refers to a respectively loose network barrier layer structure, but correspondingly leads to a lower rejection ratio. DVB working as a cross-linker, which a larger initial amount added led to smaller molecular cavities and a more condensed structure. The rejection performance of 70kDa dextran of over 90% means that membrane barrier layer consisting of 80 wt% DVB has more than 90% pores smaller than 12 nm, based on the Stokes-Einstein radius calculation in equation 4.3.

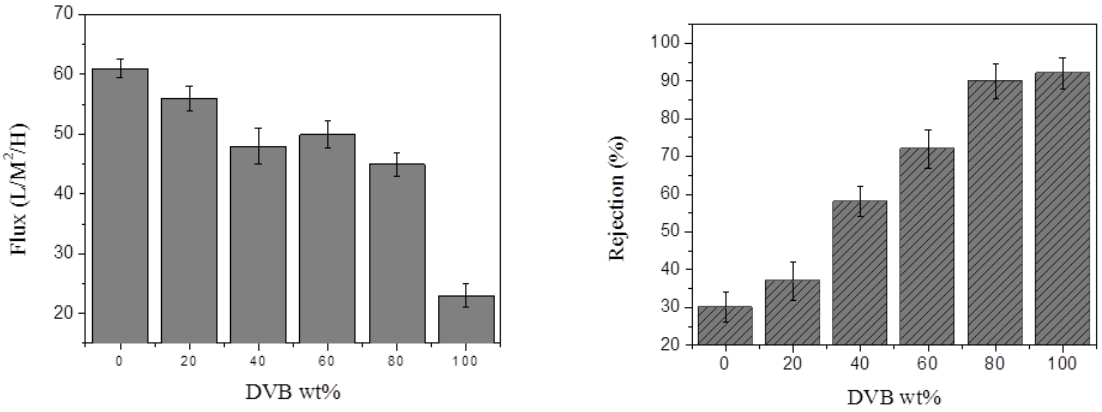

Figure 4.11 pure water flux (left) and 70 kDa dextran rejection (right) of membrane with different DVB composition

4.3.5 Membrane chemical resistance and potential applications

The styrene and DVB copolymerization generated a very rigid molecular network, making the thin film top barrier layer dense and firm. After strong acid (HCl pH = 1) and strong base (NaOH pH = 14) treatments for 48 hours each, the membrane surface morphology did not change and the membrane retained the same water flux. In addition, the membrane was also resistant to dewaxing solvent: toluene and methyl ethyl ketone (MEK) with 3 : 5 volume ratio for over 60 hours without membrane structural changes. Figure 4.12 is a SEM image of a membrane after immersion in a solvent mixture (Toluene: MEK = 3:5). It is seen both from the top view and cross-section image that no apparent difference was observable in comparison with the images before chemical treatment.

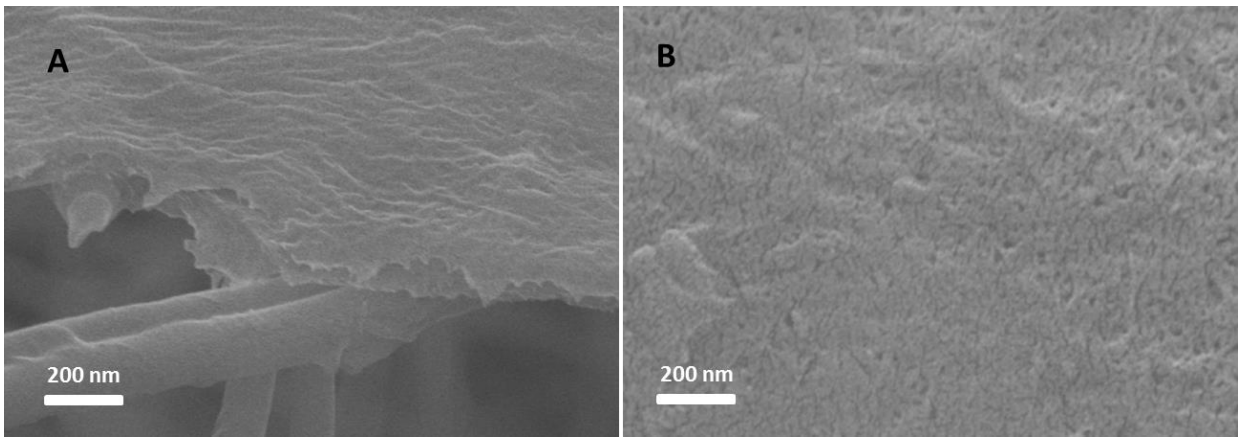

Figure 4.12 A cross-section and (B) top view of membrane after immersion in solvent mixture (Toluene: MEK = 3:5)

Since the radical polymerized UF membrane has good resistance in MEK and toluene, one of the possible applications is to separate dewaxing oil from the dewaxed solvent (MEK and toluene)[26]. Similar systems prepared by grafting polystyrene onto polyacrylonitrile (PAN) UF membranes have been applied in dewaxing oil separations [27-29]. The styrene-grafted PAN UF

membranes are reported to have a polystyrene barrier layer with a maximum pore size of 24 nm, a water contact angle of 77º, dewaxed solvent (Toluene: MEK = 3:5) flux of 0.2 $L \cdot m^{-2} \cdot h^{-1}$ at 290 psi, and a lube oil rejection of 90.2%. Although our research was limited by the testing pressure (about 290 psi) and test equipment (Steel-made dead-end cell), the highly crosslinked polymer network structure with minimum pore size 12 nm and ultra-thin barrier layer (~200 nm) with a flat surface (roughness 17 ± 5 nm) could be a promising candidate for dewaxing filtration.

4.4 Conclusions

In conclusion, a novel ultrafiltration membrane was fabricated by radical polymerization of styrene and DVB on the top of a cellulose-coated ultrafiltration composite membrane. The barrier layer polymerization network molecular cavity generates maximum pore size of 12 nm, with pure water flux of 47 ± 3 $L \cdot m^{-2} \cdot h^{-1}$. The membrane's rigid crosslinked network is strongly resistant to wastewater at both acidic and basic conditions. It is able to filter particles larger than 12 nm. In addition, the strong resistance to toluene and MEK make it a promising candidate for oil dewaxing filtration applications.

References

1. Muilenberg, T., *Water management with membrane technologies: The benefits of microfiltration.* Pollution Engineering, 2003. **35**(5): p. 22-25.
2. Mehta, A. and A.L. Zydney, *Permeability and selectivity analysis for ultrafiltration membranes.* Journal of Membrane Science, 2005. **249**(1-2): p. 245-249.

3. Shin, S.J., et al., *Preparation and characterization of polyethersulfone microfiltration membranes.* Desalination, 2005. **186**(1-3): p. 1-10.

4. Susanto, H., N. Stahra, and M. Ulbricht, *High performance polyethersulfone microfiltration membranes having high flux and stable hydrophilic property.* Journal of Membrane Science, 2009. **342**(1-2): p. 153-164.

5. Liu, Y., et al., *High-flux microfiltration filters based on electrospun polyvinylalcohol nanofibrous membranes.* Polymer, 2013. **54**(2): p. 548-556.

6. Wang, R., et al., *Electrospun nanofibrous membranes for high flux microfiltration.* Journal of Membrane Science, 2012. **392**: p. 167-174.

7. Daels, N., et al., *Potential of a functionalised nanofibre microfiltration membrane as an antibacterial water filter.* Desalination, 2011. **275**(1-3): p. 285-290.

8. Li, J.S., et al., *Preparation of alumina hollow fiber ultrafiltration membrane by filtering coating.* Chinese Journal of Catalysis, 2002. **23**(5): p. 453-456.

9. Shah, T.N., H.C. Foley, and A.L. Zydney, *Development and characterization of nanoporous carbon membranes for protein ultrafiltration.* Journal of Membrane Science, 2007. **295**(1-2): p. 40-49.

10. Facciotti, M., et al., *Deposition of thin ultrafiltration membranes on commercial SiC microfiltration tubes.* Ceramics International, 2014. **40**(2): p. 3277-3285.

11. Syafei, A.D., C.-F. Lin, and C.-H. Wu, *Removal of natural organic matter by ultrafiltration with TiO2-coated membrane under UV irradiation.* Journal of Colloid and Interface Science, 2008. **323**(1): p. 112-119.

12. Karnik, B.S., et al., *Removal of Escherichia coli after treatment using ozonation-ultrafiltration with iron oxide-coated membranes.* Ozone-Science & Engineering, 2007. **29**(2): p. 75-84.

13. Sato, A., et al., *Novel nanofibrous scaffolds for water filtration with bacteria and virus removal capability.* Journal of Electron Microscopy, 2011. **60**(3): p. 201-209.

14. Ma, H., B.S. Hsiao, and B. Chu, *Thin-film nanofibrous composite ultrafiltration membranes based on polyvinyl alcohol barrier layer containing ultra-fine cellulose nanofibers.* Abstracts of Papers of the American Chemical Society, 2011. **241**.

15. Ma, H., B.S. Hsiao, and B. Chu, *Ultrafine Cellulose Nanofibers as Efficient Adsorbents for Removal of UO22+ in Water.* Acs Macro Letters, 2012. **1**(1): p. 213-216.

16. Ma, H., et al., *Nanofibrous Microfiltration Membrane Based on Cellulose Nanowhiskers.* Biomacromolecules, 2012. **13**(1): p. 180-186.

17. Burger, C., B.S. Hsiao, and B. Chu, *Nanofibrous materials and their applications.* Annu. Rev. Mater. Res., 2006. **36**: p. 333-368.

18. Ma, H.Y., et al., *Ultrafine Polysaccharide Nanofibrous Membranes for Water Purification.* Biomacromolecules, 2011. **12**(4): p. 970-976.

19. Ma, H.Y., B.S. Hsiao, and B. Chu, *High-flux thin-film nanofibrous composite ultrafiltration membranes containing cellulose barrier layer.* Abstracts of Papers of the American Chemical Society, 2010. **240**.

20. Yang, R., et al., *Thiol-modified cellulose nanofibrous composite membranes for chromium (VI) and lead (II) adsorption.* Polymer, 2014. **55**(5): p. 1167-1176.

21. Ma, H.Y., et al., *Fabrication and characterization of cellulose nanofiber based thin-film nanofibrous composite membranes.* Journal of Membrane Science, 2014. **454**: p. 272-282.

22. Venturoli, D. and B. Rippe, *Ficoll and dextran vs. globular proteins as probes for testing glomerular permselectivity: effects of molecular size, shape, charge, and deformability.* American Journal of Physiology-Renal Physiology, 2005. **288**(4): p. F605-F613.

23. Chanda, M., Introduction to Polymer Science and Chemistry: A Problem-Solving Approach p. 379, section 6.12.

24. Odian, G., *Principles of Polymerization, 2nd ed., Wiley: New York, 1981, 196.*

25. Brandrup, J.I., E.H.; Grulke, E.A. Eds., *Polymer Handbook, 4th ed., Wiley: New York, 1999, II, 3.*

26. Zhao, Z.P., et al., *Nanofiltration membrane prepared from polyacrylonitrile ultrafiltration membrane by low-temperature plasma 2. Grafting of styrene in vapor phase.* Journal of Membrane Science, 2005. **251**(1-2): p. 239-245.

27. Chen, J., et al., *Nanofiltration membrane prepared from polyacrylonitrile ultrafiltration membrane by low-temperature plasma: 5. Grafting of styrene in vapor phase and its application.* Surface & Coatings Technology, 2007. **201**(15): p. 6789-6792.

28. Zhao, Z.P., et al., *Nanofiltration membrane prepared from polyacrylonitrile ultrafiltration membrane by low-temperature plasma: 4. Grafting of N-vinylpyrrolidone in aqueous solution.* Desalination, 2005. **184**(1-3): p. 37-44.

29. Zhao, Z.P., et al., *Nanofiltration membrane prepared from polyacrylonitrile ultrafiltration membrane by low-temperature plasma I. Graft of acrylic acid in gas.* Journal of Membrane Science, 2004. **232**(1-2): p. 1-8.

30. Kim, J.B., et al., *Preparation of TiO2 Nanoparticle from Ti-Salt Flocculated Sludge with Dye Wastewater*. Journal of Nanoscience and Nanotechnology, 2010. **10**(5): p. 3260-3265.

31. In courtesy of Dr. Christine Burger for (A) the 3D membrane structure

Chapter 5 Conclusions

Water scarcity and contamination are long term global issues. A variety of human health problems are caused by water pollution. Nanotechnology has been widely fabricated, studied, and applied in the water purification field for adsorption and separation both in academic research as well as in industry. Among these, polysaccharide-based nanofibrous materials stand out due to their nanoporous structure and tremendous potential effective sites. These can be further developed as both adsorbents and filtration media.

As presented in Chapter 2, cellulose nanofibers, produced by TEMPO oxidation method, have a uniform fiber size of 5 – 10 nm in width and a few hundred nanometers in length. These ultra-fine nanofibers have many surface carboxylate groups which can graft to cysteine to be thiol-functionalized. The thiol-modified cellulose nanofibers' adsorption efficiency of chromium and lead ions was tested as function of pH, contact time, and different initial concentration to generate maximum capacity. In addition, they were incorporated with an e-spun nanofibrous membrane to produce a MF filter candidate for heavy metal adsorption with high regeneration efficiency.

In Chapter 3, chitin nanofibers, generated from shrimp shells by a series of chemical and mechanical treatments, can produce fiber sizes ranging from 5 – 20 nm with abundant amine groups and can be well suspended in aqueous solutions. Chitin fibers were modified with thiols to remove arsenic ions from water by chelating effects, tested at different pHs and initial metal ion centration.

In Chapter 4, a novel UF membrane was fabricated based on the recently established high flux 3-layer membrane structure containing PET as the bottom substrate, e-spun PAN as the middle supporting layer, and cellulose coating as the top layer. Radical polymerization of styrene and DVB was carried out on the cellulose layer to generate a novel UF membrane with smaller pore size. The new barrier layer was created by changing various monomer compositions to achieve the optimum flux-rejection condition, producing a highly cross-linked membrane surface structure with 12 nm pore size. Future work of this project could be applying different chemicals (1,3,5-trivinylbenzene, 1,3-diisopropenylbenzene, divinyl sulfone, diviny ketone) for the crosslinking reaction to minimize and observe the corresponding membrane pore size in terms of wastewater pollutants filtration, such as dye wastewater titania (DWT) with dimension of 15 – 20 nm.

List of References

Abbas, M. A. & Latham, J. (1969). *Q J Roy Meteor Soc* **95**, 63-&.

Acharyya, S. K. & Shah, B. A. (2007). *J Environ Sci Heal A* **42**, 1795-1805.

Araki, J., Wada, M. & Kuga, S. (2001). *Langmuir* **17**, 21-27.

Back, E. L., Htun, M. T., Jackson, M. & Johanson, F. (1967). *Text Res J* **37**, 432-&.

Bang, S., Pena, M. E., Patel, M., Lippincott, L., Meng, X. & Kim, K. W. (2011). *Environ Geochem Hlth* **33**, 133-141.

Ben Issa, N., Rajakovic-Ognjanovic, V. N., Jovanovic, B. M. & Rajakovic, L. V. (2010). *Anal Chim Acta* **673**, 185-193.

Bondeson, D., Mathew, A. & Oksman, K. (2006). *Cellulose* **13**, 171-180.

Bottino, A., Capannelli, G., Comite, A., Ferrari, F. & Firpo, R. (2011). *Membr Water Treat* **2**, 63-74.

Bridge, G. (2004). *Annual Review of Environment and Resources* **29**, 205-259.

Burger, C., Hsiao, B. S. & Chu, B. (2006). *Annu. Rev. Mater. Res.* **36**, 333-368.

Cathell, M. D., Szewczyk, J. C., Bui, F. A., Weber, C. A., Wolever, J. D., Kang, J. & Schauer, C. L. (2008). *Biomacromolecules* **9**, 289-295.

Celik, I., Gallicchio, L., Boyd, K., Lam, T. K., Matanoski, G., Tao, X. G., Shiels, M., Hammond, E., Chen, L., Robinson, K. A., Caulfield, L. E., Herman, J. G., Guallar, E. & Alberg, A. J. (2008). *Environ Res* **108**, 48-55.

Chanda, M. *Introduction to Polymer Science and Chemistry: A Problem-Solving Approach* 379, section 376.312.

Chatterjee, T., Chatterjee, S. & Woo, S. H. (2009). *Chem Eng J* **148**, 414-419.

Chen, J., Li, J. D., Zhao, Z. P., Wang, D. & Chen, C. X. (2007). *Surf Coat Tech* **201**, 6789-6792.

Christoforidou, E. P., Riza, E., Kales, S. N., Hadjistavrou, K., Stoltidi, M., Kastania, A. N. & Linos, A. (2013). *J Environ Sci Heal A* **48**, 1764-1775.

Chuang, C. L., Fan, M., Xu, M., Brown, R. C., Sung, S., Saha, B. & Huang, C. P. (2005). *Chemosphere* **61**, 478-483.

Connett, P. H. & Wetterhahn, K. E. (1986). *J Am Chem Soc* **108**, 1842-1847.

Daels, N., De Vrieze, S., Sampers, I., Decostere, B., Westbroek, P., Dumoulin, A., Dejans, P., De Clerck, K. & Van Hulle, S. W. H. (2011). *Desalination* **275**, 285-290.

Dos Santos, Z. M., Caroni, A. L. P. F., Pereira, M. R., da Silva, D. R. & Fonseca, J. L. C. (2009). *Carbohyd Res* **344**, 2591-2595.

Driehaus, W., Jekel, M. & Hildebrandt, U. (1998). *J Water Serv Res Tec* **47**, 30-35.

Eguez, H. E. & Cho, E. H. (1987). *Jom-J Min Met Mat S* **39**, 38-41.

Ersahin, M. E., Ozgun, H., Dereli, R. K., Ozturk, I., Roest, K. & van Lier, J. B. (2012). *Bioresource Technol* **122**, 196-206.

Facciotti, M., Boffa, V., Magnacca, G., Jorgensen, L. B., Kristensen, P. K., Farsi, A., Konig, K., Christensen, M. L. & Yue, Y. (2014). *Ceramics International* **40**, 3277-3285.

Fan, Y., Saito, T. & Isogai, A. (2008). *Biomacromolecules* **9**, 192-198.

Fan, Y. M., Saito, T. & Isogai, A. (2009). *Carbohyd Polym* **77**, 832-838.

Fukuzumi, H., Saito, T. & Isogai, A. (2009). *Abstr Pap Am Chem S* **237**.

Gajendragad, M. R. & Agarwala, U. (1975). *Indian J Chem* **13**, 1331-1334.

Gallegos-Garcia, M., Ramirez-Muniz, K. & Song, S. X. (2012). *Min Proc Ext Met Rev* **33**, 301-315.

Gao, W., Liang, H., Ma, J., Han, M., Chen, Z. L., Han, Z. S. & Li, G. B. (2011). *Desalination* **272**, 1-8.

Gholami, M. M., Mokhtari, M. A., Aameri, A. & Fard, M. R. A. (2006). *Desalination* **200**, 725-727.

Grunert, M. & Winter, W. T. (2002). *Journal of Polymers and the Environment* **10**, 27-30.

Guan, X. H., Du, J. S., Meng, X. G., Sun, Y. K., Sun, B. & Hu, Q. H. (2012). *J Hazard Mater* **215**, 1-16.

Guo, X. J. & Chen, F. H. (2005). *Environmental science & technology* **39**, 6808-6818.

Gupta, B. K., Gupta, D. S., Dikshit, S. K. & Agarwala, U. (1977). *Indian J Chem A* **15**, 624-626.

Hao, J. M., Han, M. J., Wang, C. & Meng, X. G. (2009). *Micropor Mesopor Mat* **124**, 1-7.

Harish Prashanth, K. V. & Tharanathan, R. N. (2007). *Trends in Food Science & Technology* **18**, 117-131.

He, J. & Charlet, L. (2013). *J Hydrol* **492**, 79-88.

Hilal, N., Al-Zoubi, H., Darwish, N. A., Mohammad, A. W. & Abu Arabi, M. (2004). *Desalination* **170**, 281-308.

Huang, Z. M., Zhang, Y. Z., Kotaki, M. & Ramakrishna, S. (2003). *Compos Sci Technol* **63**, 2223-2253.

Ifuku, S., Nogi, M., Abe, K., Yoshioka, M., Morimoto, M., Saimoto, H. & Yano, H. (2009). *Biomacromolecules* **10**, 1584-1588.

Ifuku, S., Nogi, M., Abe, K., Yoshioka, M., Morimoto, M., Saimoto, H. & Yano, H. (2011). *Carbohyd Polym* **84**, 762-764.

Ifuku, S. & Saimoto, H. (2012). *Nanoscale* **4**, 3308-3318.

Jain, A. & Loeppert, R. H. (2000). *J Environ Qual* **29**, 1422-1430.

Jia, Z. S. & Li, X. L. (2002). *Chinese J Anal Chem* **30**, 846-848.

Joseph, L., Flora, J. R. V., Park, Y. G., Badawy, M., Saleh, H. & Yoon, Y. (2012). *Sep Purif Technol* **95**, 64-72.

Kanae, S. (2009). *J Health Sci* **55**, 860-864.

Karnik, B. S., Davies, S. H., Baumann, M. J. & Masten, S. J. (2007). *Ozone-Science & Engineering* **29**, 75-84.

Kim, J. B., Park, H. J., Shon, H. K., Cho, D. L., Kim, G. J., Choi, S. W. & Kim, J. H. (2010). *J Nanosci Nanotechno* **10**, 3260-3265.

Kotas, J. & Stasicka, Z. (2000). *Environ Pollut* **107**, 263-283.

Kumar, S., Ahlawat, W., Bhanjana, G., Heydarifard, S., Nazhad, M. M. & Dilbaghi, N. (2014). *J Nanosci Nanotechno* **14**, 1838-1858.

Kurhanov, A. M. (2003). *Abstr Pap Am Chem S* **226**, U495-U495.

Kurniawan, T. A., Sillanpaa, M. E. T. & Sillanpaa, M. (2012). *Crit Rev Env Sci Tec* **42**, 1233-1295.

Kwok, K. C. M., Koong, L. F., Chen, G. & McKay, G. (2014). *J Colloid Interf Sci* **416**, 1-10.

Lay, P. A. & Levina, A. (1996). *Inorg Chem* **35**, 7709-7717.

Lee, J. & Walker, H. W. (2008). *Journal of Membrane Science* **320**, 240-247.

Li, J. S., Sun, X. Y., Liu, X. D. & Wang, L. J. (2002). *Chinese Journal of Catalysis* **23**, 453-456.

Li, L., Hashaikeh, R. & Arafat, H. A. (2013). *Journal of Membrane Science* **436**, 57-67.

Li, W. X., Zhou, L. Y., Xing, W. H. & Xu, N. P. (2010). *Desalin Water Treat* **18**, 239-244.

Liu, C. P., Luo, C. L., Gao, Y., Li, F. B., Lin, L. W., Wu, C. A. & Li, X. D. (2010). *Environ Pollut* **158**, 820-826.

Liu, P., Sehaqui, H., Tingaut, P., Wichser, A., Oksman, K. & Mathew, A. P. (2014). *Cellulose* **21**, 449-461.

Liu, W., Sun, S., Cao, Z., Zhang, X., Yao, K., Lu, W. W. & Luk, K. D. K. (2005). *Biomaterials* **26**, 2705-2711.

Liu, Y., Wang, R., Ma, H., Hsiao, B. S. & Chu, B. (2013). *Polymer* **54**, 548-556.

Lu, C. Y. & Chiu, H. S. (2006). *Chem Eng Sci* **61**, 1138-1145.

Lu, M., Guan, X. H., Xu, X. H. & Wei, D. Z. (2013). *Chinese Chem Lett* **24**, 253-256.

Luo, J. & Wan, Y. (2013). *Journal of Membrane Science* **438**, 18-28.

Ma, H., Burger, C., Hsiao, B. S. & Chu, B. (2012). *Biomacromolecules* **13**, 180-186.

Ma, H., Hsiao, B. S. & Chu, B. (2011a). *Abstr Pap Am Chem S* **241**.

Ma, H., Hsiao, B. S. & Chu, B. (2012). *Acs Macro Letters* **1**, 213-216.

Ma, H. Y., Burger, C., Hsiao, B. S. & Chu, B. (2011). *Biomacromolecules* **12**, 970-976.

Ma, H. Y., Burger, C., Hsiao, B. S. & Chu, B. (2014). *Journal of Membrane Science* **454**, 272-282.

Ma, H. Y., Hsiao, B. S. & Chu, B. (2010). *Abstr Pap Am Chem S* **240**.

Ma, H. Y., Hsiao, B. S. & Chu, B. (2011b). *Polymer* **52**, 2594-2599.

Malaeb, L. & Ayoub, G. M. (2011). *Desalination* **267**, 1-8.

Maliyekkal, S. M., Philip, L. & Pradeep, T. (2009). *Chem Eng J* **153**, 101-107.

Masscheleyn, P. H., Delaune, R. D. & Patrick, W. H. (1991). *Environmental science & technology* **25**, 1414-1419.

Mathieu, J. L., Gadgil, A. J., Addy, S. E. A. & Kowolik, K. (2010). *J Environ Sci Heal A* **45**, 1446-1460.

Mcafee, B. J., Gould, W. D., Nadeau, J. C. & da Costa, A. C. A. (2001). *Sep Sci Technol* **36**, 3207-3222.

McGuigan, C. F., Hamula, C. L. A., Huang, S., Gabos, S. & Le, X. C. (2010). *Environ Rev* **18**, 291-307.

Medina, M. A. (2010). *J Hydrol Eng* **15**, 167-170.

Mehta, A. & Zydney, A. L. (2005). *Journal of Membrane Science* **249**, 245-249.

Mercier, G., Herold, C., Mareche, J. F., Cahen, S., Gleize, J., Ghanbaja, J., Lamura, G., Bellouard, C. & Vigolo, B. (2013). *New J Chem* **37**, 790-795.

Mincea, M., Negrulescu, A. & Ostafe, V. (2012). *Rev Adv Mater Sci* **30**, 225-242.

Mohammad, A. W., Ng, C. Y., Lim, Y. P. & Ng, G. H. (2012). *Food Bioprocess Tech* **5**, 1143-1156.

Mohan, D. & Pittman, C. U. (2007). *J Hazard Mater* **142**, 1-53.

Monier, M., Ayad, D. M., Wei, Y. & Sarhan, A. A. (2010). *J Hazard Mater* **177**, 962-970.

Moon, R. J., Martini, A., Nairn, J., Simonsen, J. & Youngblood, J. (2011). *Chem Soc Rev* **40**, 3941-3994.

Moore, G. T. (1907). *J Amer Med Assoc* **49**, 677-680.

Muilenberg, T. (2003). *Pollut Eng* **35**, 22-25.

Musyoka, S. M., Ngila, J. C., Moodley, B., Petrik, L. & Kindness, A. (2011). *Anal Lett* **44**, 1925-1936.

Nair, K. G. & Dufresne, A. (2003). *Biomacromolecules* **4**, 657-665.

Nguyen, V. T., Vigneswaran, S., Ngo, H. H., Shon, H. K. & Kandasamy, J. (2009). *Desalination* **236**, 363-369.

Nishimura, T. & Tozawa, K. (1985). *Cim Bull* **78**, 75-75.

Oehmen, A., Valerio, R., Llanos, J., Fradinho, J., Serra, S., Reis, M. A. M., Crespo, J. G. & Velizarov, S. (2011). *Sep Purif Technol* **83**, 137-143.

Oelkers, E. H., Hering, J. G. & Zhu, C. (2011). *Elements* **7**, 157-162.

Oksman, K., Mathew, A. P., Bondeson, D. & Kvien, I. (2006). *Compos Sci Technol* **66**, 2776-2784.

Pal, P., Ahammad, S. Z., Pattanayak, A. & Bhattacharya, P. (2007). *Water Environ Res* **79**, 357-366.

Panda, P. K. (2008). *Trans Indian Ceram S* **66**, 65-76.

Pandey, S. R., Jegatheesan, V., Baskaran, K. & Shu, L. (2012). *Rev Environ Sci Bio* **11**, 125-145.

Paul, K. (2006). *Abstr Pap Am Chem S* **231**.

Payne, J. C., ter Horst, M. A. & Godwin, H. A. (1999). *J Am Chem Soc* **121**, 6850-6855.

Pendergast, M. M., Dorin, R., Phillip, W., Weisner, U. & Hoek, E. M. V. (2012). *Abstr Pap Am Chem S* **243**.

Pham, Q. P., Sharma, U. & Mikos, A. G. (2006). *Tissue Eng* **12**, 1197-1211.

Pinisakul, A., Polprasert, C., Parkpian, P. & Satayavivad, J. (2002). *Water Sci Technol* **46**, 247-254.

Potts, D. E., Ahlert, R. C. & Wang, S. S. (1981). *Desalination* **36**, 235-264.

Raven, K. P., Jain, A. & Loeppert, R. H. (1998). *Environmental science & technology* **32**, 344-349.

Ravi Kumar, M. N. V. (2000). *Reactive and Functional Polymers* **46**, 1-27.

Raymond, L., Morin, F. G. & Marchessault, R. H. (1993). *Carbohyd Res* **246**, 331-336.

Reschke, G. & Gelbin, D. (1982). *Chem Tech-Leipzig* **34**, 114-120.

Riddles, P. W., Blakeley, R. L. & Zerner, B. (1979). *Analytical biochemistry* **94**, 75-81.

Riddles, P. W., Blakeley, R. L. & Zerner, B. (1983). *Method Enzymol* **91**, 49-60.

Rodionova, G., Eriksen, O. & Gregersen, O. (2012). *Cellulose* **19**, 1115-1123.

Rodriguez-Lado, L., Sun, G. F., Berg, M., Zhang, Q., Xue, H. B., Zheng, Q. M. & Johnson, C. A. (2013). *Science* **341**, 866-868.

Rodriguez, A., Ovejero, G., Mestanza, M. & Garcia, J. (2012). *Desalin Water Treat* **45**, 191-205.

Rorech, G. J. & Bond, S. G. (1993). *I&Cs-Instr Con Syst* **66**, 35-37.

Sato, A., Wang, R., Ma, H., Hsiao, B. S. & Chu, B. (2011). *Journal of Electron Microscopy* **60**, 201-209.

Schwarzenbach, R. P., Egli, T., Hofstetter, T. B., von Gunten, U. & Wehrli, B. (2010). *Annu Rev Env Resour* **35**, 109-136.

Seidel, A., Waypa, J. J. & Elimelech, M. (2001). *Environ Eng Sci* **18**, 105-113.

Shah, T. N., Foley, H. C. & Zydney, A. L. (2007). *Journal of Membrane Science* **295**, 40-49.

Shen, L. & Patel, M. K. (2008). *Journal of Polymers and the Environment* **16**, 154-167.

Shen, W., Chen, S. Y., Shi, S. K., Li, X., Zhang, X., Hu, W. L. & Wang, H. P. (2009). *Carbohyd Polym* **75**, 110-114.

Shin, S. J., Kim, J. P., Kim, H. J., Jeon, J. H. & Min, B. R. (2005). *Desalination* **186**, 1-10.

Singh, S. K., Ghosh, A. K., Kumar, A., Kislay, K., Kumar, C., Tiwari, R. R., Parwez, R., Kumar, N. & Imam, M. D. (2014). *Int J Environ Res* **8**, 49-60.

Sonina, A. N., Uspenskii, S. A., Vikhoreva, G. A., Filatov, Y. N. & Gal'braikh, L. S. (2011). *Fibre Chem+* **42**, 350-358.

Sorlier, P., Denuziere, A., Viton, C. & Domard, A. (2001). *Biomacromolecules* **2**, 765-772.

Styles, P. M., Chanda, M. & Rempel, G. L. (1996). *React Funct Polym* **31**, 89-102.

Su, Y., Burger, C., Hsiao, B. S. & Chu, B. (2014). *Journal of Applied Crystallography* **47**, 788-798.

Sullivan, C., Tyrer, M., Cheeseman, C. R. & Graham, N. J. D. (2010). *Sci Total Environ* **408**, 1770-1778.

Susanto, H., Stahra, N. & Ulbricht, M. (2009). *Journal of Membrane Science* **342**, 153-164.

Syafei, A. D., Lin, C.-F. & Wu, C.-H. (2008). *J Colloid Interf Sci* **323**, 112-119.

Tajc, S. G., Tolbert, B. S., Basavappa, R. & Miller, B. L. (2004). *J Am Chem Soc* **126**, 10508-10509.

Tang, S. S. & Chang, G. G. (1996). *J Biochem-Tokyo* **119**, 1182-1188.

Tseng, T. & Edwards, M. (1999). *J Am Water Works Ass* **91**, 159-170.

Van der Bruggen, B. (2009). *J Appl Polym Sci* **114**, 630-642.

Venturoli, D. & Rippe, B. (2005). *Am J Physiol-Renal* **288**, F605-F613.

Wai, C. M., Wang, J. S. & Yang, M. H. (2003). *Biogeochemistry of Environmentally Important Trace Elements* **835**, 210-231.

Wang, J. W. J., Bejan, D. & Bunce, N. J. (2005). *Ind Eng Chem Res* **44**, 3384-3388.

Wang, L. C., Chen, X. G., Liu, C. S., Li, P. W. & Zhou, P. M. (2008). *J Polym Sci Pol Phys* **46**, 1419-1429.

Wang, R., Guan, S., Sato, A., Wang, X., Wang, Z., Yang, R., Hsiao, B. S. & Chu, B. (2013). *Journal of Membrane Science*.

Wang, R., Liu, Y., Li, B., Hsiao, B. S. & Chu, B. (2012). *Journal of Membrane Science* **392**, 167-174.

Wang, Y. & Santiago-Aviles, J. J. (2011). *Integr Ferroelectr* **126**, 60-76.

Wang, Y. X., Ma, T., Ryzhenko, B. N., Limantseva, O. A. & Cherkasova, E. V. (2009). *Geochem Int+* **47**, 713-724.

Wojciech, B., Celińska, E., Dembczyński, R., Szymanowska, D., Nowacka, M., Jesionowski, T. & Grajek, W. (2013). *Journal of Membrane Science* **427**, 118-128.

Wool, R. P., Khot, S. N., LaScala, J. J., Bunker, S. P., Lu, J., Thielemans, W., Can, E., Morye, S. S. & Williams, G. I. (2002). *Advancing Sustainability through Green Chemistry and Engineering* **823**, 177-204.

Wu, Z. M., Cheng, Z. H. & Ma, W. (2012). *Bioresource Technol* **104**, 807-809.

Xia, S. J., Dong, B. Z., Zhang, Q. L., Xu, B., Gao, N. Y. & Causseranda, C. (2007). *Desalination* **204**, 374-379.

Xie, K. L., Jing, L. X., Zhao, W. G. & Zhang, Y. L. (2011). *J Appl Polym Sci* **122**, 2864-2868.

Yang, R., Aubrecht, K. B., Ma, H., Wang, R., Grubbs, R. B., Hsiao, B. S. & Chu, B. (2014). *Polymer* **55**, 1167-1176.

Yang, Y. Q., Chen, R. Z. & Xing, W. H. (2011). *Sep Purif Technol* **76**, 373-377.

Yarin, A. L., Koombhongse, S. & Reneker, D. H. (2001). *J Appl Phys* **90**, 4836-4846.

Ying, W. C. & Weber, W. J. (1979). *J Water Pollut Con F* **51**, 2661-2677.

Yoshida, T., Yamauchi, H. & Sun, G. F. (2004). *Toxicol Appl Pharm* **198**, 243-252.

Zhang, X. Z., Jiang, K., Tian, Z. B., Huang, W. Q. & Zhao, L. (2008). *J Appl Polym Sci* **110**, 3934-3940.

Zhao, Z. P., Li, J. D., Chen, J. & Chen, C. X. (2005). *Journal of Membrane Science* **251**, 239-245.